FER-LIKE IRON DEFICIENCY-INDUCED TRANSCRIPTION FACTOR (FIT) accumulates in homo- and heterodimeric complexes in dynamic and inducible nuclear condensates associated with speckle components

Short title: FIT localizes in condensates

Ksenia Trofimov[1], Regina Gratz[1,§], Rumen Ivanov[1], Yvonne Stahl[2,3], Petra Bauer[1,3,*], Tzvetina Brumbarova[1,*]

[1] Institute of Botany, Heinrich-Heine-University, 40225 Düsseldorf, Germany
[2] Institute for Developmental Genetics, Heinrich-Heine-University, 40225 Düsseldorf, Germany
[3] Cluster of Excellence on Plant Science (CEPLAS), Heinrich-Heine-University, 40225 Düsseldorf, Germany
***** Shared corresponding authors: Tzvetina Brumbarova (Tzvetina.Brumbarova@hhu.de), Petra Bauer (Petra.Bauer@hhu.de)
[§] Present address: Department of Forest Genetics and Plant Physiology, Swedish University of Agricultural Sciences, 90183 Umeå, Sweden

The author responsible for distribution of materials integral to the findings presented in this article in accordance with the policy described in the Instructions for Authors (https://academic.oup.com/plcell/pages/General-Instructions) is: Petra Bauer (Petra.Bauer@hhu.de).

Highlights

- FIT undergoes light-induced, reversible condensation and localizes to nuclear bodies (NBs), likely via liquid-liquid phase separation
- Functionally relevant Ser271/272 defines an intrinsically disordered region and influences NB formation dynamics
- NBs are preferential sites for FIT dimerization with FIT and bHLH039, dependent on Ser271/272
- FIT NBs colocalize with NB markers related to splicing and light signaling
- Light conditions inducing NBs are linked with active FIT, in agreement with elevated FIT target gene expression in roots

Keywords

bHLH039, condensates, FIT, FRET, intrinsically disordered region, blue light, liquid-liquid phase separation, nuclear body, speckle, SR45

33 **Abbreviations**

34 bHLH	basic helix-loop-helix
35 bHLH039	BASIC HELIX-LOOP-HELIX039
36 C	mCherry
37 FIT	FER-LIKE IRON DEFICIENCY-INDUCED TRANSCRIPTION FACTOR
38 FLIM	fluorescence lifetime imaging microscopy
39 FRAP	fluorescence recovery after photobleaching
40 FRET	fluorescence resonance energy transfer
41 G	GFP
42 GFP	GREEN FLUORESCENT PROTEIN
43 IDR	intrinsically disordered region
44 LLPS	liquid-liquid phase separation
45 mCherry	monomeric Cherry
46 mRFP	monomeric RED FLUORESCENT PROTEIN
47 NB	nuclear body
48 NP	nucleoplasm
49 PB	photobody
50 R	mRFP
51 TF	transcription factor

Abstract

Some nuclear proteins undergo condensation, but the functional importance remains often unclear. The basic helix-loop-helix (bHLH) FER-LIKE IRON DEFICIENCY-INDUCED TRANSCRIPTION FACTOR (FIT) integrates internal and external signals to control iron acquisition and growth. The previously described C-terminal residues Ser271/272 allow FIT to form active complexes with subgroup Ib bHLH factors such as bHLH039. FIT has lower nuclear mobility than mutant FITmSS271AA. Here, we show that FIT undergoes a light-inducible subnuclear partitioning into nuclear condensates that we termed FIT nuclear bodies (NBs). FIT NB characteristics were examined using a standardized FIT NB analysis procedure coupled with different types of quantitative and qualitative microscopy-based approaches. FIT condensates were reversible and likely formed by liquid-liquid phase separation. FIT accumulated preferentially in FIT NBs versus nucleoplasm when engaged in protein complexes with itself and with bHLH039. FITmSS271AA, instead, localized to NBs with different dynamics. FIT colocalized with splicing and light signaling NB markers. The light conditions inducing NBs were linked with active FIT and elevated FIT target gene expression in roots. Hence, the inducible highly dynamic FIT condensates link active transcription factor complexes with posttranscriptional regulation processes and light. Inducible FIT nuclear condensates may affect nuclear mobility and integrate environmental and Fe nutrition signals.

Introduction

As sessile organisms, plants must adjust to an ever-changing environment. Read-out of environmental cues and rapid acclimation are necessary to ensure the plant's vitality. Accordingly, plants control micronutrient uptake. Overaccumulation causes toxicity but lack of a micronutrient leads to deficiency symptoms. Even though iron is one of the most abundant elements in the soil, its bioavailability as micronutrient is limited in most soils, rendering iron uptake a challenge for plants (Römheld and Marschner, 1986; Wedepohl, 1995).

An essential regulatory protein needed for iron acquisition is the basic helix-loop-helix (bHLH) transcription factor (TF) FER-LIKE IRON DEFICIENCY-INDUCED TRANSCRIPTION FACTOR (FIT; Colangelo and Guerinot, 2004; Jakoby et al., 2004; Yuan et al., 2005; Bauer et al., 2007). FIT is activated upon iron deficiency downstream of a cascade of bHLH TFs (Zhang et al., 2015; Li et al., 2016; Liang et al., 2017; Kim et al., 2019; Gao et al., 2020) and of a calcium-sensing protein kinase able to target phosphorylation site Ser271/272 of FIT (Gratz et al., 2019). FIT alone is not sufficient to upregulate iron acquisition, while it is active in a heterodimeric complex together with a member of the bHLH subgroup Ib such as bHLH039 (Yuan et al., 2008; Wang et al., 2013). Furthermore, FIT action is regulated through protein-protein contacts with multiple key players of hormonal and abiotic stress signaling pathways (Lingam et al., 2011; Le et al., 2016; Wild et al., 2016; Cui et al., 2018; Gratz et al., 2019, 2020). Thus, FIT behaves as a regulatory hub in root cells that perceives external and internal cues to adjust iron acquisition with growth (Schwarz and Bauer, 2020; Kanwar et al., 2021).

The subcellular localization of the FIT-bHLH039 module is remarkable. bHLH039 alone is inactive and present mainly close to the plasma membrane in cytoplasmic foci, while bHLH039 together with FIT localizes in the nucleus (Trofimov et al., 2019). FIT is predominately localized in the nucleus but not as mobile compared to mutant FITmSS271AA, that is a less active mutant form of FIT (Gratz et al., 2019). Subcellular partitioning of proteins involved in nutrient uptake has until now not been enough in the focus of research to understand the significance of the differing subcellular localization patterns.

One prominent type of subnuclear partitioning is conferred by biomolecular condensates, or nuclear bodies (NBs). NBs are membrane-less, nuclear sub-compartments, which can be of stable or dynamic nature. To form condensates, proteins

105 need to have particular features that enable protein interactions and compaction in three-
106 dimensional space. IDRs are flexible protein regions that allow conformational changes,
107 and thus various interactions, leading to the required multivalency of a protein for
108 condensate formation (Tarczewska and Greb-Markiewicz, 2019; Emenecker et al., 2020).
109 As Arabidopsis TFs are enriched in IDRs (Strader et al., 2022) it is not unlikely that the
110 resulting multivalency in TFs drives condensation and results in microenvironments for
111 interaction, probably more often than so far studied. IDRs are particularly characteristic in
112 bHLH TFs in vertebrates and invertebrates (Tarczewska and Greb-Markiewicz, 2019),
113 suggesting that this feature may also be relevant for the bHLH TFs of plants. One
114 possibility for condensates to form is to undergo liquid-liquid phase separation (LLPS). In
115 this process, a solution is demixed into two or more phases (Emenecker et al., 2020). This
116 mechanism has been examined in simplified *in vitro* systems, but the involvement of
117 different cell components renders the mechanism more complex *in vivo* (Fang et al., 2019;
118 Riback et al., 2020; Zhu et al., 2021).

119 NBs comprise an immense variety of types, and plants and animals share several
120 of them, e.g. the nucleolus, Cajal bodies, and speckles. The nucleolus is involved in
121 transcription of ribosomal DNA, processing of ribosomal RNA, and ribosome biogenesis
122 (Kalinina et al., 2018; Lafontaine et al., 2021). Nucleoli share components and function
123 with Cajal bodies, which are e.g. ribonucleoproteins and RNA processing (Love et al.,
124 2017; Trinkle-Mulcahy and Sleeman, 2017). Speckles are known spliceosomal sites
125 (Reddy et al., 2012; Galganski et al., 2017). Plant-specific NBs are photobodies (PBs),
126 which are triggered by light, temperature, and circadian clock (Pardi and Nusinow, 2021).
127 PBs harbor regulatory complexes of the photomorphogenic responses, including
128 photoreceptors like phytochromes (phy) and bHLH TFs belonging to the
129 PHYTOCHROME INTERACTING FACTORs (PIFs; Pardi and Nusinow, 2021). Another
130 trigger for inducible and reversible condensate formation is temperature (Jung et al., 2020;
131 Zhu et al., 2021).

132 NBs may act as hubs integrating environmental signals (Emenecker et al., 2020;
133 Meyer, 2020). Especially PBs may combine external cues, such as light, as an input signal
134 to steer developmental processes (Kaiserli et al., 2015; Meyer, 2020; Pardi and Nusinow,
135 2021). It is proposed that the formation of NBs could be an ancient mechanism for spatial
136 organization within the nucleus (Emenecker et al., 2020). As more evidence on

137 condensation in plants arises, this topic remains barely examined in the scope of plant
138 nutrition.

139 The motivation for our study was to elucidate the mechanism behind subcellular
140 distribution and nuclear mobility of FIT. We had found an interesting hint that FIT may
141 undergo light-inducible and reversible nuclear condensation, when we detected FIT
142 nuclear bodies (NBs). We developed a standardized FIT NB analysis procedure and
143 applied it to characterize quantitative and qualitative aspects of the dynamic NB formation
144 using different microscopy-based techniques. Thereby, we were able to link FIT NB
145 formation with the activity status of FIT to form functional protein complexes. We found
146 that splicing and light signaling were also associated with FIT NBs. Thus, this study lays
147 ground for FIT NBs being regulatory hubs steering nutritional signalling, and associating
148 functional significance to FIT protein condensate formation.

149 **Results**

150 **FIT localizes to NBs in light-inducible and dynamic manner likely as a result of LLPS**

151 The TF FIT has a dynamic mobility and capacity to form TF complexes inside plant
152 cells (Gratz et al., 2019; Trofimov et al., 2019). To explore possible mechanisms for
153 dynamic FIT subcellular localization, we performed a microscopic study on FIT-GFP
154 protein localization in the root epidermis of the root differentiation zone of 5-d-old iron-
155 deficient seedlings of *Arabidopsis thaliana* (Arabidopsis), where FIT is active and iron
156 acquisition occurs (FIT_{pro}:FIT-GFP, this study; $35S_{pro}$:FIT-GFP, Gratz et al., 2019). At first
157 microscopic inspection, FIT-GFP was evenly distributed within the nucleus (t= 0 in
158 **Figure 1A**, FIT_{pro}:FIT-GFP; t= 0 in **Supplemental Figure S1A**, $35S_{pro}$:FIT-GFP), as
159 expected (Gratz et al., 2019; Trofimov et al., 2019). We report and characterize here a
160 previously unknown localization behavior of FIT that we found to be coupled with its
161 activity status. We observed, when whole seedlings were exposed to 488 nm laser light
162 for several minutes or when they had been shifted from a white light growth chamber into
163 one with blue light for a time of up to two hours, that FIT became re-localized at the
164 subnuclear level. After a lag time, FIT-GFP was present in one to four discrete spots per
165 nucleus, visible after 40 min earliest, sometimes taking up to 120 min to appear (t= 90
166 minutes in **Figure 1A**, FIT_{pro}:FIT-GFP; t= 40 min in **Supplemental Figure S1A**,
167 $35S_{pro}$:FIT-GFP). Hence, FIT-GFP was re-localized in light-inducible manner at the
168 subnuclear level, irrespective of either of the two promoters used. During the imaging

169 process or an additional hour of darkness, these spots disappeared (**Figure 1A**, t= 120
170 min), indicating that the formation of these spots was reversible. The observation of FIT
171 nuclear spots in the root epidermis of the root differentiation zone was very interesting,
172 suggesting that these might perhaps be NBs containing FIT. However, further inspection
173 of the nuclear spots in root cells in this differentiating root zone was hampered by several
174 difficulties, namely the small size and low accessibility of the nucleus, and especially
175 considering the long lag time for detecting the nuclear spots. These factors made it
176 impossible for us to apply quantitative fluorescence microscopy techniques to draw
177 validated conclusions on the nature, dynamics, and functional significance of nuclear
178 spots in root epidermis cells of the root differentiation zone of iron-deficient seedlings.
179 We previously employed a reliable plant cell assay for studying FIT functionality,
180 and we adapted it to study the characteristics of FIT NBs (Gratz et al., 2019, 2020;
181 Trofimov et al., 2019). Using this assay, FIT-GFP that was transiently expressed in
182 *Nicotiana benthamiana* (*N. benthamiana*) leaf epidermis cells under a β-estradiol-
183 inducible promoter to control protein expression showed a very similar re-localization of
184 FIT-GFP into nuclear spots as observed in the Arabidopsis root epidermis, again triggered
185 by treatment with a 488 nm laser light stimulus. Differences were, however, the duration
186 of the lag time needed to observe this phenomenon, and the number of nuclear spots. As
187 in Arabidopsis, FIT-GFP localized initially in uniform manner to the entire nucleus (t=0) of
188 *N. benthamiana* leaf epidermis cells. A short duration of 1 min 488 nm laser light excitation
189 induced the formation of FIT-GFP signals in discrete spots inside the nucleus after a lag
190 time of only five minutes (t=5; **Figure 1B and Supplemental Movie S1A**). The nuclear
191 FIT spots were systematically initiated, and nearly all nuclei in the imaged leaf disk
192 showed numerous spots. A similar laser light excitation procedure was previously found
193 to elicit PB formation of cryptochrome2 (CRY2) in Arabidopsis protoplasts and HEK293T
194 cells (Wang et al., 2021). We deduced that the spots of FIT-GFP signal were NBs. FIT NB
195 formation was not dependent on the fluorescent tag, as it was similar for FIT-mCherry
196 when co-excited with 488 nm laser light (**Figure 1C**). Another TF and interactor of FIT,
197 ZINC FINGER OF ARABIDOPSIS THALIANA12-GFP (ZAT12-GFP; Le et al., 2016), did
198 not localize to NBs under the same imaging conditions (**Figure 1D and Supplemental**
199 **Movie S1B**). Therefore, we concluded that FIT localization to NBs was a specificity of FIT
200 and that formation of FIT NBs was not artificially caused by fluorescent tags or the imaging
201 setup. Importantly, the *N. benthamiana* epidermis expression system was suited to control

202 the parameters for light-induced triggering of FIT NBs and their quantitative analysis by
203 fluorescence microscopy. We then developed a standardized experimental procedure for
204 qualitative and quantitative FIT NB analysis in *N. benthamiana* (hereafter named
205 'standardized FIT NB analysis procedure'; **Supplemental Figure S1B**).

206 Liquid-liquid phase separation (LLPS) is a possible way for condensate formation,
207 and liquid-like features are quantifiable by mobility and shape analysis within condensates
208 (Shin et al., 2017; Wang et al., 2021). We used the standardized FIT NB analysis
209 procedure to examine whether this could also be a mechanism underlying the FIT NB
210 formation. Mobility of FIT NBs was tested with the fluorescence recovery after
211 photobleaching (FRAP) approach (Bancaud et al., 2010; Trofimov et al., 2019) by
212 recording the recovery of the fluorescence intensity over time in a bleached NB
213 (**Figure 1E-G**). According to relative fluorescence intensity the fluorescence signal
214 recovered to a high extent with FIT NBs (**Figure 1F**), and the calculated mobile fraction
215 of the NB protein was on average 80% (**Figure 1G**). Shape analysis of FIT NBs showed
216 that the NBs reached a high circularity score (**Figure 1H**). According to Wang et al. (2021),
217 fluorescence recovery and circularity scores as the ones measured for FIT NBs reflect
218 high mobility and circular shape. Thus, FIT NBs behave in a liquid-like manner suggesting
219 that LLPS might be the mechanism leading to FIT NB formation.

220 In summary, FIT-GFP forms light-inducible FIT NBs in roots and upon transient
221 expression in *N. bethamiana* leaf epidermis cells. The developed standardized FIT NB
222 analysis procedure was well suited for investigating dynamic properties of light-induced
223 FIT NBs and characterizing them as the likely result of LLPS. Because of these properties,
224 it is justified to term them 'FIT NBs'. We hypothesized that NB formation is a feature of the
225 FIT protein that provides regulatory specificity, and we subsequently investigated this
226 hypothesis using the developed standardized FIT NB analysis procedure in all subsequent
227 assays below.

228 **FIT forms homodimeric complexes preferentially in NBs, dependent on Ser271/272**

229 Next, we asked which properties of the FIT protein enable NB formation. Residue
230 Ser271/272 is important for the homo- and heterodimerization capacity of FIT (Gratz et
231 al., 2019). We therefore asked whether this site has an influence on FIT NB formation,
232 and we compared the ability for NB formation of phospho-mutated FIT with that of wild-
233 type FIT-GFP protein. The phospho-mimicking FITmS272E protein did not show

234 significant changes in its behavior compared to wild-type FIT in the work of Gratz et al.
235 (2019). However, the FITmSS271AA-GFP mutant was less able to mediate induction of
236 iron deficiency responses and its properties differed from wild-type FIT-GFP (Gratz et al.,
237 2019). Hence, we focused on comparing the nuclear NB-forming characteristics between
238 wild-type FIT-GFP and FITmSS271AA-GFP mutant.

239 FITmSS271AA-GFP also localized to NBs, however with different dynamics. The
240 formation of FITmSS271AA NBs was delayed in time (**Figure 2A**; t=15 instead of t=5).
241 While FIT-GFP NB formation started in the first minutes after excitation (**Supplemental**
242 **Movie S1A**), FITmSS271AA-GFP NB formation occurred earliest 10 min after excitation
243 (**Supplemental Movie S1C**). In addition, NB number and size of FITmSS271AA-GFP
244 were decreased in comparison to the ones from wild-type FIT-GFP (**Figure 2, B and C**).
245 Hence, the dynamics of NB formation were dependent on Ser271/272.

246 The process of condensation is facilitated when proteins possess IDRs, since,
247 importantly, IDRs may engage in numerous interactions in space due to rapid
248 conformational changes (Tarczewska and Greb-Markiewicz, 2019; Emenecker et al.,
249 2020). The three-dimensional conformation of wild-type FIT had predicted stretches of
250 intrinsic disorganization, peaking before and at the basic region of the bHLH domain, and
251 two in the C-terminal part, one of them around the Ser271/272 site (termed $IDR^{Ser271/272}$;
252 **Supplemental Figure S2A**). In contrast, in the FITmSS271AA mutant this C-terminal
253 region was no longer classified as IDR (**Supplemental Figure S2B**). This underlined the
254 significance of the Ser271/272 site, not only for interaction but also for FIT NB formation.

255 We then tested whether FIT homodimerization was preferentially associated with
256 NB formation. For that, we investigated whether FIT-GFP shows a differentiated
257 homodimerization strength, first, inside the NBs versus the nucleoplasm (NP), and
258 second, as wild-type FIT versus the mutant FITmSS271AA-GFP protein by performing
259 anisotropy (or homo-FRET) measurements. Energy transfer between the same kind of
260 fluorescently tagged proteins leads to depolarization of the emitted light (Stahl et al., 2013;
261 Weidtkamp-Peters et al., 2022). Fluorescence anisotropy (FA) describes this
262 depolarization and gives hints on the dimerization and oligomerization status of a protein
263 as the FA value decreases (**Figure 3A**). We measured FA before (t=0) and after NB
264 formation (t=5 for FIT and t=15 for FITmSS271AA), and analyzed the homodimerization
265 strength for the whole nucleus, the NBs, and the residual NP (**Figure 3B-D**). Free GFP

266 and GFP-GFP constructs were used as references for monomers and dimers (**Figure 3C**
267 **and D**).
268 Whole nucleus FA values were lower at t=5 than at t=0 for FIT-GFP. Additionally,
269 FA values were lower within the NBs compared to the NP (**Figure 3C**). Compared to wild-
270 type FIT-GFP, FA values were not reduced for mutant FITmSS271AA-GFP at t=15
271 compared to t=0. Also, the FA values did not differ between NBs and NP for the mutant
272 protein (**Figure 3D**). This indicated the presence of homodimeric FIT complexes in NBs.
273 In summary, wild-type FIT had better capacities to localize to NBs than mutant
274 FITmSS271AA, presumably due its $IDR^{Ser271/272}$ at the C-terminus. NBs were nuclear sites
275 in which FIT formed preferentially homodimeric protein complexes.

276 **FIT-bHLH039 interaction complexes preferentially accumulate in FIT NBs**

277 FIT engages in protein-protein interactions with bHLH039 to steer iron uptake
278 target gene induction in the nucleus, while mutant FITmSS271AA protein is less active in
279 interacting with bHLH039 (Gratz et al., 2019). Hence, we tested whether FIT also interacts
280 with bHLH039 preferentially inside NBs and whether mutant FITmSS271AA differs in this
281 ability from wild-type FIT protein. bHLH039 alone does not localize inside the nucleus but
282 requires FIT for nuclear localization (Trofimov et al., 2019), so that bHLH039 was not used
283 alone to test its subnuclear localization.
284 Upon co-expression, FIT-GFP and bHLH039-mCherry colocalized fully in NBs that
285 resembled the previously described FIT NBs. In the beginning, both proteins were
286 uniformly distributed within the nucleus (t=0), and later became localized in NBs (t=5;
287 **Figure 4A**).
288 We then examined the heterodimerization strength of FIT-GFP and bHLH039-
289 mCherry, and FITmSS271AA-GFP and bHLH039-mCherry by FRET-fluorescence
290 lifetime imaging microscopy (FRET-FLIM) measurements. In case of protein interaction
291 (close proximity, ≤10 nm), energy transfer between a fluorescently tagged donor and a
292 fluorescently tagged acceptor decreases the fluorescence lifetime of the donor
293 (**Figure 4B;** Borst and Visser, 2010; Weidtkamp-Peters and Stahl, 2017). We quantified
294 the fluorescence lifetime of FIT-GFP and FITmSS271AA-GFP respective of
295 heterodimerization before (t=0) and after NB formation (t=5 for FIT and t=15 for
296 FITmSS271AA) in the whole nucleus, in NBs, and in the NP (**Figure 4C-E**). FIT-GFP and
297 FITmSS271AA-GFP (donor only) served as negative controls.

298 Fluorescence lifetime was decreased for the pair FIT-GFP and bHLH039-mCherry
299 at t=5 within NBs compared to all other measured areas (**Figure 4D**). In contrast to that,
300 the fluorescence lifetime decreased for the pair FITmSS271AA-GFP and bHLH039-
301 mCherry at t=15 was not different between NBs and NP (**Figure 4E**). This indicated that
302 heterodimeric complexes accumulated preferentially in FIT NBs.
303 In summary, heterodimerization of FIT with bHLH039 was spatially concentrated in
304 NBs versus the remaining nuclear space and was less prominent for FITmSS271AA.
305 Hence, the capacity of FIT to form an active TF complex was coupled with its presence in
306 NBs. The occurrence of FIT homo- and heterodimerization preferentially in NBs suggests
307 that FIT protein interaction may drive condensation. We therefore concluded that FIT NBs
308 may be sites with active TF complexes for iron deficiency response regulation.

309 **FIT NBs colocalize with speckle components**

310 Numerous NB types are known, and they are associated with particular proteins
311 that are indicative of the NB type. To further understand the identity, dynamics, and
312 function of FIT NBs, we co-expressed FIT-GFP with seven different NB markers from The
313 Plant Nuclear Marker collection (NASC) and observed NB formation and protein
314 colocalization before (t=0) and after FIT NB formation (t=5). In cases where we detected
315 a colocalization with FIT-GFP, we analyzed the localization of NB markers also in the
316 single expression at t=0 and at t=5 after the 488 nm excitation, to detect potentially
317 different patterns in single and co-expression.
318 All seven NB markers were expressed together with FIT-GFP, and according to the
319 resulting extent of colocalization we subdivided them into three different types. The first
320 type (type I) did not colocalize with FIT-GFP neither at t=0 nor at t=5. This was the case
321 for the Cajal body markers coilin-mRFP and U2 snRNP-specific protein U2B”-mRFP
322 (**Supplemental Figure S3**; Lorković et al., 2004; Collier et al., 2006). Coilin-mRFP
323 localized into a NB within and around the nucleolus (**Supplemental Figure S3A**). The
324 NBs of U2B”-mRFP were also close to the nucleolus (**Supplemental Figure S3B**).
325 Hence, FIT-GFP was not associated with Cajal bodies.
326 The second type (type II) of NB markers were partially colocalized with FIT-GFP.
327 This included the speckle components ARGININE/SERINE-RICH45-mRFP (SR45) and
328 the serine/arginine-rich matrix protein SRm102-mRFP. SR45 is involved in splicing and
329 alternative splicing and is part of the spliceosome in speckles (Ali et al., 2003), and was

330 recently found to be involved in splicing of iron homeostasis genes (Fanara et al., 2022).
331 SRm102 is a speckle component (Kim et al., 2016). SR45-mRFP localized barely in the
332 NP but inside few and very large NBs that remained constant at t=0 and t=5. FIT-GFP did
333 not colocalize in those NBs at t=0, however, it colocalized with the large SR45-mRFP NBs
334 at t=5 (**Figure 5A**). FIT-GFP also localized in typical FIT NBs in the residual NP at t=5
335 (**Figure 5A**). SRm102-mRFP showed low expression in the NP and stronger expression
336 in a few NBs that also remained constant at t=0 and t=5. FIT-GFP colocalized with
337 SRm102-mRFP in only few instances at t=5, but not t=0, while most FIT NBs did not
338 colocalize with SRm102-mRFP NBs (**Figure 5B**). Both SR45-mRFP and SRm102-mRFP
339 had the same localization pattern at t=0 and t=5, irrespective of FIT-GFP co-expression
340 or 488 nm excitation (**Supplemental Figure S4**). These type II NB markers seemed to
341 recruit FIT-GFP into NBs after 488 nm excitation that were present (pre-existing) before
342 FIT-GFP NB formation, while FIT-GFP localized additionally in separate FIT NBs. Hence,
343 FIT became associated with splicing components and speckles upon the light trigger.
344 A third type (type III) of three NBs markers, namely UAP56H2-mRFP, P15H1-
345 mRFP, and PININ-mRFP, were fully colocalized with FIT-GFP. Until now, these NB
346 marker proteins are not well described in plants. UAP56H2 is a RNA helicase, which is
347 involved in mRNA export (Kammel et al., 2013). P15H1 was found as a putative
348 Arabidopsis orthologue of an exon junction complex component in humans (Pendle et al.,
349 2005), while PININ has a redundant role to its paralogue apoptotic chromatin
350 condensation inducer in the nucleus (ACINUS) in alternative splicing (Bi et al., 2021).
351 UAP56H2-mRFP and P15H1-mRFP did not localize in NBs and were not responsive to
352 the 488 nm excitation when expressed alone or together with FIT-GFP at t=0 (**Figure 6,**
353 **A and B and Supplemental Figure S4, C and D**). When co-expressed with FIT-GFP and
354 following the 488 nm excitation, at t=5, the two NB markers adopted the FIT NB pattern
355 and colocalized with FIT-GFP in FIT NBs (**Figure 6, A and B**). PININ-mRFP was also
356 uniformly distributed in the nucleus at t=0 like FIT-GFP and fully colocalized with FIT NBs
357 at t=5 (**Figure 6C**). But curiously, PININ-mRFP showed a very different localization in the
358 single expression. Predominately, it localized to a very large NB besides several small
359 NBs with no expression in the NP at t=0 and at t=5 (**Supplemental Figure S4E**). Thus,
360 FIT-GFP recruited these type III NB marker and speckle proteins fully into FIT NBs. Since
361 type III NB markers are also potentially involved in splicing and mRNA export from the
362 nucleus, these same functions may be relevant in FIT NBs.

363 Taken together, the colocalization studies underlined the dynamic behavior of
364 inducible FIT NB formation. FIT NBs had a speckle function, in which on the one hand FIT
365 was recruited itself into pre-existing splicing-related NBs (SR45-mRFP and SRm102-
366 mRFP, type II), while on the other hand it also recruited speckle-localized proteins into
367 FIT NBs (UAP56H2-mRFP, P15H1-mRFP, and PININ-mRFP, type III).

368 **PB components influence FIT NB localization and formation**

369 PBs are plant-specific condensates which harbor various light signaling
370 components (Kircher et al., 2002; Bauer et al., 2004). Among them are the bHLH TFs of
371 the PIF family. As key regulators of photomorphogenesis, they integrate light signals in
372 various developmental and physiological response pathways (Leivar and Monte, 2014;
373 Pham et al., 2018). Indeed, PIF4 may control iron responses in Arabidopsis based on
374 computational analysis of iron deficiency response gene expression networks
375 (Brumbarova and Ivanov, 2019) and both PIF proteins intersect with blue light signaling
376 (Ni et al., 1998; Oh et al., 2004; Pedmale et al., 2016). We tested in the same manner as
377 described above for NB markers, whether FIT NBs coincide with two of the described PB
378 markers, PIF3-mCherry and PIF4-mCherry (Van Buskirk et al., 2014; Qiu et al., 2019,
379 2021).

380 We detected distinct localization patterns for PIF3-mCherry and PIF4-mCherry. At
381 t=0, PIF3-mCherry was predominantly localized in a single large PB (**Figure 7A**). In
382 general, localization of single expressed PIF3-mCherry remained unchanged at t=0 and
383 t=15 (**Supplemental Figure S5A**). Upon co-expression, FIT-GFP was initially not present
384 in PIF3-mCherry PB at t=0. After 488 nm excitation and at t=5, FIT NBs were still not
385 visible. Instead, FIT-GFP accumulated and finally colocalized with the large PIF3-mCherry
386 PB at t=15, while the typical FIT NBs did not appear (**Figure 7A**).

387 PIF4-mCherry localized in two different patterns, and both differed substantially
388 from that of PIF3-mCherry. In the one pattern at t=0, PIF4-mCherry was not localized to
389 any PBs, but instead was uniformly distributed in the NP as was the case for FIT-GFP.
390 Such a pattern was also seen at t=15, and then neither PIF4-mCherry nor FIT-GFP were
391 localized in any PBs/NBs (**Figure 7B**). In the other pattern, PIF4-mCherry and FIT-GFP
392 localized in multiple PBs at t=0 and t=15, whereas none of them corresponded
393 morphologically to the typical FIT NBs (**Figure 7C**). The same two localization patterns

394 were also found for PIF4-mCherry in the single expression, whereby 488 nm excitation
395 did not alter PIF4-mCherry localization (**Supplemental Figure S5, B and C**).
396 Hence, FIT was able to localize to PBs when co-expressed with PIF3 and PIF4,
397 raising the possibility that FIT is a key regulator to cross-connect iron acquisition regulation
398 and light signaling pathways.

399 **Blue light has a promoting effect on iron acquisition responses downstream of FIT**

400 Previous studies have shown that iron uptake by FIT is diurnally and circadian
401 clock-regulated (Vert et al., 2003; Santi and Schmidt, 2009; Salomé et al., 2013). Knowing
402 that FIT NB formation was light-dependent as well as promoting the interaction of the FIT-
403 bHLH039 complex, and that FIT NBs were colocalizing with light signaling and PB
404 components, we reasoned that plants exposed to the FIT NB-forming light cues may show
405 differential FIT-dependent iron uptake responses with respect to control plants exposed
406 to the regular light conditions. To test this, we grew wild-type Arabidopsis plants for 5 d
407 under iron sufficient and iron deficient conditions under white light and exposed the plants
408 additionally for 1 d to blue light. As a control for light quality, we also included exposure to
409 red and far-red light and darkness besides the regular white light. We measured molecular
410 iron uptake responses known to be under the control of FIT-bHLH039 in roots (Gratz et
411 al., 2019).
412 Iron reductase activity is increased in roots when FIT and bHLH039 are activated
413 in response to iron deficiency in our growth system (Gratz et al., 2019). Iron reductase
414 activity was higher under iron deficient conditions compared to iron sufficient conditions
415 under all white light controls, as expected (**Figure 8A-D**). Interestingly, when seedlings
416 were exposed to blue light for a day, they induced iron reductase activity in the iron
417 deficient versus iron sufficient condition more than in the white light control (**Figure 8A**).
418 On the other hand, exposure to red light did not change the iron reductase activity
419 compared to the white light control (**Figure 8B**), while exposure to far-red light or darkness
420 abolished the induction (**Figure 8, C and D**). Hence, only exposure to blue light had an
421 extra promoting effect on iron uptake in the seedlings compared with the other tested light
422 qualities.
423 Increased iron acquisition under iron deficiency and enhanced iron reductase
424 activity require FERRIC REDUCTASE-OXIDASE2 (FRO2) protein (Yi and Guerinot, 1996;
425 Robinson et al., 1999), and *FRO2* to be induced, along with *IRON REGULATED*

426 *TRANSPORTER1* (*IRT1*; Eide et al., 1996; Korshunova et al., 1999). *FRO2* and *IRT1* are
427 target genes of FIT-bHLH039 in our growth system (Gratz et al., 2019, 2020). As a readout
428 of the activity of the FIT-bHLH039 complex, we examined gene regulation of *FRO2* and
429 *IRT1* as well as *FIT* and *BHLH039* under the same light conditions as described above.
430 Previously, it was shown that the expression of *IRT1* and *FRO2* was downregulated under
431 iron deficient conditions in darkness compared to iron deficient conditions in white light,
432 while the opposite was true for *FIT* (Santi and Schmidt, 2009).

433 Under white light conditions, gene expression for all four genes was tested in four
434 independent samples. In 15 out of the 16 cases, gene expression of *FIT*, *BHLH039*, *FRO2*
435 and *IRT1* was significantly higher under iron deficient than sufficient conditions, as
436 expected, and in only one case for *FIT*, it was similar and not significantly enhanced
437 (**Figure 9A-P, with exception of E**, *FIT*). Under blue light, *FIT* and *BHLH039* expression
438 was induced upon iron deficiency in the same manner as in white light (**Figure 9, A and**
439 **B**), whereas *FRO2* and *IRT1* were induced to a higher level in response to iron deficiency
440 in blue light versus white light (**Figure 9A-D**). Again, plant responses were different upon
441 exposure to other light conditions. *FIT* and *IRT1* were similarly induced, while *BHLH039*
442 and *FRO2* were even less induced by iron deficiency under red light than white light
443 (**Figure 9E-H**). In both, the far-red light and darkness situations, *FIT* was induced under
444 iron deficiency versus deficiency, while on the other side, *BHLH039*, *FRO2* and *IRT1* were
445 not induced at all in these light conditions (**Figure 9I-P**). *FIT* was similarly induced under
446 far-red light and white light (**Figure 9I**), whereas in darkness it was even induced to higher
447 level (**Figure 9M**), as previously reported (Santi and Schmidt, 2009).

448 To sum up, the FIT-bHLH039-dependent target gene expression is similarly light
449 quality-dependent as the FIT-bHLH039-dependent iron reductase activity. Hence, very
450 interestingly, blue light cues which lead to FIT NB formation, promote FIT-bHLH039-
451 dependent iron uptake responses, fitting with the above finding that FIT NBs are linked
452 with active TF complexes in condensates.

453 **Discussion**

454 In this study, we uncovered a previously unknown phenomenon, the blue light-
455 induced and reversible accumulation of FIT condensates in FIT NBs. LLPS was most
456 likely the underlying mechanism for this highly dynamic process. FIT NBs were enriched
457 in active FIT TF complexes that are required for iron deficiency gene regulation. FIT

458 associated with speckles and PBs in a highly dynamic fashion, indicating a function in
459 transcriptional and post-transcriptional control. Blue light exposure resulted in enhanced
460 molecular FIT-bHLH039-dependent iron acquisition responses. Based on these data, we
461 propose that FIT NBs are dynamic microenvironments with active FIT TF complexes that
462 possibly are hubs to enhance and cross-connect transcriptional iron deficiency gene
463 expression with post-transcriptional regulation and light signaling.

464 **A standardized procedure for FIT NB induction was crucial to delineate the**
465 **characteristics of FIT NBs in reliable manner**

466 A major aim of this study was to characterize the nature and potential function of
467 light-induced FIT NBs. To be able to apply the quantitative microscopy-based techniques,
468 we needed to control the appearance of NBs in reliable manner. This was clearly a
469 limitation for inspection of root epidermis cells of the root differentiation zone in iron-
470 deficient plants in which FIT-controlled iron uptake takes place. Not every root epidermis
471 cell showed NBs and only few FIT NBs were detectable after a delay of 40 min to 120 min.
472 Since condensation depleted FIT protein in the nucleoplasm, the remaining low FIT
473 protein concentration can be the reason why FIT NBs remained few in number in the
474 Arabidopsis root cells. The *N. benthamiana* protein expression system did not present
475 these limitations and high-quality measurement data were obtained for all experimental
476 series. Furthermore, this expression system is a well-established and widely utilized
477 system in plant biology (Martin et al., 2009; Bleckmann et al., 2010; Leonelli et al., 2016;
478 Burkart et al., 2022). The developed standardized assay generated reliable and accurate
479 data for statistical analysis and quantification to conclude about FIT NB characteristics.

480 Condensation likely explains the reduced mobility of FIT-GFP versus
481 FITmSS271AA-GFP seen in a previous study (Gratz et al., 2019). In liquid state,
482 condensates are still more mobile than in the solid one. The condensate formation was
483 reversible, speaking in favor of a liquid state of the condensates. According to FRAP data,
484 FIT NBs maintained a dynamic exchange of FIT protein with the surrounding NP. FIT NBs
485 were also mostly of circular shape. Circular condensates appear as droplets, in contrast
486 to solid-like condensates that are irregularly shaped (Shin et al., 2017). These
487 characteristics speak in favor of liquid-like features, suggesting that LLPS underlies FIT
488 NB formation. A similar situation was described for CRY2 PBs, which were also reversible
489 and of circular shape with mobile protein inside PBs (Wang et al., 2021). bHLH039 was

490 found accumulated in cytoplasmic foci at the cell periphery (Trofimov et al., 2019). In such
491 foci, bHLH039 was immobile, and we suspect it was in a non-functional state in the
492 absence of FIT. This underlines the understanding that liquid condensates such as FIT
493 NBs are dynamic microenvironments, whereas immobile condensates point rather
494 towards a solid and pathological state (Shin et al., 2017).

495 In conclusion, the properties of liquid condensation along with the findings that it
496 occurred irrespective of the fluorescence protein tag preferentially with wild-type FIT, but
497 with different dynamics for the mutant FITmSS271AA and not at all for ZAT12, allowed us
498 to coin the term of 'FIT NBs'.

499 **IDR$^{Ser271/272}$ was crucial for interaction and NB formation of FIT**

500 FIT NBs were hotspots for FIT interaction, allowing to assume that they are
501 integrated in the iron deficiency response as interaction hubs. FIT formed homodimers
502 and heterodimers with bHLH039 preferentially in NBs compared with the NP. These
503 abilities distinguished wild-type FIT and mutant FITmSS271AA. According to these
504 findings FITmSS271AA was less successful in interacting within NBs, indicating that wild-
505 type FIT is a multivalent protein and IDR$^{Ser271/272}$ is important for that. bHLH proteins
506 interact with other proteins via the helix-loop-helix interface, which may certainly also be
507 the case for FIT. Our study supports previous reports that FIT protein interaction via its C-
508 terminus is relevant (Lingam et al., 2011; Le et al., 2016; Gratz et al., 2019). The property
509 of being able to interact via the HLH and via the C-terminal domain allows FIT to be
510 multivalent. It could not be distinguished whether FIT homodimers were a prerequisite for
511 the localization of bHLH039 in NBs or whether FIT-bHLH039 complexes also initiated NBs
512 on their own.

513 The predicted C-terminal FIT IDR$^{Ser271/272}$ was relevant for NB formation capacity.
514 IDRs are often required for protein interactions of hub proteins since the flexible IDRs
515 adapt to interactions with multiple protein partners and are therefore crucial for
516 multivalency (Tarczewska and Greb-Markiewicz, 2019; Emenecker et al., 2020; Salladini
517 et al., 2020). Besides, evidence exists that the amino acid composition of IDRs is crucial
518 for condensation (Powers et al., 2019; Emenecker et al., 2021; Huang et al., 2022). Very
519 interestingly, posttranslational modification in form of phosphorylation within IDRs is
520 suggested to be a mechanism to regulate condensate formation (Owen and Shewmaker,
521 2019). Ser271/272 is targeted by a FIT-interacting protein kinase that was shown to affect

522 FIT activity *in vivo* and FIT phosphorylation *in vitro* (Gratz et al., 2019). Hence,
523 phosphorylation of Ser271/272 might perhaps be a trigger for NB formation *in vivo*.

524 **Formation of FIT NB could happen *de novo* but also associate with pre-existing**
525 **condensates in the nucleus**

526 FIT may have formed FIT NBs as entirely newly formed structures upon the light
527 trigger. But it is also possible that FIT joined pre-existing NBs, which then became the
528 structures we termed FIT NBs. Partial or full colocalization of FIT-GFP with NB and PB
529 markers revealed the remarkably high and intriguing dynamic nature of FIT NBs and
530 suggests that both possibilities are plausible. FIT NBs are light-triggered, and this speaks
531 in favor of pre-existing NBs. Since FIT does not possess light-responsive domains, it is
532 most likely that a light-responsive protein must be inducing FIT NB formation. The basic
533 leucine zipper TF ELONGATED HYPOCOTYL5 (HY5) could be a good candidate, since
534 HY5 is a mobile protein involved in iron acquisition in tomato (Gao et al., 2021; Guo et al.,
535 2021) and acts positively on iron uptake and gene expression of *FIT*, *FRO2*, and *IRT1* in
536 Arabidopsis (Mankotia et al., 2023). Possibly activation and condensation involve not only
537 the studied NB and PB markers but also potentially signaling proteins or further scaffold
538 proteins that are part of the multivalent protein complexes in FIT NBs. On the other hand,
539 FIT-GFP accumulated not only in FIT NBs but also in the pre-existing NBs with type II NB
540 markers (SR45 and SRm102) after the FIT NB induction procedure. In this respect, type II
541 markers were similar to PIF3 and PIF4. FIT-GFP was recruited to pre-existing PBs and
542 again only after the light trigger. Interestingly, typical FIT NB formation did not occur in the
543 presence of PB markers, indicating that they must have had a strong effect on recruiting
544 FIT. Overall, the dynamics of FIT colocalization with type II NB and PB markers suggest
545 that these condensates dictated FIT condensation in their own pre-existing NBs/PBs. This
546 recruiting process could be navigated via protein-protein interaction since this is the
547 driving force of condensation (Kaiserli et al., 2015; Emenecker et al., 2020).

548 Speaking in favor of a *de novo* FIT NB formation is the localization with type III NB
549 markers. The three fully colocalizing type III NB markers (UAP56H2, P15H1 and PININ)
550 accumulated only in FIT NBs upon co-expression with FIT and mostly not on their own.
551 The same was true for bHLH039, that joined FIT in FIT NBs, showing that FIT not only
552 facilitated bHLH039 nuclear localization (Trofimov et al., 2019) but also condensation.
553 Interestingly, FIT was able to change PININ nuclear localization. In single expression,

554 PININ was localized to a major large NB, but in colocalization with FIT it joined the typical
555 FIT NBs. This suggests that FIT dictates bHLH039 and type III NB markers and highlights
556 that FIT is also able to set the tone for NB formation. Hence, FIT can recruit other proteins
557 into NBs, and it is possible that FIT forms its own NBs. Protein-protein interaction could
558 underly this recruitment, as evident for bHLH039 (Kaiserli et al., 2015; Emenecker et al.,
559 2020). Ultimately, as a high diversification of condensates exists, a combination of newly
560 formed NBs and localization to pre-existing NBs cannot be ruled out. Given the variety of
561 proteins localizing in condensates, effort in isolating FIT NBs and identification of proteins
562 within FIT NBs is necessary to further uncover the driving forces of FIT NB formation.

563 **FIT NBs might have a transcriptional and post-transcriptional function**

564 Since the type II and III markers are splicing components, the colocalization studies
565 suggest that FIT NBs are speckles. On the one hand, the speckle nature coincides well
566 with the dynamic nature of FIT NBs. Like FIT NBs, speckles are highly dynamic. They are
567 forming around transcriptionally active sites in the interchromatin regions recruiting
568 several protein functions like mRNA synthesis, maturation, splicing and export (Reddy et
569 al., 2012; Galganski et al., 2017). The type II speckle component SR45, for instance, was
570 shown to be a highly mobile protein in speckles and required phosphorylation for proper
571 speckle localization (Ali et al., 2003; Reddy et al., 2012). These processes fit well to the
572 described FIT NB attributes. On the other hand, speckle components are also linked with
573 epigenetic mechanisms (Mikulski et al., 2022). The characterization of FIT NBs as
574 speckles is interesting because regulation of splicing and epigenetic regulation is
575 associated with iron deficiency gene expression. Genes were spliced incorrectly in a *sr45-*
576 *1* null mutant Arabidopsis line, and gene expression of *FIT* and FIT target genes was
577 increased in *sr45-1* seedlings, showing that an interplay between SR45 and the iron
578 uptake machinery exists (Fanara et al., 2022). Alternative splicing was detected for FIT
579 targets and the *BHLH* subgroup Ib genes in iron-deficient versus iron-sufficient conditions
580 (Li et al., 2013). Hence, FIT NBs may regulate iron uptake gene expression at
581 posttranscriptional level. Notably, PININ (type III), together with ACINUS, were shown to
582 stabilize SR45 (type II) in plants (Bi et al., 2021). Further, UAP56H2, P15H1, and PININ
583 (type III) are connected to SR45 and SRm102 (type II) in mammalian cells as all being
584 part of the exon junction complex and interacting with each other (Lin et al., 2004; Pendle
585 et al., 2005). This is an interesting parallel, as it suggests that type II and type III marker

586 localization is conserved across kingdoms, underlying the ancient nature of condensates.
587 Indeed, SR45 and PININ located to a very large NB in non-induced cells. This opens the
588 possibility that the two proteins might localize to the same speckle, as also might FIT.
589 Taken together, the observations confirm the high diversification and complexity of FIT
590 NBs and speckles (Lorković et al., 2008) and it is tempting to speculate that FIT might
591 regulate splicing and alternative splicing of its target genes by recruiting speckle
592 components.

593 *FIT* is itself a direct target of FIT and the FIT-bHLH039 complex (Wang et al., 2007;
594 Naranjo-Arcos et al., 2017), and perhaps FIT NB speckles appear at the *FIT* transcription
595 site. Indeed, coupling of transcription with splicing or alternative splicing is an established
596 idea in the mammalian field, and evidence for co-transcriptional splicing in plants is also
597 recently rising (Nojima et al., 2015; Zhu et al., 2018; Chaudhary et al., 2019). Mediator
598 complex condensation was shown to drive transcriptional control (Boija et al., 2018) and
599 interestingly, FIT was also shown to interact with Mediator complexes, directly and
600 indirectly (Yang et al., 2014; Zhang et al., 2014). Besides, other studies suggest TF
601 condensation to be involved in transcriptional regulation (Kaiserli et al., 2015; Huang et
602 al., 2022). Possibly, the basic region of FIT and bHLH039 might be accessible for DNA
603 binding either within or outside of NBs to regulate target genes (Boija et al., 2018; Brodsky
604 et al., 2020). In further studies, it will be interesting to analyze whether DNA and mRNA
605 FIT targets are present inside FIT NBs and whether FIT may also interact directly with
606 other speckle components.

607 The interesting finding that blue light exposure not only caused the formation of FIT
608 NBs, that we could link with active TF complexes, but also promoted FIT-bHLH039-
609 dependent iron mobilization responses can be interpreted as follows: FIT NBs may indeed
610 serve the rapid rearrangement of TFs to enhance target gene expression and subsequent
611 physiological responses. Changes of the light spectrum over the day could serve as a cue
612 for a high photosynthetic period, such a high blue light component, and induce stronger
613 iron uptake. Due to photosynthesis, chloroplasts and photosynthetically active leaves may
614 serve as a major sink for iron. Under far-red light, which is as shade signal, and in
615 darkness, photosynthetic activity is lowered. In turn, lower amounts of iron may be
616 acquired. Regulation of FIT protein abundance occurs rather on the posttranslational level
617 than on transcriptional (Lingam et al., 2011; Meiser et al., 2011; Gratz et al., 2019, 2020).
618 On the other hand, *FIT* is itself a target of FIT-bHLH039 (Wang et al. 2007). The fact that

619 *FIT* gene expression is differently regulated from *IRT1* and *FRO2* depending on light
620 quality is intriguing. Perhaps FIT protein is readily available during the day. The formation
621 and dissociation of NBs could be a fast way to adjust iron uptake and specifically uncouple
622 *IRT1* and *FRO2* from FIT regulation and therefore adapt even better to environmental
623 changes. Reversibility of FIT condensation might rapidly switch off the process, possibly
624 by phosphorylation triggers leading to inactivation of FIT (Gratz et al., 2020). Reversibility
625 of condensates was shown in the context of light, temperature, or stresses, once the
626 stimulus was removed (Jung et al., 2020; Wang et al., 2021; Zhu et al., 2021; Chen et al.,
627 2022; Wang et al., 2022). This supports the hypothesis that plant condensates are hubs
628 for fast adaptation to external cues.

629 As we focused to characterize the phenomenon, the physiological integration and
630 regulation of the induction of FIT NB formation can be subject of future studies. The rapid
631 speed by which FIT NB appeared within 5 min in *N. benthamiana* leaf cells speaks in favor
632 of protein rearrangement rather than protein synthesis. The long duration of FIT NB
633 formation after blue light induction in Arabidopsis roots suggests that signal transduction
634 was more complex and possibly involved intracellular or even cell-to-cell and long-
635 distance leaf-to-root signaling. In how far a long-distance signal or a signaling cascade
636 triggered by light is involved in FIT NB formation in roots remains to be investigated, but
637 CRY1/CRY2 and HY5 are promising candidates for further studies, as their involvement
638 in iron deficiency response regulation has been highlighted (Gao et al., 2021; Guo et al.,
639 2021; Mankotia et al., 2023). Since Arabidopsis germinates in the light, it is well
640 conceivable that the FIT NB-forming property is part of a seedling establishment
641 procedure during early phases when roots can be exposed in the light. In order to undergo
642 phase separation, a certain protein concentration must be reached (Bracha et al., 2018).
643 Since FIT protein is subject of proteasomal turnover in roots, FIT NB formation may
644 depend on FIT protein interaction partners in roots that need to be activated (Lingam et
645 al., 2011; Meiser et al., 2011).

646 In summary, FIT localizes to dynamic and reversible NBs. FIT NBs contain active
647 TF complexes for iron acquisition gene expression and are speckles that link
648 transcriptional with post-transcriptional regulation. The appearance of FIT NBs is inducible
649 by blue light, a condition that promotes iron mobilization responses, and light regulated
650 PB components are connected with FIT NBs and vice versa (**Figure 10**). It will be
651 interesting in the future to test hormonal and environmental triggers that may stabilize FIT

652 protein prior to examining the initiation of FIT NBs in root physiological situations and to
653 investigate the effects on transcriptional and posttranscriptional regulation of FIT targets.

654 **Materials and methods**

655 **Plant material and growth conditions**

656 *Arabidopsis thaliana* experiments were conducted with the Col-0 accession.
657 Arabidopsis line FIT_{pro}:FIT-GFP used for imaging was obtained as follows: First, the
658 FIT_{pro}:FIT-GFP construct was obtained in a plant gene expression binary vector via
659 GreenGate cloning (Lampropoulos et al., 2013). *FIT* promoter sequence of 2012 bp
660 upstream of the CDS was cloned into pGGA000 entry vector using pFIT GG fw and pFIT
661 GG rv primers with respective overhang sequences (**Supplemental Table S1**). FIT CDS
662 (954 bp, without stop codon) was cloned into pGGC000 entry vector using cFIT GG fw
663 and cFIT GG rv primers with respective overhang sequences (**Supplemental Table S1**).
664 The final construct was created via the GreenGate reaction with the pGGZ001 destination
665 vector, containing the entry vectors pGGA000 FIT promoter, pGGB003 *B-dummy* for N-
666 tag, pGGA000 FIT CDS, pGGD001 *linker*-GFP, pGGE009 *UBQ10* terminator, and
667 pGGF001 $p^{d}MAS^{e}$:$BastaR^{f}$:$t^{g}MAS$, and verified by sequencing. The plasmid was
668 transferred to *Rhizobium radiobacter* pSOUP strain (GV3103). Transgenic plants (in Col-
669 0 wild-type background) were obtained by floral dip transformation (Clough and Bent,
670 1998) and subsequent Basta selection. *Arabidopsis thaliana* 2x35S_{pro}:FIT-GFP/*fit-3* line
671 used for imaging was previously described in Gratz et al. (2019).

672 *Arabidopsis thaliana* FIT_{pro}:FIT-GFP seedlings were used for localization studies.
673 Seeds were sterilized and grown upright on Hoagland medium plates (macronutrients:
674 1.5 mM $Ca(NO_3)_2 \cdot 4H_2O$, 0.5 mM KH_2PO_4, 1.25 mM KNO_3, 0.75 mM $MgSO_4 \cdot 7H_2O$;
675 micronutrients: 0.075 µM $(NH_4)6Mo_7O_{24} \cdot 4H_2O$, 1.5 µM $CuSO_4 \cdot 5H_2O$, 50 µM H_3BO_3,
676 50 µM KCl, 10 µM $MnSO_4 \cdot H_2O$, 2 µM $ZnSO_4 \cdot 7H_2O$; 1.4 % (w/v) plant agar, 1 % (w/v)
677 sucrose, pH 5.8) with no iron supply for 5 d under long day conditions (16 h light/8 h dark)
678 at 21°C in a plant chamber (CLF Plant Climatics) under white light (120 µmol m^{-2} s^{-1}).

679 For iron reductase activity assays and gene expression analysis, *Arabidopsis*
680 *thaliana* seedlings were sterilized and grown upright on Hoagland medium plates with
681 either no iron supply or with 50 µM FeNaEDTA supply for 5 d under long day conditions
682 (16 h light/8 h dark) at 21°C in a plant chamber (CLF Plant Climatics) under white light
683 (120 µmol m^{-2} s^{-1}). For different light treatments plates were transferred to LED light
684 chambers (CLF Plant Climatics) for 1 d under continuous blue light (70 µmol m^{-2} s^{-1}),
685 continuous red light (55 µmol m^{-2} s^{-1}), continuous far-red light (65 µmol m^{-2} s^{-1}) or
686 darkness. White light was used as control (125 µmol m^{-2} s^{-1}).

687 *Nicotiana benthamiana* plants were grown in the greenhouse facility for approx. 4
688 weeks under long day conditions (16 h light/8 h dark) for use in transient protein
689 expression experiments.

690 **Root iron reductase activity assay**

691 6-d-old seedlings were grown as described in the text. Root iron reductase activity
692 was determined as described in Le *et al.* (2016). Plants were washed with 0.1 M
693 $Ca(NO_3)_2 \cdot 4H_2O$ and subsequently incubated for 1 h in darkness at room temperature in
694 the iron reductase solution (300 µM Ferrozine, 100 µM FeNaEDTA). The absorbance of
695 the ferrozine-Fe^{2+} complex was measured at 562 nm and used to calculate the root iron
696 reductase activity normalized to root fresh weight.

697 **Gene expression analysis by RT-qPCR**

698 6-d-old seedlings were grown as described in the text. The reverse transcription-
699 real time-quantitative polymerase chain reaction (RT-qPCR) procedure and analysis is
700 described in Abdallah and Bauer (2016). Briefly, plant material was harvested, using three
701 biological replicates, and shock frozen. RNA was extracted (peqGOLD Plant RNA Kit,
702 PEQLAB). Subsequently, an amount of 0.5 µg of total RNA was used for cDNA synthesis
703 (Thermo Scientific). Diluted cDNA, SYBR green master mix (Thermo Scientific) and
704 respective primers (**Supplemental Table S1**) were pipetted in a 96 well plate and qPCR
705 was performed with two technical duplicates with the CFX96 Touch™ Real-Time PCR
706 Detection System (Bio-Rad). qPCR data were analyzed, and quantification was obtained
707 according to the mass standard curve analysis procedure. Normalization was performed
708 using the reference gene *ELONGATION FACTOR1A* (*EFc*). Statistical analysis was
709 performed with absolute normalized gene expression levels.

710 **Microscopy of *Arabidopsis thaliana* seedlings**

711 Protein localization studies in roots of 5-d-old seedlings of the *Arabidopsis thaliana*
712 line FIT_{pro}:FIT-GFP and $35S_{pro}$:FIT-GFP were performed with the widefield microscope
713 ELYRA PS (Zeiss) equipped with a EMCCD camera. To induce FIT NB formation, whole
714 seedlings were exposed to 488 nm laser light for several minutes. GFP was excited with
715 a 488 nm laser and detected with a BP 495-575 + LP 750 beam splitter. Images were
716 acquired with the C-Apochromat 63x/1.2 W Korr M27 (Zeiss) objective, pixel dwell time of

717 1.6 µs and frame size of 512x512. Pictures were processed with the manufacturer's
718 software ZEN lite (Zeiss).

719 **Generation of fluorescent constructs**

720 All constructs used in this study are listed in **Supplemental Table S2**. Generation
721 of fluorescent translational C-terminal fusion of PIF3 and PIF4 with mCherry was
722 performed with Gateway Cloning. CDS of *PIF3* was amplified with the PIF3 GW fw and
723 PIF3 GW rv primers (**Supplemental Table S1**), and CDS of *PIF4* was amplified with the
724 PIF4 GW fw and PIF4 GW rv primers (**Supplemental Table S1**), and introduced into the
725 entry vector pDONR207 via the BP reaction (Life Technologies) and subsequently into
726 the inducible pABind $35S_{pro}$:mCherry destination vector (Bleckmann et al., 2010) via the
727 LR reaction (Life Technologies). Finally, *Rhizobium radiobacter* was transformed with the
728 constructs for transient transformation of *Nicotiana benthamiana* leaf epidermal cells.

729 **Transient transformation of *Nicotiana benthamiana* leaf epidermal cells**

730 Transient protein expression was performed in *Nicotiana benthamiana* leaf
731 epidermal cells according to Bleckmann et al. (2010). This was performed for localization
732 studies, FRAP measurements, anisotropy (homo-FRET) measurements, FRET-FLIM
733 measurements, and NB quantification. Cultures of *Rhizobium radiobacter* containing the
734 construct of interest (**Supplemental Table S2**) were incubated overnight and cell were
735 pelleted and dissolved in AS medium (250 µM acetosyringone (in DMSO), 5 % (w/v)
736 sucrose, 0.01 % (v/v) silwet, 0.01 % (w/v) glucose). An OD_{600nm} of 0.4 was set for all
737 constructs. A *Rhizobium radiobacter* strain containing the silencing repressor p19 vector
738 (Shamloul et al., 2014) was used additionally for bHLH039-mCherry to enhance
739 expression. After 1 h incubation on ice the suspension was infiltrated with a syringe into
740 the abaxial side of the leaf. *Nicotiana benthamiana* plants were kept under long day
741 conditions (16 h light/8 h dark) in the laboratory after infiltration. Imaging was performed
742 2-3 d after infiltration. Expression of constructs with an inducible 35S promoter was
743 induced 16 h prior to imaging with β-estradiol (20 µM β-estradiol (in DMSO), 0.1 % (v/v)
744 Tween 20).

745 **Confocal microscopy**

746 For localization studies a confocal laser scanning microscope LSM780 (Zeiss) was
747 used. Imaging was controlled by the ZEN 2.3 SP1 FP3 (Black) (Zeiss) software. GFP was

748 excited with a 488 nm laser and detected in the range of 491-553 nm. mCherry and mRFP
749 were excited with a 561 nm laser and detected in the range of 562-626 nm. Fluorophore
750 crosstalk was minimized by splitting of the excitation tracks and reduction of emission
751 spectrum overlap. Images were acquired with the C-Apochromat 40x/1.20 W Korr M27
752 (Zeiss) objective, zoom factor of 8, pinhole set to 1,00 AU, pixel dwell time of 1.27 µs and
753 frame size of 1.024x1.024. Z-stacks for quantification were taken with the same settings,
754 except with pixel dwell time of 0.79 µs and frame size of 512x512. Pictures were
755 processed with the manufacturer's software ZEN lite (Zeiss).

756 **Standardized FIT NB analysis procedure**

757 Following *Nicotiana benthamiana* leaf infiltration with *Rhizobium radiobacter*, FIT-
758 GFP protein expression was induced after 2-3 d by β-estradiol, as described above. 16 h
759 later, a leaf disc was excised and FIT-GFP fluorescence signals were recorded (t=0). The
760 leaf disc was excited with 488 nm laser light for 1 min. 5 min later, FIT-GFP accumulation
761 in FIT NBs was observed (t= 5 min). See **Supplemental Figure S1**. This procedure was
762 modified by using different time points for NB analysis and different constructs
763 (**Supplemental Table S2**) and co-expression as indicated in the text. Imaging was
764 performed at the respective wavelengths for detection of GFP and mRFP/mCherry.

765 **FRAP measurements**

766 FRAP measurements (Bancaud et al., 2010; Trofimov et al., 2019) were performed
767 at the confocal laser scanning microscope LSM780 (Zeiss). Imaging was controlled by the
768 ZEN 2.3 SP1 FP3 (Black) (Zeiss) software. GFP was excited with a 488 nm laser and
769 detected in the range of 491-553 nm. Images were acquired with the C-Apochromat
770 40x/1.20 W Korr M27 (Zeiss) objective, zoom factor of 8, pinhole set to 2,43 AU, pixel
771 dwell time of 1.0 µs, frame size of 256x256, and 300 frames. After 20 frames, a NB was
772 bleached with 50 iterations and 100% 488 nm laser power. Fluorescence intensity was
773 recorded for the bleached NB (ROI), a non-bleached region equal in size to the NB (BG)
774 as well as for the total image (Tot). Values were calculated and processed in Excel
775 (Microsoft Corporation). Background subtraction and normalization to calculate the
776 relative fluorescence intensity was performed as follows: [(ROI(t)-BG(t)/Tot(T)-
777 BG(t))*(Tot(t0)-BG(t0)/ROI(t0)-BG(t0))]. The mobile fraction was calculated as follows:
778 $[(F_{end}-F_{post})/(F_{pre}-F_{post})*100]$. F_{pre} marks the average of the 20 values before bleaching,
779 F_{post} marks the value right after the bleaching, and F_{end} marks the average of the 280

780 values after the bleaching. Pictures were processed with the manufacturer's software ZEN
781 lite (Zeiss).

782 **Anisotropy (homo-FRET) measurements**

783 Anisotropy measurements (Stahl et al., 2013; Weidtkamp-Peters et al., 2022) were
784 performed at the confocal laser scanning microscope LSM780 (Zeiss) equipped with a
785 polarization beam splitter, bandpass filter (520/35), and a single-photon counting device
786 HydraHarp (PicoQuant) with avalanche photo diodes (τ-SPADs). Emission was detected
787 in parallel and perpendicular orientation. Rhodamine 110 was used to determine the G
788 factor to correct for the differential parallel and perpendicular detector sensitivity.
789 Calibration of the system was performed for every experiment and measurements were
790 conducted in darkness. Free GFP and GFP-GFP were used as references for mono- and
791 dimerization, respectively. GFP was excited with a linearly polarized pulsed (32 MHz)
792 485 nm laser and 0.05-1 µW output power. Measurements were recorded with a C-
793 Apochromat 40x/1.20 W Korr M27 (Zeiss) objective, zoom factor of 8, pixel dwell time of
794 12.5 µs, objective frame size of 256x256, and 40 frames. Measurements were controlled
795 with the manufacturer's ZEN 2.3 SP1 FP3 (Black) (Zeiss) software and SymPhoTime 64
796 (PicoQuant) software. SymPhoTime 64 (PicoQuant) software was used for analysis in the
797 respective regions of interest (whole nucleus, NB, NP) and to generate color-coded FA
798 value images. Minimal photon count was set to 200.

799 **FRET-FLIM measurements**

800 FRET-FLIM measurements (Borst and Visser, 2010; Weidtkamp-Peters and Stahl,
801 2017) were taken at the confocal laser scanning microscope FV3000 (Olympus) equipped
802 with a multi-photon counting device MultiHarp 150 (PicoQuant) with avalanche photo
803 diodes (τ-SPADs) and bandpass filter (520/35). Erythrosine B (quenched in saturated
804 potassium iodide) was used to record the Instrument Response Function to correct for the
805 time between laser pulse and detection. Calibration of the system was performed for every
806 experiment and measurements were conducted in darkness. FIT-GFP and
807 FITmSS271AA-GFP were used as negative controls (donor only), FIT-GFP or
808 FITmSS271AA-GFP (donor) and bHLH039-mCherry (acceptor) as FRET pair. GFP was
809 excited with a linearly polarized pulsed (32 MHz) 485 nm laser and 0.01-0.1 µW output
810 power. Measurements were recorded with a UPLSAPO 60XW (Olympus) objective, zoom
811 factor of 8, pixel dwell time of 12.5 µs, objective frame size of 256x256, and 60 frames.

812 Measurements were controlled with the manufacturer's FV31S-SW (Olympus) software
813 and SymPhoTime 64 (PicoQuant) software. SymPhoTime 64 (PicoQuant) software was
814 used for analysis in the respective regions of interest (whole nucleus, NB, NP) and to
815 generate color-coded fluorescence lifetime value images. Number of parameters for the
816 fit depended on the region of interest.

817 **Circularity quantification**

818 Circularity quantification was performed with the software ImageJ (National
819 Institutes of Health). Full intensity projection images were generated from Z-stacks in the
820 ZEN lite (Zeiss) software and exported as TIFF (no compression, all dimensions). Images
821 were duplicated in ImageJ and converted to RGB and 8-bit. Correct scale was set (in µm)
822 under 'Analyze' - 'Set Scale'. Threshold for the intensity limit (areas below that limit were
823 not considered for quantification) was set under 'Image' - 'Adjust' - 'Threshold' and was
824 set manually for every image. To separate the nuclear bodies better, 'Process' - 'Binary' -
825 'Watershed' was used. Parameters that should be quantified were selected under
826 'Analyze' - 'Set Measurements'. To perform the analysis, 'Analyze' - 'Analyze Particles'
827 was selected. Calculated values were further processed in Excel (Microsoft Corporation).

828 **Nuclear body quantification**

829 Nuclear body quantification was performed with the software ImageJ (National
830 Institutes of Health) and additional plugin '3D Object Counter'. Z-stacks were exported
831 from the ZEN lite (Zeiss) software as TIFF (no compression, all dimensions) first. In
832 ImageJ, Z-stacks were converted to RGB and 8-bit. Correct scale was set (in µm) under
833 'Properties'. Parameters that should be quantified were selected under 'Plugins' - '3D
834 Object Counter' - 'Set 3D Measurements'. To perform the analysis, 'Plugins' - '3D Object
835 Counter' - '3D object counter' was selected. Threshold for the intensity limit (areas below
836 that limit were not considered for quantification) was set manually for every z-stack.
837 Calculated values were further processed in Excel (Microsoft Corporation). Only size
838 between 0,01-15 μm^3 was considered.

839 **Protein domain prediction**

840 IDRs in FIT/FITmSS271AA were predicted with the tool PONDR-VLXT
841 (www.pondr.com, Molecular Kinetics, Inc.). According to the sequence of the protein, a
842 PONDR score was determined for each amino acid. A score above 0.5 indicates intrinsic

843 disorder. The bHLH domain of FIT was predicted with InterPro (www.ebi.ac.uk/interpro,
844 EMBL-EBI).

845 **Statistical analysis**

846 Line and bar diagrams represent the mean and standard deviation. Box plots show
847 25-75 percentile with min-max whiskers, mean as small square and median as line.
848 Graphs and statistical analysis were created and performed with OriginPro (OriginLab
849 Corporation). Data was tested for normal distribution with the Shapiro-Wilk test. Statistical
850 significance of data with normal distribution was tested by one-way Anova with Tukey
851 post-hoc test. Statistical significance of data with non-normal distribution was tested by
852 Mann-Whitney test. Different letters indicate statistically significant differences ($P < 0.05$).
853 Illustrations were created with BioRender.com.

854 **Accession numbers**

855 Sequence data from this article can be found in the EMBL/GenBank data libraries
856 under accession numbers*: bHLH039* (AT3G56980), *COILIN* (AT1G13030), *FIT*
857 (AT2G28160), *FRO2* (AT1G01580), *IRT1* (AT4G19690), *P15H1* (AT1G11570), *PIF3*
858 (AT1G09530), *PIF4* (AT2G43010), *PININ* (AT1G15200), *SR45* (AT1G16610), *SRm102*
859 (AT2G29210), *U2B"* (AT2G30260), *UAP56H2* (AT5G11170), and *ZAT12* (AT5G59820).

860 **Figures**

861 **Figure 1.** FIT accumulated in nuclear condensates, termed FIT nuclear bodies (NBs) in a
862 light-inducible manner, most likely following liquid-liquid phase separation (LLPS).

863 **Figure 2.** The FIT C-terminal Ser271/272 site was important for the capacity of FIT to
864 localize to NBs.

865 **Figure 3.** FIT was present in homodimeric protein complexes in NBs, dependent on
866 Ser271/272 site.

867 **Figure 4.** FIT was present in heterodimeric protein complexes with bHLH039 in NBs,
868 dependent on Ser271/272 site.

869 **Figure 5.** Two NB markers and splicing components were present in NBs (designated
870 type II), revealing the dynamics of FIT to accumulate in NBs.

871 **Figure 6.** Three NB markers and speckle components became localized in FIT NBs and
872 colocalized fully with FIT (designated type III), suggesting that FIT NBs have speckle
873 function.

874 **Figure 7.** FIT colocalized with photobody (PB) markers in distinct PBs.

875 **Figure 8.** Root iron reductase activity is promoted under blue light.

876 **Figure 9.** Induction of FIT target gene expression is enhanced under blue light.

877 **Figure 10.** Schematic summary models illustrating the dynamics of FIT NB formation,
878 suggesting that FIT NBs are related to transcriptional and posttranscriptional regulation in
879 speckles.

880 **Supplemental Data**

881 **Supplemental Figure S1.** FIT NBs induced by blue light and a standardized FIT NB
882 analysis procedure was developed to analyze the characteristics and dynamics of FIT
883 NBs. (Supports Figure 1)

884 **Supplemental Figure S2.** An intrinsically disordered region, $IDR^{Ser271/272}$, is present in the
885 FIT C-terminus and disrupted in the FITmSS271AA mutant. (Supports Figure 2, 3, and 4)

886 **Supplemental Figure S3.** FIT NBs did not colocalize with Cajal body components
887 (designated type I). (Supports Figure 5 and 6)

888 **Supplemental Figure S4.** Type II and III NB markers are similarly localized upon single
889 expression as upon co-expression with FIT, except PININ. (Supports Figure 5 and 6)

890 **Supplemental Figure S5.** PB markers are similarly localized upon single expression and
891 upon co-expression with FIT. (Supports Figure 7)

892 **Supplemental Table S1.** List of primers used in this study.

893 **Supplemental Table S2.** List of vectors used in this study.

894 **Supplemental Movie S1.** Light induction triggers the formation of NBs with FIT and
895 FITmSS271AA with different dynamics. (Supports Figure 1 and 2)

896 **Acknowledgements**

897 We thank Elke Wieneke and Monique Eutebach (Institute of Botany, Heinrich-
898 Heine-University, Düsseldorf, Germany) for excellent technical assistance. We
899 acknowledge the contribution of the student Daniel Torno. We thank Rebecca C. Burkart
900 (Institute of Developmental Genetics, Heinrich-Heine-University, Düsseldorf, Germany),
901 Sebastian Hänsch and Stefanie Weidtkamp-Peters (Center for Advanced Imaging,
902 Heinrich-Heine-University, Düsseldorf, Germany) for help and advice with microscopy and
903 data analysis. K.T. is an associate member of the DFG-funded International Graduate
904 School for Plant Science iGRAD*plant* (IRTG 2466 "Network, exchange, and training
905 program to understand plant resource allocation"), Düsseldorf, Germany.

906 **Funding**

907 This work was funded by Deutsche Forschungsgemeinschaft (DFG, German
908 Research Foundation) under GRK F020512056 (NEXT*plant*), SFB 1208 project B05, and
909 Germany´s Excellence Strategy – EXC-2048/1 – project ID 390686111. Funding for
910 instrumentation: Zeiss ELYRA PS: DFG- INST 208/613-1 FUGG; Zeiss LSM780 + 4-
911 channel FLIM extension (Picoquant): DFG- INST 208/551-1 FUGG; Olympus FV3000
912 Confocal Laser Scanning Microscope with 4-channel FLIM extension (PicoQuant
913 rapidFLIM): DFG- INST 1358/44-1 FUGB.

914 K.T., R.I., Y.S., P.B. and T.B. designed the research; K.T. performed research;
915 K.T., R.I., Y.S., and T.B. analyzed data; R.G. contributed key materials; K.T. wrote the
916 paper; P.B. acquired funding; all authors reviewed and edited the article.

References

Abdallah, H. Ben and Bauer, P. (2016). Quantitative reverse transcription-qPCR-based gene expression analysis in plants. Methods Mol. Biol. **479**: 9–24.

Ali, G.S., Golovkin, M., and Reddy, A.S.N. (2003). Nuclear localization and in vivo dynamics of a plant-specific serine/arginine-rich protein. Plant J. **36**: 883–893.

Bancaud, A., Huet, S., Rabut, G., and Ellenberg, J. (2010). Fluorescence Perturbation Techniques to Study Mobility and Molecular Dynamics of Proteins in Live Cells: FRAP, Photoactivation, Photoconversion, and FLIP. Cold Spring Harb. Protoc.: 1303–1325.

Bauer, D., Viczían, A., Kircher, S., Nobis, T., Nitschke, R., Kunkel, T., Panigrahi, K.C.S., Ádám, É., Fejes, E., Schäfer, E., and Nagy, F. (2004). Constitutive Photomorphogenesis 1 and Multiple Photoreceptors Control Degradation of Phytochrome Interacting Factor 3, a Transcription Factor Required for Light Signaling in Arabidopsis. Plant Cell **16**: 1433–1445.

Bauer, P., Ling, H.Q., and Guerinot, M. Lou (2007). FIT, the FER-LIKE IRON DEFICIENCY INDUCED TRANSCRIPTION FACTOR in Arabidopsis. Plant Physiol. Biochem. **45**: 260–261.

Bi, Y. et al. (2021). Arabidopsis ACINUS is O-glycosylated and regulates transcription and alternative splicing of regulators of reproductive transitions. Nat. Commun. **12**: 1–13.

Bleckmann, A., Weidtkamp-Peters, S., Seidel, C.A.M., and Simon, R. (2010). Stem Cell Signaling in Arabidopsis Requires CRN to Localize CLV2 to the Plasma Membrane. Plant Physiol. **152**: 166–176.

Boija, A. et al. (2018). Transcription Factors Activate Genes through the Phase-Separation Capacity of Their Activation Domains. Cell **175**: 1842–1855.

Borst, J.W. and Visser, A.J.W.G. (2010). Fluorescence lifetime imaging microscopy in life sciences. Meas. Sci. Technol. **21**: 1–21.

Bracha, D., Walls, M.T., Wei, M.T., Zhu, L., Kurian, M., Avalos, J.L., Toettcher, J.E., and Brangwynne, C.P. (2018). Mapping Local and Global Liquid Phase Behavior in Living Cells Using Photo-Oligomerizable Seeds. Cell **175**: 1467–1480.

Brumbarova, T. and Ivanov, R. (2019). The Nutrient Response Transcriptional Regulome of Arabidopsis. iScience **19**: 358–368.

Burkart, R.C., Strotmann, V.I., Kirschner, G.K., Akinci, A., Czempik, L., Dolata, A.,

950 **Maizel, A., Weidtkamp-Peters, S., and Stahl, Y.** (2022). PLETHORA-WOX5
951 interaction and subnuclear localization control Arabidopsis root stem cell
952 maintenance. EMBO Rep. **23**: 1–18.
953 **Van Buskirk, E.K., Reddy, A.K., Nagatani, A., and Chen, M.** (2014). Photobody
954 Localization of Phytochrome B Is Tightly Correlated with Prolonged and Light-
955 Dependent Inhibition of Hypocotyl Elongation in the Dark. Plant Physiol. **165**: 595–
956 607.
957 **Chen, D., Lyu, M., Kou, X., Li, J., Yang, Z., Gao, L., Li, Y., Fan, L., Shi, H., and**
958 **Zhong, S.** (2022). Integration of light and temperature sensing by liquid-liquid
959 phase separation of phytochrome B. Mol. Cell **82**: 1–15.
960 **Clough, S.J. and Bent, A.F.** (1998). Floral dip: a simplified method for Agrobacterium-
961 mediated transformation of Arabidopsis thaliana. Plant J. **16**: 735–743.
962 **Colangelo, E.P. and Guerinot, M. Lou** (2004). The Essential Basic Helix-Loop-Helix
963 Protein FIT1 Is Required for the Iron Deficiency Response. Plant Cell **16**: 3400–
964 3412.
965 **Collier, S., Pendle, A., Boudonck, K., van Rij, T., Dolan, L., and Shaw, P.** (2006). A
966 Distant Coilin Homologue Is Required for the Formation of Cajal Bodies in
967 Arabidopsis. Mol. Biol. Cell **17**: 2942–2951.
968 **Cui, Y., Chen, C.L., Cui, M., Zhou, W.J., Wu, H.L., and Ling, H.Q.** (2018). Four IVa
969 bHLH Transcription Factors Are Novel Interactors of FIT and Mediate JA Inhibition
970 of Iron Uptake in Arabidopsis. Mol. Plant **11**: 1166–1183.
971 **Eide, D., Broderius, M., Fett, J., and Guerinot, M. Lou** (1996). A novel iron-regulated
972 metal transporter from plants identified by functional expression in yeast. Proc. Natl.
973 Acad. Sci. **93**: 5624–5628.
974 **Emenecker, R.J., Holehouse, A.S., and Strader, L.C.** (2020). Emerging Roles for
975 Phase Separation in Plants. Dev. Cell **55**: 69–83.
976 **Emenecker, R.J., Holehouse, A.S., and Strader, L.C.** (2021). Sequence determinants
977 of in cell condensate morphology, dynamics, and oligomerization as measured by
978 number and brightness analysis. Cell Commun. Signal. **19**: 1–15.
979 **Fanara, S., Schloesser, M., Hanikenne, M., and Motte, P.** (2022). Altered metal
980 distribution in the sr45-1 Arabidopsis mutant causes developmental defects. Plant J.
981 **110**: 1332–1352.
982 **Fang, X., Wang, L., Ishikawa, R., Li, Y., Fiedler, M., Liu, F., Calder, G., Rowan, B.,**

983 **Weigel, D., Li, P., and Dean, C.** (2019). Arabidopsis FLL2 promotes liquid–liquid
984 phase separation of polyadenylation complexes. Nature **569**: 265–269.
985 **Galganski, L., Urbanek, M.O., and Krzyzosiak, W.J.** (2017). Nuclear speckles:
986 Molecular organization, biological function and role in disease. Nucleic Acids Res.
987 **45**: 10350–10368.
988 **Gao, F., Robe, K., Bettembourg, M., Navarro, N., Rofidal, V., Santoni, V., Gaymard,**
989 **F., Vignols, F., Roschzttardtz, H., Izquierdo, E., and Dubos, C.** (2020). The
990 Transcription Factor bHLH121 Interacts with bHLH105 (ILR3) and Its Closest
991 Homologs to Regulate Iron Homeostasis in Arabidopsis. Plant Cell **32**: 508–524.
992 **Gao, Y.-Q., Bu, L.-H., Han, M.-L., Wang, Y.-L., Li, Z.-Y., Liu, H.-T., and Chao, D.-Y.**
993 (2021). Long-distance blue light signalling regulates phosphate deficiency-induced
994 primary root growth inhibition. Mol. Plant **14**: 1–15.
995 **Gratz, R. et al.** (2019). CIPK11-Dependent Phosphorylation Modulates FIT Activity to
996 Promote Arabidopsis Iron Acquisition in Response to Calcium Signaling. Dev. Cell
997 **48**: 726–740.
998 **Gratz, R., Brumbarova, T., Ivanov, R., Trofimov, K., Tünnermann, L., Ochoa-**
999 **Fernandez, R., Blomeier, T., Meiser, J., Weidtkamp-Peters, S., Zurbriggen, M.,**
1000 **and Bauer, P.** (2020). Phospho-mutant activity assays provide evidence for
1001 alternative phospho-regulation pathways of the transcription factor FER-LIKE IRON
1002 DEFICIENCY-INDUCED TRANSCRIPTION FACTOR. New Phytol. **225**: 250–267.
1003 **Guo, Z., Xu, J., Wang, Y., Hu, C., Shi, K., Zhou, J., Xia, X., Zhou, Y., Foyer, C.H., and**
1004 **Yu, J.** (2021). The phyB-dependent induction of HY5 promotes iron uptake by
1005 systemically activating FER expression. EMBO Rep. **22**: 1–15.
1006 **Huang, X., Xiao, N., Zou, Y., Xie, Y., Tang, L., Zhang, Y., Yu, Y., Li, Y., and Xu, C.**
1007 (2022). Heterotypic transcriptional condensates formed by prion-like paralogous
1008 proteins canalize flowering transition in tomato. Genome Biol. **23**: 1–21.
1009 **Jakoby, M., Wang, H.Y., Reidt, W., Weisshaar, B., and Bauer, P.** (2004). FRU
1010 (BHLH029) is required for induction of iron mobilization genes in Arabidopsis
1011 thaliana. FEBS Lett. **577**: 528–534.
1012 **Jung, J.-H. et al.** (2020). A prion-like domain in ELF3 functions as a thermosensor in
1013 Arabidopsis. Nature **585**: 256–260.
1014 **Kaiserli, E., Páldi, K., O'Donnell, L., Batalov, O., Pedmale, U. V., Nusinow, D.A.,**
1015 **Kay, S.A., and Chory, J.** (2015). Integration of Light and Photoperiodic Signaling in

1016 Transcriptional Nuclear Foci. Dev. Cell **35**: 311–321.
1017 **Kalinina, N.O., Makarova, S., Makhotenko, A., Love, A.J., and Taliansky, M.** (2018).
1018 The Multiple Functions of the Nucleolus in Plant Development, Disease and Stress
1019 Responses. Front. Plant Sci. **9**: 1–19.
1020 **Kammel, C., Thomaier, M., Sørensen, B.B., Schubert, T., Längst, G., Grasser, M.,**
1021 **and Grasser, K.D.** (2013). Arabidopsis DEAD-Box RNA Helicase UAP56 Interacts
1022 with Both RNA and DNA as well as with mRNA Export Factors. PLoS One **8**: 1–12.
1023 **Kanwar, P., Baby, D., and Bauer, P.** (2021). Interconnection of iron and osmotic stress
1024 signalling in plants: is FIT a regulatory hub to cross-connect abscisic acid
1025 responses? Plant Biol. **23**: 31–38.
1026 **Kim, D.W., Jeon, S.J., Hwang, S.M., Hong, J.C., and Bahk, J.D.** (2016). The C3H-
1027 type zinc finger protein GDS1/C3H42 is a nuclear-speckle-localized protein that is
1028 essential for normal growth and development in Arabidopsis. Plant Sci. **250**: 141–
1029 153.
1030 **Kim, S.A., Lacroix, I.S., Gerber, S.A., and Guerinot, M. Lou** (2019). The iron
1031 deficiency response in Arabidopsis thaliana requires the phosphorylated
1032 transcription factor URI. Proc. Natl. Acad. Sci. **116**: 24933–24942.
1033 **Kircher, S., Gil, P., Kozma-Bognár, L., Fejes, E., Speth, V., Husselstein-Muller, T.,**
1034 **Bauer, D., Ádám, É., Schäfer, E., and Nagy, F.** (2002). Nucleocytoplasmic
1035 Partitioning of the Plant Photoreceptors Phytochrome A, B, C, D, and E Is
1036 Regulated Differentially by Light and Exhibits a Diurnal Rhythm. Plant Cell **14**:
1037 1541–1555.
1038 **Korshunova, Y.O., Eide, D., Clark, W.G., Guerinot, M. Lou, and Himadri, B.** (1999).
1039 The IRT1 protein from Arabidopsis thaliana is a metal transporter with a broad
1040 substrate range. Plant Mol. Biol. **40**: 37–44.
1041 **Lafontaine, D.L.J., Riback, J.A., Bascetin, R., and Brangwynne, C.P.** (2021). The
1042 nucleolus as a multiphase liquid condensate. Nat. Rev. Mol. Cell Biol. **22**: 165–182.
1043 **Lampropoulos, A., Sutikovic, Z., Wenzl, C., Maegele, I., Lohmann, J.U., and Forner,**
1044 **J.** (2013). GreenGate - A Novel, Versatile, and Efficient Cloning System for Plant
1045 Transgenesis. PLoS One **8**: 1–15.
1046 **Le, C.T.T., Brumbarova, T., Ivanov, R., Stoof, C., Weber, E., Mohrbacher, J., Fink-**
1047 **Straube, C., and Bauer, P.** (2016). ZINC FINGER OF ARABIDOPSIS
1048 THALIANA12 (ZAT12) Interacts with FER-LIKE IRON DEFICIENCY-INDUCED

1049 TRANSCRIPTION FACTOR (FIT) Linking Iron Deficiency and Oxidative Stress
1050 Responses. Plant Physiol. **170**: 540–557.
1051 **Leivar, P. and Monte, E.** (2014). PIFs: Systems Integrators in Plant Development. Plant
1052 Cell **26**: 56–78.
1053 **Leonelli, L., Erickson, E., Lyska, D., and Niyogi, K.K.** (2016). Transient expression in
1054 Nicotiana benthamiana for rapid functional analysis of genes involved in non-
1055 photochemical quenching and carotenoid biosynthesis. Plant J. **88**: 375–386.
1056 **Li, W., Lin, W.-D., Ray, P., Lan, P., and Schmidt, W.** (2013). Genome-Wide Detection
1057 of Condition-Sensitive Alternative Splicing in Arabidopsis Roots. Plant Physiol. **162**:
1058 1750–1763.
1059 **Li, X., Zhang, H., Ai, Q., Liang, G., and Yu, D.** (2016). Two bHLH Transcription
1060 Factors, bHLH34 and bHLH104, Regulate Iron Homeostasis in Arabidopsis
1061 thaliana. Plant Physiol. **170**: 2478–2493.
1062 **Liang, G., Zhang, H., Li, X., Ai, Q., and Yu, D.** (2017). bHLH transcription factor
1063 bHLH115 regulates iron homeostasis in Arabidopsis thaliana. J. Exp. Bot. **68**:
1064 1743–1755.
1065 **Lin, C.L., Leu, S., Lu, M.C., and Ouyang, P.** (2004). Over-expression of SR-cyclophilin,
1066 an interaction partner of nuclear pinin, releases SR family splicing factors from
1067 nuclear speckles. Biochem. Biophys. Res. Commun. **321**: 638–647.
1068 **Lingam, S., Mohrbacher, J., Brumbarova, T., Potuschak, T., Fink-Straube, C.,**
1069 **Blondet, E., Genschik, P., and Bauer, P.** (2011). Interaction between the bHLH
1070 Transcription Factor FIT and ETHYLENE INSENSITIVE3/ETHYLENE
1071 INSENSITIVE3-LIKE1 Reveals Molecular Linkage between the Regulation of Iron
1072 Acquisition and Ethylene Signaling in Arabidopsis. Plant Cell **23**: 1815–1829.
1073 **Lorković, Z.J., Hilscher, J., and Barta, A.** (2008). Co-localisation studies of
1074 Arabidopsis SR splicing factors reveal different types of speckles in plant cell nuclei.
1075 Exp. Cell Res. **314**: 3175–3186.
1076 **Lorković, Z.J., Hilscher, J., and Barta, A.** (2004). Use of Fluorescent Protein Tags to
1077 Study Nuclear Organization of the Spliceosomal Machinery in Transiently
1078 Transformed Living Plant Cells. Mol. Biol. Cell **15**: 3233–3243.
1079 **Love, A.J., Yu, C., Petukhova, N. V., Kalinina, N.O., Chen, J., and Taliansky, M.E.**
1080 (2017). Cajal bodies and their role in plant stress and disease responses. RNA Biol.
1081 **14**: 779–790.

1082 **Mankotia, S., Singh, D., Monika, K., Kalra, M., Meena, H., Meena, V., Yadav, R.K.,**
1083 **Pandey, A.K., and Satbhai, S.B.** (2023). ELONGATED HYPOCOTYL 5 regulates
1084 BRUTUS and affects iron acquisition and homeostasis in Arabidopsis thaliana.
1085 Plant J.: 1–18.
1086 **Martin, K., Kopperud, K., Chakrabarty, R., Banerjee, R., Brooks, R., and Goodin,**
1087 **M.M.** (2009). Transient expression in Nicotiana benthamiana fluorescent marker
1088 lines provides enhanced definition of protein localization, movement and
1089 interactions in planta. Plant J. **59**: 150–162.
1090 **Meiser, J., Lingam, S., and Bauer, P.** (2011). Posttranslational Regulation of the Iron
1091 Deficiency Basic Helix-Loop-Helix Transcription Factor FIT Is Affected by Iron and
1092 Nitric Oxide. Plant Physiol. **157**: 2154–2166.
1093 **Meyer, H.M.** (2020). In search of function: nuclear bodies and their possible roles as
1094 plant environmental sensors. Curr. Opin. Plant Biol. **58**: 33–40.
1095 **Mikulski, P., Wolff, P., Lu, T., Nielsen, M., Echevarria, E.F., Zhu, D., Questa, J.I.,**
1096 **Saalbach, G., Martins, C., and Dean, C.** (2022). VAL1 acts as an assembly
1097 platform co-ordinating co-transcriptional repression and chromatin regulation at
1098 Arabidopsis FLC. Nat. Commun. **13**: 1–12.
1099 **Naranjo-Arcos, M.A., Maurer, F., Meiser, J., Pateyron, S., Fink-Straube, C., and**
1100 **Bauer, P.** (2017). Dissection of iron signaling and iron accumulation by
1101 overexpression of subgroup Ib bHLH039 protein. Sci. Rep. **7**: 1–12.
1102 **Ni, M., Tepperman, J.M., and Quail, P.H.** (1998). PIF3, a Phytochrome-Interacting
1103 Factor Necessary for Normal Photoinduced Signal Transduction, Is a Novel Basic
1104 Helix-Loop-Helix Protein. Cell **95**: 657–667.
1105 **Oh, E., Kim, J., Park, E., Kim, J.-I., Kang, C., and Choi, G.** (2004). PIL5, a
1106 Phytochrome-Interacting Basic Helix-Loop-Helix Protein, Is a Key Negative
1107 Regulator of Seed Germination in Arabidopsis thaliana. Plant Cell **16**: 3045–3058.
1108 **Owen, I. and Shewmaker, F.** (2019). The Role of Post-Translational Modifications in
1109 the Phase Transitions of Intrinsically Disordered Proteins. Int. J. Mol. Sci. **20**: 1–14.
1110 **Pardi, S.A. and Nusinow, D.A.** (2021). Out of the Dark and Into the Light: A New View
1111 of Phytochrome Photobodies. Front. Plant Sci. **12**: 1–15.
1112 **Pedmale, U. V., Huang, S.-S.C., Zander, M., Cole, B.J., Hetzel, J., Ljung, K., Reis,**
1113 **P.A.B., Sridevi, P., Nito, K., Nery, J.R., Ecker, J.R., and Chory, J.** (2016).
1114 Cryptochromes Interact Directly with PIFs to Control Plant Growth in Limiting Blue

1115 Light. Cell **164**: 233–245.
1116 **Pendle, A.F., Cark, G.P., Boon, R., Lewandowska, D., Lam, Y.W., Andersen, J.,**
1117 **Mann, M., Lamond, A.I., Brown, J.W.S., and Shaw, P.J.** (2005). Proteomic
1118 Analysis of the Arabidopsis Nucleolus Suggests Novel Nucleolar Functions. Mol.
1119 Biol. Cell **16**: 260–269.
1120 **Pham, V.N., Kathare, P.K., and Huq, E.** (2018). Phytochromes and Phytochrome
1121 Interacting Factors. Plant Physiol. **176**: 1025–1038.
1122 **Powers, S.K. et al.** (2019). Nucleo-cytoplasmic Partitioning of ARF Proteins Controls
1123 Auxin Responses in Arabidopsis thaliana. Mol. Cell **76**: 177–190.
1124 **Qiu, Y., Li, M., Kim, R.J.A., Moore, C.M., and Chen, M.** (2019). Daytime temperature is
1125 sensed by phytochrome B in Arabidopsis through a transcriptional activator
1126 HEMERA. Nat. Commun. **10**: 1–13.
1127 **Qiu, Y., Pasoreck, E.K., Yoo, C.Y., He, J., Wang, H., Bajracharya, A., Li, M., Larsen,**
1128 **H.D., Cheung, S., and Chen, M.** (2021). RCB initiates Arabidopsis
1129 thermomorphogenesis by stabilizing the thermoregulator PIF4 in the daytime. Nat.
1130 Commun. **12**: 1–13.
1131 **Reddy, A.S.N., Day, I.S., Gohring, J., and Barta, A.** (2012). Localization and Dynamics
1132 of Nuclear Speckles in Plants. Plant Physiol. **158**: 67–77.
1133 **Riback, J.A., Zhu, L., Ferrolino, M.C., Tolbert, M., Mitrea, D.M., Sanders, D.W., Wei,**
1134 **M.-T., Kriwacki, R.W., and Brangwynne, C.P.** (2020). Composition-dependent
1135 thermodynamics of intracellular phase separation. Nature **581**: 209–214.
1136 **Robinson, N.J., Procter, C.M., Connolly, E.L., and Guerinot, M. Lou** (1999). A ferric-
1137 chelate reductase for iron uptake from soils. Nature **397**: 694–697.
1138 **Römheld, V. and Marschner, H.** (1986). Mobilization of iron in the rhizosphere of
1139 different plant species. Adv. Plant Nutr. **2**: 155–204.
1140 **Salladini, E., Jørgensen, M.L.M., Theisen, F.F., and Skriver, K.** (2020). Intrinsic
1141 Disorder in Plant Transcription Factor Systems: Functional Implications. Int. J. Mol.
1142 Sci. **21**: 1–35.
1143 **Salomé, P.A., Oliva, M., Weigel, D., and Krämer, U.** (2013). Circadian clock
1144 adjustment to plant iron status depends on chloroplast and phytochrome function.
1145 EMBO J. **32**: 511–523.
1146 **Santi, S. and Schmidt, W.** (2009). Dissecting iron deficiency-induced proton extrusion
1147 in Arabidopsis roots. New Phytol. **183**: 1072–1084.

1148 **Schwarz, B. and Bauer, P.** (2020). FIT, a regulatory hub for iron deficiency and stress
1149 signaling in roots, and FIT-dependent and -independent gene signatures. J. Exp.
1150 Bot. **71**: 1694–1705.
1151 **Shamloul, M., Trusa, J., Mett, V., and Yusibov, V.** (2014). Optimization and Utilization
1152 of Agrobacterium-mediated Transient Protein Production in Nicotiana. J. Vis. Exp.
1153 **86**: 1–13.
1154 **Shin, Y., Berry, J., Pannucci, N., Haataja, M.P., Toettcher, J.E., and Brangwynne,**
1155 **C.P.** (2017). Spatiotemporal Control of Intracellular Phase Transitions Using Light-
1156 Activated optoDroplets. Cell **168**: 159–171.
1157 **Stahl, Y. et al.** (2013). Moderation of Arabidopsis root Stemness by CLAVATA1 and
1158 ARABIDOPSIS CRINKLY4 Receptor Kinase Complexes. Curr. Biol. **23**: 362–371.
1159 **Strader, L., Weijers, D., and Wagner, D.** (2022). Plant transcription factors - being in
1160 the right place with the right company. Curr. Opin. Plant Biol. **65**: 1–8.
1161 **Tarczewska, A. and Greb-Markiewicz, B.** (2019). The Significance of the Intrinsically
1162 Disordered Regions for the Functions of the bHLH Transcription Factors. Int. J. Mol.
1163 Sci. **20**: 1–20.
1164 **Trinkle-Mulcahy, L. and Sleeman, J.E.** (2017). The Cajal body and the nucleolus: “In a
1165 relationship” or “It’s complicated”? RNA Biol. **14**: 739–751.
1166 **Trofimov, K., Ivanov, R., Eutebach, M., Acaroglu, B., Mohr, I., Bauer, P., and**
1167 **Brumbarova, T.** (2019). Mobility and localization of the iron deficiency-induced
1168 transcription factor bHLH039 change in the presence of FIT. Plant Direct **3**: 1–11.
1169 **Vert, G.A., Briat, J.F., and Curie, C.** (2003). Dual Regulation of the Arabidopsis High-
1170 Affinity Root Iron Uptake System by Local and Long-Distance Signals. Plant
1171 Physiol. **132**: 796–804.
1172 **Wang, B., Zhang, H., Huai, J., Peng, F., Wu, J., Lin, R., and Fang, X.** (2022).
1173 Condensation of SEUSS promotes hyperosmotic stress tolerance in Arabidopsis.
1174 Nat. Chem. Biol. **18**: 1361–1369.
1175 **Wang, H.Y., Klatte, M., Jakoby, M., Bäumlein, H., Weisshaar, B., and Bauer, P.**
1176 (2007). Iron deficiency-mediated stress regulation of four subgroup Ib BHLH genes
1177 in Arabidopsis thaliana. Planta **226**: 897–908.
1178 **Wang, N., Cui, Y., Liu, Y., Fan, H., Du, J., Huang, Z., Yuan, Y., Wu, H., and Ling,**
1179 **H.Q.** (2013). Requirement and Functional Redundancy of Ib Subgroup bHLH
1180 Proteins for Iron Deficiency Responses and Uptake in Arabidopsis thaliana. Mol.

1181 Plant **6**: 503–513.
1182 **Wang, X., Jiang, B., Gu, L., Chen, Y., Mora, M., Zhu, M., Noory, E., Wang, Q., and**
1183 **Lin, C.** (2021). A photoregulatory mechanism of the circadian clock in Arabidopsis.
1184 Nat. Plants **7**: 1397–1408.
1185 **Wedepohl, K.H.** (1995). The composition of the continental crust. Geochim.
1186 Cosmochim. Acta **59**: 1217–1232.
1187 **Weidtkamp-Peters, S., Rehwald, S., and Stahl, Y.** (2022). Homo-FRET Imaging to
1188 Study Protein–Protein Interaction and Complex Formation in Plants. In Plant
1189 Synthetic Biology: Methods and Protocols, M.D. Zurbriggen, ed (Springer US: New
1190 York, NY), pp. 197–208.
1191 **Weidtkamp-Peters, S. and Stahl, Y.** (2017). The Use of FRET/FLIM to Study Proteins
1192 Interacting with Plant Receptor Kinases. In Plant Receptor Kinases: Methods and
1193 Protocols, R.B. Aalen, ed (Springer New York: New York, NY), pp. 163–175.
1194 **Wild, M., Davière, J.M., Regnault, T., Sakvarelidze-Achard, L., Carrera, E., Lopez**
1195 **Diaz, I., Cayrel, A., Dubeaux, G., Vert, G., and Achard, P.** (2016). Tissue-Specific
1196 Regulation of Gibberellin Signaling Fine-Tunes Arabidopsis Iron-Deficiency
1197 Responses. Dev. Cell **37**: 190–200.
1198 **Yang, Y., Ou, B., Zhang, J., Si, W., Gu, H., Qin, G., and Qu, L.-J.** (2014). The
1199 Arabidopsis Mediator subunit MED16 regulates iron homeostasis by associating
1200 with EIN3/EIL1 through subunit MED25. Plant J. **77**: 838–851.
1201 **Yi, Y. and Guerinot, M. Lou** (1996). Genetic evidence that induction of root Fe(III)
1202 chelate reductase activity is necessary for iron uptake under iron deficiency. Plant J.
1203 **10**: 835–844.
1204 **Yuan, Y., Wu, H., Wang, N., Li, J., Zhao, W., Du, J., Wang, D., and Ling, H.Q.** (2008).
1205 FIT interacts with AtbHLH38 and AtbHLH39 in regulating iron uptake gene
1206 expression for iron homeostasis in Arabidopsis. Cell Res. **18**: 385–397.
1207 **Yuan, Y.X., Zhang, J., Wang, D.W., and Ling, H.Q.** (2005). AtbHLH29 of Arabidopsis
1208 thaliana is a functional ortholog of tomato FER involved in controlling iron
1209 acquisition in strategy I plants. Cell Res. **15**: 613–621.
1210 **Zhang, J., Liu, B., Li, M., Feng, D., Jin, H., Wang, P., Liu, J., Xiong, F., Wang, J., and**
1211 **Wang, H.** (2015). The bHLH Transcription Factor bHLH104 Interacts with IAA-
1212 LEUCINE RESISTANT3 and Modulates Iron Homeostasis in Arabidopsis. Plant Cell
1213 **27**: 787–805.

1214 **Zhang, Y., Wu, H., Wang, N., Fan, H., Chen, C., Cui, Y., Liu, H., and Ling, H.-Q.**
1215 (2014). Mediator subunit 16 functions in the regulation of iron uptake gene
1216 expression in Arabidopsis. New Phytol. **203**: 770–783.
1217 **Zhu, P., Lister, C., and Dean, C.** (2021). Cold-induced Arabidopsis FRIGIDA nuclear
1218 condensates for FLC repression. Nature **599**: 657–661.
1219
1220
1221 **Figures and figure legends**
1222

1223 **Figure 1: FIT accumulated in nuclear condensates, termed FIT nuclear bodies (NBs)**
1224 **in a light-inducible manner, most likely following liquid-liquid phase separation**
1225 **(LLPS).**

1226 A, Induction of FIT NBs in Arabidopsis root epidermis cells of the root differentiation
1227 zone. Left, light microscopy overview image of a 5-d-old Arabidopsis seedling (proFIT:FIT-
1228 GFP) grown under iron deficiency. Right, nuclear localization of FIT-GFP in the root
1229 epidermis cells as indicated in the overview image, at t=0, t=90, and t=120 min. FIT-GFP
1230 signals were evenly distributed in the nucleus at t=0 min, and after induction by excitation
1231 with 488 nm laser NB formation accumulated in NBs at t=90 min, then disappeared as
1232 shown at t=120 min. Note that root epidermis cells developed few NBs, sometimes taking
1233 up to two hours to appear. Three independent experiments with three plants were
1234 conducted. In the indicated region of interest, approximately a quarter of the root
1235 epidermis cells showed NBs. A representative image from one nucleus is shown. B-D,
1236 Fluorescence protein analysis in transiently transformed *N. benthamiana* leaf epidermis
1237 cells. Confocal images of B, FIT-GFP, C, FIT-mCherry, and D, ZAT12-GFP at t=0 and
1238 t=5 min. At t=0 min, FIT-GFP and FIT-mCherry showed an even distribution within the
1239 nucleus. Following a 488 nm laser excitation, numerous NBs were clearly visible in all
1240 examined transformed cells at t=5 min. These NBs were termed FIT NBs. Under the same
1241 imaging conditions, ZAT12-GFP did not show NB formation. According to these results, a
1242 standardized FIT NB analysis procedure was set up (**Supplemental Figure S1B**). See
1243 also **Supplemental Movie S1A-C**. Representative images from two to three independent
1244 experiments. E-G, FRAP measurements to test for liquid-like behavior of FIT NBs, using
1245 the standardized FIT NB analysis procedure in transiently transformed *N. benthamiana*
1246 leaf epidermis cells. E, Representative images of the fluorescent signal during a FRAP
1247 experiment, taken before bleaching (0 s) and recovery of fluorescence at three time points
1248 after bleaching from 3 s to 45 s within the circled region of a NB. F, Line diagram
1249 representing the relative fluorescence during a FRAP measurement for 10 NBs, showing
1250 a high fluorescence recovery rate of FIT-GFP within NBs. Dark green line, mean value;
1251 light green filled area, variation. G, Box plot diagram representing the mobile fraction of
1252 FIT-GFP calculated based on the relative fluorescence recovery in F. The diagram
1253 indicates high mobility of FIT. The mean was calculated from 10 NBs from 10 nuclei from
1254 a transformed plant. Three independent experiments were conducted, one representative
1255 result is shown. H, Box plot diagram representing quantification of the FIT NB shape with

1256 the software ImageJ (National Institutes of Health), indicating that FIT NBs have circular
1257 shape. Mobility and circularity characteristics indicate that FIT NBs are most likely liquid
1258 condensates that are the result of LLPS. The mean was calculated from all NBs visible in
1259 15 nuclei from a transformed plant. Two independent experiments were conducted, one
1260 representative result is shown.

1261 Box plots show 25-75 percentile with min-max whiskers, mean as small square and
1262 median as line. Scale bars of nuclei images, 2 µm; scale bar full seedling, 1 mm.
1263 Arrowheads indicate NBs. G = GFP; C = mCherry.

1264 **Figure 2: The FIT C-terminal Ser271/272 site was important for the capacity of FIT**
1265 **to localize to NBs.**

1266 A, Confocal images of nuclear localization of FITmSS271AA-GFP at t=0 and
1267 t=15 min. FITmSS271AA-GFP accumulated in NBs, but NB formation required a longer
1268 time compared to FIT-GFP. See also **Supplemental Movie S1, A and C**. Two
1269 independent experiments. Representative images from one nucleus. B, Bar diagrams
1270 showing in B, number of NBs, and in C, the sizes of NBs with FIT-GFP and
1271 FITmSS271AA-GFP at t=5/15 min. NB number and size were determined with the
1272 software ImageJ (National Institute of Health). FIT-GFP accumulated in more and larger
1273 NBs than FITmSS271AA-GFP. See **Supplemental Movie S1, A and C**. FITmSS271AA-
1274 GFP lacks $IDR^{Ser271/272}$. This IDR may be relevant for FIT NB formation (**Supplemental**
1275 **Figure S2**). In B and C, bar diagrams represent the mean and standard deviation for a
1276 quantification of 15 nuclei from a transformed plant (n = 15). Two experiments were
1277 conducted, one representative result is shown.

1278 Statistical analysis was performed with the Mann-Whitney test. Different letters
1279 indicate statistically significant differences ($P < 0.05$). Scale bar: 2 µm. Arrowheads
1280 indicate NBs. G = GFP. Analysis was conducted in transiently transformed
1281 *N. benthamiana* leaf epidermis cells, following the standardized FIT NB analysis
1282 procedure.

1283 **Figure 3: FIT was present in homodimeric protein complexes in NBs, dependent on**
1284 **Ser271/272 site.**

1285 Anisotropy (or homo-FRET) measurements of FIT-GFP and FITmSS271AA-GFP
1286 to determine homodimerization strength. A, Schematic illustration of the anisotropy
1287 principle. Energy transfer between the same kind of fluorescently tagged proteins leads
1288 to depolarization of the emitted light. Extent of the depolarization gives a hint on
1289 dimerization and oligomerization of a protein as the fluorescence anisotropy (FA) value
1290 decreases. B, Representative images showing color-coded FA values of FIT-GFP and
1291 FITmSS271AA at t=0 and t=5/15 min. C-D, Box plots representing quantification of FA
1292 values. FA was measured at t=0 within the whole nucleus and at t =5/15 min within the
1293 whole nucleus, in NBs and in residual NP. Free GFP and GFP-GFP served as references
1294 for mono- and dimerization. FA values for C, FIT-GFP, and D, FITmSS271AA-GFP. In C
1295 and D, FA values were calculated from 10-15 nuclei from a transformed plant (n = 10-15).
1296 Two experiments were conducted, one representative result is shown. C and D show the
1297 same free GFP and GFP-GFP references because both measurements were performed
1298 on the same day. FA values decreased for FIT-GFP, but not FITmSS271AA-GFP, in the
1299 whole nucleus (compare t=0 with t=5/15 min). FA values were also lowered in NBs versus
1300 NP in the case of FIT-GFP but not FITmSS271AA-GFP (compare t=5/15 min of NBs and
1301 NP). This indicates stronger homodimerization of FIT than FITmSS271AA-GFP in the
1302 whole nucleus and in NBs. $IDR^{Ser271/272}$ may therefore be relevant for FIT NB formation
1303 and FIT homodimerization (**Supplemental Figure S2**).

1304 Box plots show 25-75 percentile with min-max whiskers, mean as small square and
1305 median as line. Statistical analysis was performed with one-way ANOVA and Tukey post-
1306 hoc test. Different letters indicate statistically significant differences ($P < 0.05$). Scale bar:
1307 2 µm. Arrowheads indicate NBs. G = GFP. Fluorescence protein analysis was conducted
1308 in transiently transformed *N. benthamiana* leaf epidermis cells, following the standardized
1309 FIT NB analysis procedure.

1310 **Figure 4: FIT was present in heterodimeric protein complexes with bHLH039 in NBs,**
1311 **dependent on Ser271/272 site.**
1312 A, Confocal images with colocalization of FIT-GFP and bHLH039-mCherry in the
1313 nucleus. Both proteins were evenly distributed within the nucleus at t=0 and colocalized
1314 fully in FIT NBs at t=5 min. Two independent experiments with two plants each.
1315 Representative images from one nucleus. B-E, FRET-FLIM measurements to determine
1316 heterodimerization strength of FIT and FITmSS271AA with bHLH039, respectively. FIT-
1317 GFP and FITmSS271AA-GFP (donor only) served as negative controls. B, Schematic
1318 illustration of the FRET-FLIM principle. Energy transfer occurs between two different
1319 fluorophores. One fluorophore acts as the donor and the other as the acceptor of the
1320 energy. In case of interaction (close proximity, ≤10 nm) the fluorescence lifetime of the
1321 donor decreases. C, Representative images showing color-coded fluorescence lifetime
1322 values of FIT-GFP and FITmSS271AA-GFP co-expressed with bHLH039-mCherry at t=0
1323 and t=5/15 min. D-E, Box plots diagrams representing FRET-FLIM measurements at t=0
1324 within the whole nucleus and at t=5/15 min within the whole nucleus, inside NBs and in
1325 residual NP. Lifetime values represent measurements of 10 nuclei from a transformed
1326 plant (n = 10). Two experiments were conducted, one representative result is shown.
1327 Fluorescence lifetime was reduced for the pair of FIT-GFP and bHLH039-mCherry in NBs
1328 versus NP at t=5 min, indicating protein interaction preferentially inside NBs. Fluorescence
1329 lifetime values were not significantly different for the pair FITmSS271AA-GFP and
1330 bHLH039-mCherry in this same comparison at t=15 min, indicating that this pair did not
1331 preferentially interact in NBs. $IDR^{Ser271/272}$ may therefore be relevant for FIT NB formation,
1332 and FIT homo- and heterodimerization (**Supplemental Figure S2**).
1333 Box plots show 25-75 percentile with min-max whiskers, mean as small square and
1334 median as line. Statistical analysis was performed with one-way ANOVA and Tukey post-
1335 hoc test. Different letters indicate statistically significant differences ($P < 0.05$). Scale bar:
1336 2 µm. Arrowheads indicate NBs. G = GFP; C = mCherry. Fluorescence protein analysis
1337 was conducted in transiently transformed *N. benthamiana* leaf epidermis cells, following
1338 the standardized FIT NB analysis procedure.

1339 **Figure 5: Two NB markers and splicing components were present in NBs**
1340 **(designated type II), revealing the dynamics of FIT to accumulate in NBs.**
1341 Confocal images showing localization of FIT-GFP and NB markers (type II) upon
1342 co-expression in the nucleus at t=0 and t=5 min. Co-expression of FIT-GFP with A, SR45-
1343 mRFP, and B, SRm102-mRFP. Type II NB markers localized inside NBs at t=0 and
1344 t=5 min. Similar localization patterns were observed upon single expression, showing that
1345 SR45 and SRm102 are present in distinct NB types (compare with **Supplemental**
1346 **Figure S4, A and B**). FIT-GFP colocalized with type II markers in their distinct NBs at
1347 t=5 min, but not t=0. FIT-GFP additionally localized in FIT NBs at t=5 min. Type II markers
1348 were not present in FIT NBs, while FIT-GFP became recruited into the distinct type II NBs
1349 upon the light trigger. Hence, FIT NBs could be associated with speckle components.
1350 Scale bar: 2 µm. Filled arrowheads indicate colocalization in NBs, empty
1351 arrowheads indicate no colocalization in NBs. G = GFP; R = mRFP. Fluorescence protein
1352 analysis was conducted in transiently transformed *N. benthamiana* leaf epidermis cells,
1353 following the standardized FIT NB analysis procedure. Representative images from two
1354 to five independent experiments are shown. For data with type I markers (no
1355 colocalization) and type III markers (full colocalization) see **Supplemental Figure S3** and
1356 **Figure 6**.

1357 **Figure 6: Three NB markers and speckle components became localized in FIT NBs**
1358 **and colocalized fully with FIT (designated type III), suggesting that FIT NBs have**
1359 **speckle function.**

1360 Confocal images showing localization of FIT-GFP and NB markers (type III) upon
1361 co-expression in the nucleus at t=0 and t=5 min. Co-expression of FIT-GFP with A,
1362 UAP56H2-mRFP, B, P15H1-mRFP, and C, PININ-mRFP. All three type III NB markers
1363 were homogeneously distributed and colocalized with FIT-GFP in the nucleus at t=0, while
1364 they colocalized with FIT-GFP in FIT NBs at t=5 min. UAP56H2-mRFP and P15H1-mRFP
1365 showed homogeneous localization in the single expression at both t=0 and t=5 min
1366 (compare with **Supplemental Figure S4, C and D**), while PININ-mRFP localized mainly
1367 in one large and several small NBs upon single expression at t=0 and t=5 min (compare
1368 with **Supplemental Figure S4E**). Hence, these three markers adopted the localization of
1369 FIT-GFP upon co-expression and suggest that FIT NBs have a speckle function.

1370 Scale bar: 2 μm. Arrowheads indicate colocalization within NBs. G = GFP; R =
1371 mRFP. Fluorescence protein analysis was conducted in transiently transformed
1372 *N. benthamiana* leaf epidermis cells, following the standardized FIT NB analysis
1373 procedure. Representative images from four to seven independent experiments are
1374 shown. For data with type I markers (no colocalization) and type II markers (partial
1375 colocalization) see **Supplemental Figure S** and **Figure 5**.

1376 **Figure 7: FIT colocalized with photobody (PB) markers in distinct PBs.**

1377 Confocal images showing localization of FIT-GFP and PB markers upon co-
1378 expression in the nucleus at t=0 and t=15 min. Co-expression of FIT-GFP with A, PIF3-
1379 mCherry, and B and C, PIF4-mCherry, in B, showing a typical pattern with absence of NBs
1380 (ca. 50% of nuclei), in C, showing a typical pattern with presence of NBs (ca. 50% of cells).
1381 When FIT-GFP was co-expressed with PB markers, FIT NBs did not appear at t=5 min,
1382 but instead, FIT-GFP colocalized with PB markers in PBs at t=15 min. A, PIF3-mCherry
1383 localized predominantly to a single large PB at t=0 and t=15 min. FIT-GFP colocalized
1384 with PIF3-mCherry in this single large PB at t=15 min. B, PIF4-mCherry and FIT-GFP were
1385 both homogeneously distributed in the nucleoplasm at t=0 and t=15 min. In C, FIT-GFP
1386 colocalized with PIF4-mCherry in PBs at t=0 and t=15 min. The same localization patterns
1387 were found for PIF3-mCherry and PIF4-mCherry upon single expression (compare with
1388 **Supplemental Figure S5**). Hence, FIT-GFP was recruited to the two distinct types of PIF3
1389 and PIF4 PBs, whereas PIF3 and PIF4 were not recruited to FIT NBs. This suggests that
1390 FIT NBs are affected by the presence of PIF3- and PIF4-containing PBs and a connection
1391 to light signaling exists.

1392 Scale bar: 2 µm. Arrowheads indicate colocalization in PBs. G = GFP; C = mCherry.
1393 Fluorescence protein analysis was conducted in transiently transformed *N. benthamiana*
1394 leaf epidermis cells, following the standardized FIT NB analysis procedure.
1395 Representative images from four to six independent experiments are shown.

1396 **Figure 8. Root iron reductase activity is promoted under blue light.**

1397 Root iron reductase activity assay on 6-d-old Arabidopsis seedlings grown under
1398 white light for 5 d under iron deficient and iron sufficient conditions and then exposed for
1399 1 d to blue, red, far-red light or darkness, or in parallel as control to white light. A, Induction
1400 of iron reductase activity upon iron deficiency versus sufficiency was higher under blue
1401 light than compared to the white light control. B, Exposure to red light did not change the
1402 iron reductase activity compared to the white light control. C-D, Plants exposed to far-red
1403 light and darkness did not show induction of iron reductase activity under iron deficient
1404 conditions compared to the iron deficient conditions.

1405 Two experiments were conducted, one representative result is shown. Bar
1406 diagrams represent the mean and standard deviation of four replicates with four seedlings
1407 each (n=4). Statistical analysis was performed with one-way ANOVA and Tukey post-hoc
1408 test. Different letters indicate statistically significant differences ($P < 0.05$).

1409 **Figure 9. Induction of FIT target gene expression is enhanced under blue light.**

1410 Gene expression analysis of iron deficiency genes *FIT*, *BHLH039*, *FRO2*, and *IRT1*
1411 on 6-d-old Arabidopsis seedlings grown under white light for 5 d under iron deficient and
1412 iron sufficient conditions and then exposed for 1 d to blue, red, far-red light or darkness,
1413 or in parallel as control to white light. A-B, *FIT* and *bHLH039* gene induction in response
1414 to low iron supply did not change after blue light exposure compared to the white light
1415 control. C-D, *FRO2* and *IRT1* gene expression increased after blue light exposure in iron
1416 deficient conditions compared to respective iron sufficient condition and white light control.
1417 E, *FIT* gene expression did not change after red light exposure compared to the white light
1418 control. F-G, *BHLH039* and *FRO2* gene expression decreased after red light exposure in
1419 iron deficient conditions compared to respective iron sufficient condition and white light
1420 control. H, *IRT1* gene expression did not change after red light exposure compared to the
1421 white light control. I, *FIT* gene expression did not change after far-red light exposure
1422 compared to the white light control. J-L, *BHLH039*, *FRO2*, and *IRT1* gene expression
1423 decreased after far-red light exposure in iron deficient conditions compared to white light
1424 deficient condition, comparable to the respective iron sufficient condition and iron
1425 sufficient white light control. M, *FIT* gene expression was higher in darkness under iron
1426 deficient conditions compared to respective iron sufficient condition and white light control.
1427 N-P, *BHLH039*, *FRO2*, and *IRT1* gene expression decreased after being exposed to
1428 darkness in iron deficient conditions compared to white light deficient condition,
1429 comparable to the respective iron sufficient condition and iron sufficient white light control.

1430 Two experiments were conducted, one representative result is shown. Bar
1431 diagrams represent the mean and standard deviation of three replicates with twelve
1432 seedlings and two technical replicates each (n=4). Statistical analysis was performed with
1433 one-way ANOVA and Tukey post-hoc test. Different letters indicate statistically significant
1434 differences ($P < 0.05$).

1435 **Figure 10: Summary model illustrating the effect of blue light on FIT NB formation**
1436 **and iron uptake, suggesting that FIT NBs are related to transcriptional and**
1437 **posttranscriptional regulation in speckles and that blue light has a promoting effect**
1438 **on iron uptake.**

1439 FIT accumulates in FIT NBs upon induction with blue light. FIT NBs are reversible,
1440 dynamic and of circular shape and may undergo LLPS. FIT homodimers and FIT-
1441 bHLH039 heterodimers are present in FIT NBs. FIT-bHLH039 is an active TF complex for
1442 upregulating the expression of iron acquisition genes in roots (Gratz et al., 2019). Hence,
1443 FIT NBs are subnuclear sites related to transcriptional regulation and because of their
1444 colocalization with speckle components, also to speckles. Blue light enhances root iron
1445 reductase activity and gene expression of *FRO2* and *IRT1*, all of which are downstream
1446 of FIT-bHLH039. In summary, FIT NBs are blue light-inducible subnuclear sites where
1447 active TF complexes of FIT and bHLH039 accumulate, linking transcriptional and
1448 posttranscriptional regulation in speckles with a promoting blue light effect on iron uptake.

Figure 1

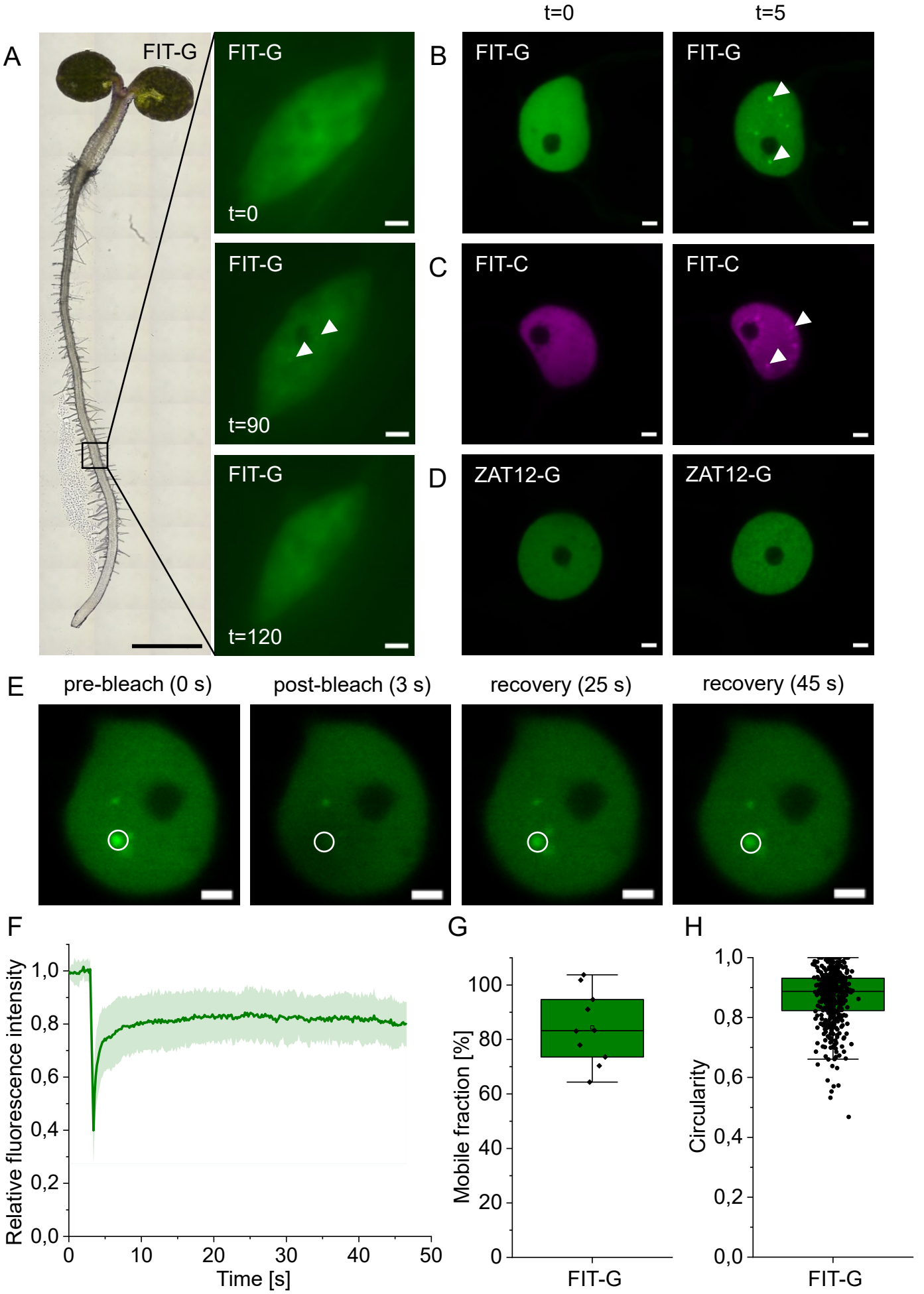
A
FIT-G
FIT-G
t=0
FIT-G
t=90
FIT-G
t=120
B
t=0
t=5
FIT-G
FIT-G
C
FIT-C
FIT-C
D
ZAT12-G
ZAT12-G
E
pre-bleach (0 s)
post-bleach (3 s)
recovery (25 s)
recovery (45 s)
F
Relative fluorescence intensity
1,0
0,8
0,6
0,4
0,2
0,0
0
10
20
30
40
50
Time [s]
G
Mobile fraction [%]
100
80
60
40
20
0
FIT-G
H
Circularity
1,0
0,8
0,6
0,4
0,2
0,0
FIT-G

Figure 1: FIT accumulated in nuclear condensates, termed FIT nuclear bodies (NBs) in a light-inducible manner, most likely following liquid-liquid phase separation (LLPS).

A, Induction of FIT NBs in Arabidopsis root epidermis cells of the root differentiation zone. Left, light microscopy overview image of a 5-d-old Arabidopsis seedling (proFIT:FIT-GFP) grown under iron deficiency. Right, nuclear localization of FIT-GFP in the root epidermis cells as indicated in the overview image, at t=0, t=90, and t=120 min. FIT-GFP signals were evenly distributed in the nucleus at t=0 min, and after induction by excitation with 488 nm laser NB formation accumulated in NBs at t=90 min, but also disappeared as shown at t=120 min. Note that root epidermis cells developed few NBs, sometimes taking up to two hours to appear. Three independent experiments with three plants were conducted. In the indicated region of interest, approximately a quarter of the root epidermis cells showed NBs. A representative image from one nucleus is shown. B-D, Fluorescence protein analysis in transiently transformed *N. benthamiana* leaf epidermis cells. Confocal images of B, FIT-GFP, C, FIT-mCherry, and D, ZAT12-GFP at t=0 and t=5 min. At t=0 min, FIT-GFP and FIT-mCherry showed an even distribution within the nucleus. Following a 488 nm laser excitation, numerous NBs were clearly visible in all examined transformed cells at t=5 min. These NBs were termed FIT NBs. Under the same imaging conditions, ZAT12-GFP did not show NB formation. According to these results, a standardized FIT NB analysis procedure was set up (**Supplemental Figure S1B**). See also **Supplemental Movie S1A-C**. Representative images from two to three independent experiments. E-G, FRAP measurements to test for liquid-like behavior of FIT NBs, using the standardized FIT NB analysis procedure in transiently transformed *N. benthamiana* leaf epidermis cells. E, Representative images of the fluorescent signal during a FRAP experiment, taken before bleaching (0 s) and recovery of fluorescence at three time points after bleaching from 3 s to 45 s within the circled region of a NB. F, Line diagram representing the relative fluorescence during a FRAP measurement for 10 NBs, showing a high fluorescence recovery rate of FIT-GFP within NBs. Dark green line, mean value; light green filled area, variation. G, Box plot diagram representing the mobile fraction of FIT-GFP calculated based on the relative fluorescence recovery in F. The diagram indicates high mobility of FIT. The mean was calculated from 10 NBs from 10 nuclei from a transformed plant. Three independent experiments were conducted, one representative result is shown. H, Box plot diagram representing quantification of the FIT NB shape with the software ImageJ (National Institutes of Health), indicating that FIT NBs have circular shape. Mobility and circularity characteristics indicate that FIT NBs are most likely liquid condensates that are the result of LLPS. The mean was calculated from all NBs visible in 15 nuclei from a transformed plant. Two independent experiments were conducted, one representative result is shown.

Box plots show 25-75 percentile with min-max whiskers, mean as small square and median as line. Scale bars of nuclei images, 2 µm; scale bar full seedling, 1 mm. Arrowheads indicate NBs. G = GFP; C = mCherry.

Figure 2

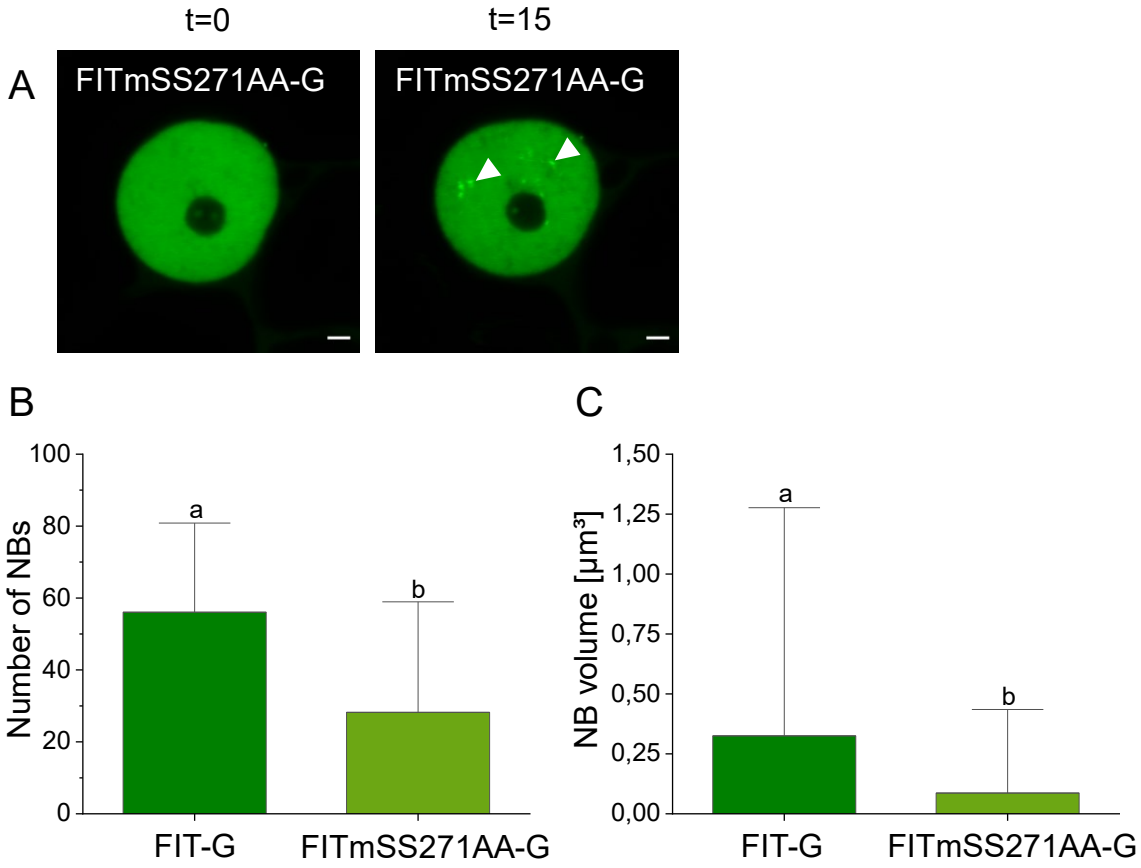
t=0
t=15
A
FITmSS271AA-G
FITmSS271AA-G
B
Number of NBs
100
80
60
40
20
0
a
b
FIT-G
FITmSS271AA-G
C
NB volume [µm³]
1,50
1,25
1,00
0,75
0,50
0,25
0,00
a
b
FIT-G
FITmSS271AA-G

Figure 2: The FIT C-terminal Ser271/272 site was important for the capacity of FIT to localize to NBs.

A, Confocal images of nuclear localization of FITmSS271AA-GFP at t=0 and t=15 min. FITmSS271AA-GFP accumulated in NBs, but NB formation required a longer time compared to FIT-GFP. See also **Supplemental Movie S1, A and C**. Two independent experiments. Representative images from one nucleus. B, Bar diagrams showing in B, number of NBs, and in C, the sizes of NBs with FIT-GFP and FITmSS271AA-GFP at t=5/15 min. NB number and size were determined with the software ImageJ (National Institute of Health). FIT-GFP accumulated in more and larger NBs than FITmSS271AA-GFP. See **Supplemental Movie S1, A and C**. FITmSS271AA-GFP lacks $IDR^{Ser271/272}$. This IDR may be relevant for FIT NB formation (**Supplemental Figure S2**). In B and C, bar diagrams represent the mean and standard deviation for a quantification of 15 nuclei from a transformed plant (n = 15). Two experiments were conducted, one representative result is shown.

Statistical analysis was performed with the Mann-Whitney test. Different letters indicate statistically significant differences ($P < 0.05$). Scale bar: 2 µm. Arrowheads indicate NBs. G = GFP. Analysis was conducted in transiently transformed *N. benthamiana* leaf epidermis cells, following the standardized FIT NB analysis procedure.

Figure 3

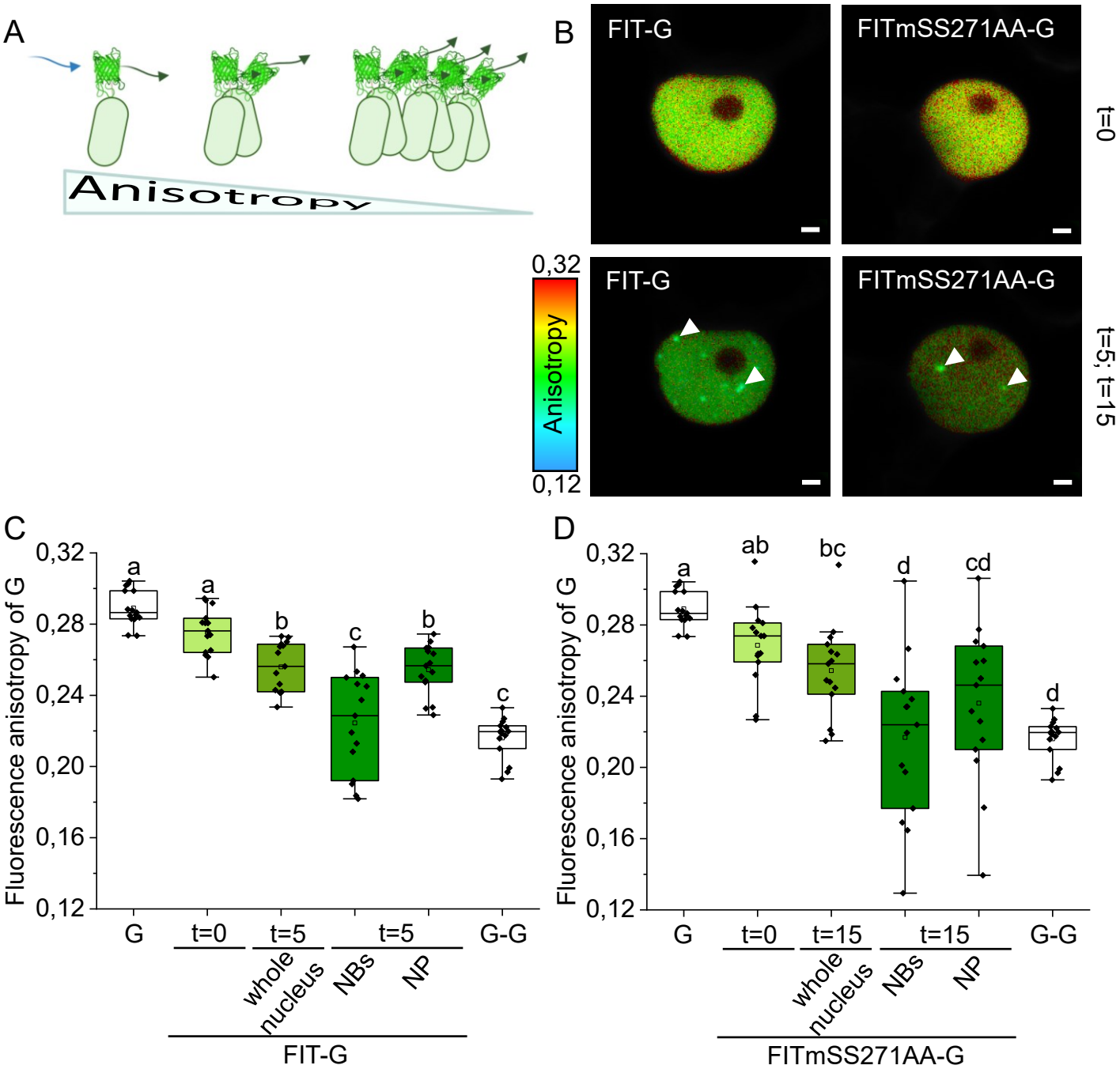
A
Anisotropy
B
FIT-G
FITmSS271AA-G
t=0
0,32
Anisotropy
0,12
FIT-G
FITmSS271AA-G
t=5; t=15
C
Fluorescence anisotropy of G
0,32
0,28
0,24
0,20
0,16
0,12
a
a
b
c
b
c
G
t=0
t=5
t=5
G-G
whole nucleus
NBs
NP
FIT-G
D
Fluorescence anisotropy of G
0,32
0,28
0,24
0,20
0,16
0,12
a
ab
bc
d
cd
d
G
t=0
t=15
t=15
G-G
whole nucleus
NBs
NP
FITmSS271AA-G

Figure 3: FIT was present in homodimeric protein complexes in NBs, dependent on Ser271/272 site.

Anisotropy (or homo-FRET) measurements of FIT-GFP and FITmSS271AA-GFP to determine homodimerization strength. A, Schematic illustration of the anisotropy principle. Energy transfer between the same kind of fluorescently tagged proteins leads to depolarization of the emitted light. Extent of the depolarization gives a hint on dimerization and oligomerization of a protein as the fluorescence anisotropy (FA) value decreases. B, Representative images showing color-coded FA values of FIT-GFP and FITmSS271AA at t=0 and t=5/15 min. C-D, Box plots representing quantification of FA values. FA was measured at t=0 within the whole nucleus and at t =5/15 min within the whole nucleus, in NBs and in residual NP. Free GFP and GFP-GFP served as references for mono- and dimerization. FA values for C, FIT-GFP, and D, FITmSS271AA-GFP. In C and D, FA values were calculated from 10-15 nuclei from a transformed plant (n = 10-15). Two experiments were conducted, one representative result is shown. C and D show the same free GFP and GFP-GFP references because both measurements were performed on the same day. FA values decreased for FIT-GFP, but not FITmSS271AA-GFP, in the whole nucleus (compare t=0 with t=5/15 min). FA values were also lowered in NBs versus NP in the case of FIT-GFP but not FITmSS271AA-GFP (compare t=5/15 min of NBs and NP). This indicates stronger homodimerization of FIT than FITmSS271AA-GFP in the whole nucleus and in NBs. $IDR^{Ser271/272}$ may therefore be relevant for FIT NB formation and FIT homodimerization (**Supplemental Figure S2**).

Box plots show 25-75 percentile with min-max whiskers, mean as small square and median as line. Statistical analysis was performed with one-way ANOVA and Tukey post-hoc test. Different letters indicate statistically significant differences ($P < 0.05$). Scale bar: 2 µm. Arrowheads indicate NBs. G = GFP. Fluorescence protein analysis was conducted in transiently transformed *N. benthamiana* leaf epidermis cells, following the standardized FIT NB analysis procedure.

Figure 4

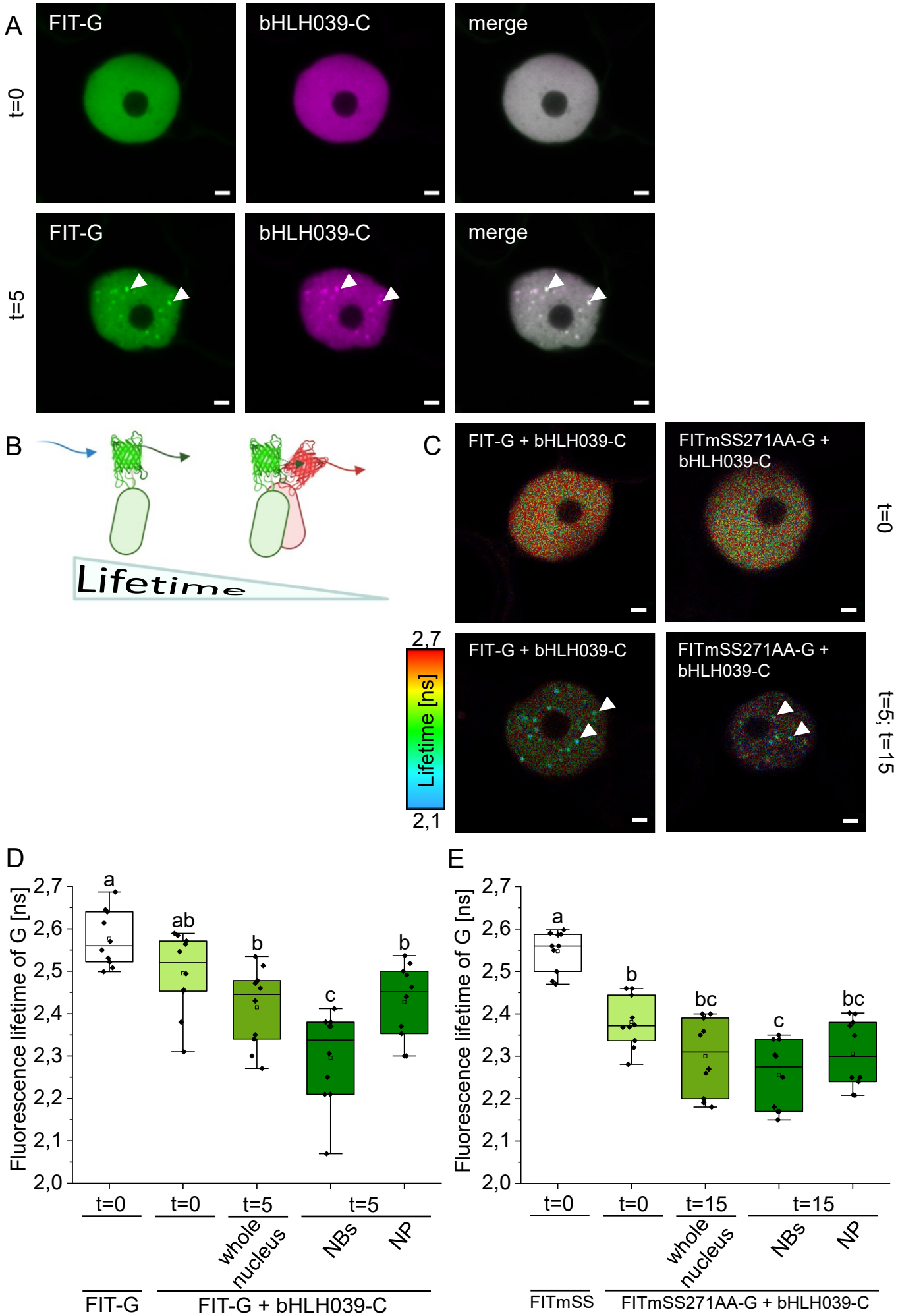
A
FIT-G
bHLH039-C
merge
t=0
t=5
B
Lifetime
C
FIT-G + bHLH039-C
FITmSS271AA-G + bHLH039-C
t=0
t=5; t=15
2,7
Lifetime [ns]
2,1
D
Fluorescence lifetime of G [ns]
2,7
2,6
2,5
2,4
2,3
2,2
2,1
2,0
a
ab
b
c
b
t=0
t=0
t=5
t=5
whole nucleus
NBs
NP
FIT-G
FIT-G + bHLH039-C
E
Fluorescence lifetime of G [ns]
a
b
bc
c
bc
t=0
t=0
t=15
t=15
whole nucleus
NBs
NP
FITmSS
FITmSS271AA-G + bHLH039-C

Figure 4: FIT was present in heterodimeric protein complexes with bHLH039 in NBs, dependent on Ser271/272 site.

A, Confocal images with colocalization of FIT-GFP and bHLH039-mCherry in the nucleus. Both proteins were evenly distributed within the nucleus at t=0 and colocalized fully in FIT NBs at t=5 min. Two independent experiments with two plants each. Representative images from one nucleus. B-E, FRET-FLIM measurements to determine heterodimerization strength of FIT and FITmSS271AA with bHLH039, respectively. FIT-GFP and FITmSS271AA-GFP (donor only) served as negative controls. B, Schematic illustration of the FRET-FLIM principle. Energy transfer occurs between two different fluorophores. One fluorophore acts as the donor and the other as the acceptor of the energy. In case of interaction (close proximity, ≤10 nm) the fluorescence lifetime of the donor decreases. C, Representative images showing color-coded fluorescence lifetime values of FIT-GFP and FITmSS271AA-GFP co-expressed with bHLH039-mCherry at t=0 and t=5/15 min. D-E, Box plots diagrams representing FRET-FLIM measurements at t=0 within the whole nucleus and at t=5/15 min within the whole nucleus, inside NBs and in residual NP. Lifetime values represent measurements of 10 nuclei from a transformed plant (n = 10). Two experiments were conducted, one representative result is shown. Fluorescence lifetime was reduced for the pair of FIT-GFP and bHLH039-mCherry in NBs versus NP at t=5 min, indicating protein interaction preferentially inside NBs. Fluorescence lifetime values were not significantly different for the pair FITmSS271AA-GFP and bHLH039-mCherry in this same comparison at t=15 min, indicating that this pair did not preferentially interact in NBs. $IDR^{Ser271/272}$ may therefore be relevant for FIT NB formation, and FIT homo- and heterodimerization (**Supplemental Figure S2**).

Box plots show 25-75 percentile with min-max whiskers, mean as small square and median as line. Statistical analysis was performed with one-way ANOVA and Tukey post-hoc test. Different letters indicate statistically significant differences ($P < 0.05$). Scale bar: 2 µm. Arrowheads indicate NBs. G = GFP; C = mCherry. Fluorescence protein analysis was conducted in transiently transformed *N. benthamiana* leaf epidermis cells, following the standardized FIT NB analysis procedure.

Figure 5

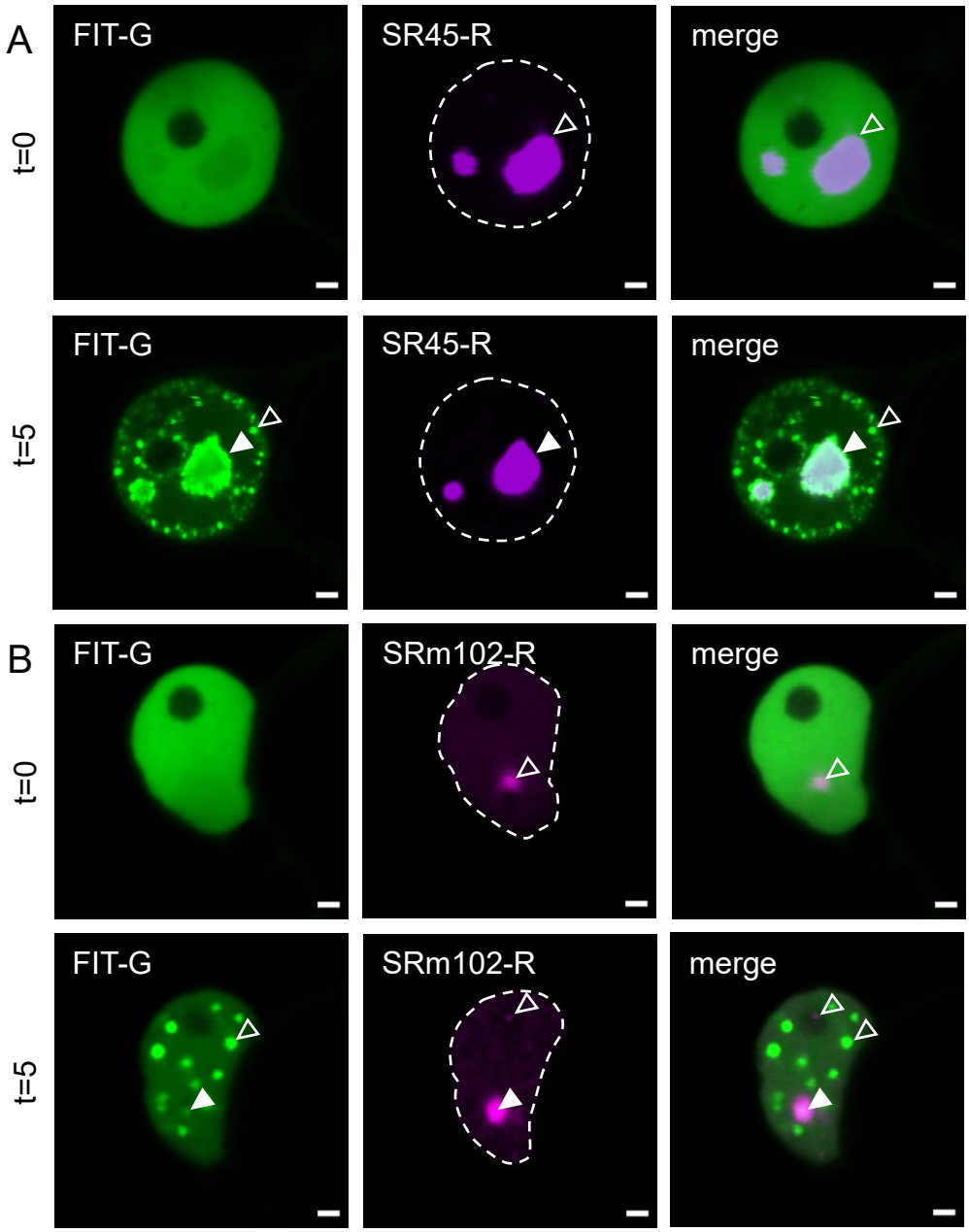

Figure 5: Two NB markers and splicing components were present in NBs (designated type II), revealing the dynamics of FIT to accumulate in NBs.

Confocal images showing localization of FIT-GFP and NB markers (type II) upon co-expression in the nucleus at t=0 and t=5 min. Co-expression of FIT-GFP with A, SR45-mRFP, and B, SRm102-mRFP. Type II NB markers localized inside NBs at t=0 and t=5 min. Similar localization patterns were observed upon single expression, showing that SR45 and SRm102 are present in distinct NB types (compare with **Supplemental Figure S4, A and B**). FIT-GFP colocalized with type II markers in their distinct NBs at t=5 min, but not t=0. FIT-GFP additionally localized in FIT NBs at t=5 min. Type II markers were not present in FIT NBs, while FIT-GFP became recruited into the distinct type II NBs upon the light trigger. Hence, FIT NBs could be associated with speckle components.

Scale bar: 2 µm. Filled arrowheads indicate colocalization in NBs, empty arrowheads indicate no colocalization in NBs. G = GFP; R = mRFP. Fluorescence protein analysis was conducted in transiently transformed *N. benthamiana* leaf epidermis cells, following the standardized FIT NB analysis procedure. Representative images from two to five independent experiments are shown. For data with type I markers (no colocalization) and type III markers (full colocalization) see **Supplemental Figure S3** and **Figure 6**.

Figure 6

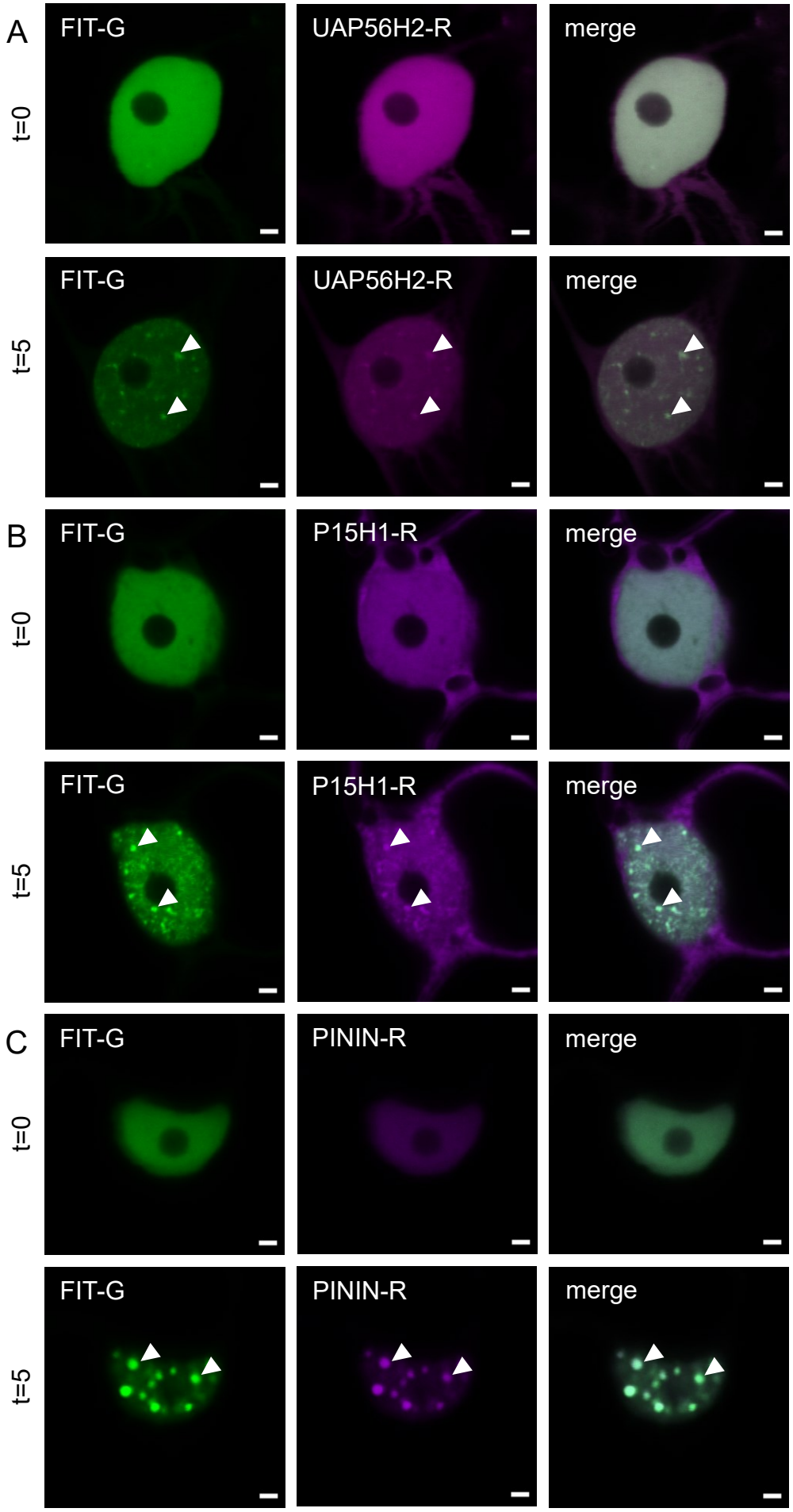
A
t=0
FIT-G
UAP56H2-R
merge
t=5
FIT-G
UAP56H2-R
merge
B
t=0
FIT-G
P15H1-R
merge
t=5
FIT-G
P15H1-R
merge
C
t=0
FIT-G
PININ-R
merge
t=5
FIT-G
PININ-R
merge

Figure 6: Three NB markers and speckle components became localized in FIT NBs and colocalized fully with FIT (designated type III), suggesting that FIT NBs have speckle function.

Confocal images showing localization of FIT-GFP and NB markers (type III) upon co-expression in the nucleus at t=0 and t=5 min. Co-expression of FIT-GFP with A, UAP56H2-mRFP, B, P15H1-mRFP, and C, PININ-mRFP. All three type III NB markers were homogeneously distributed and colocalized with FIT-GFP in the nucleus at t=0, while they colocalized with FIT-GFP in FIT NBs at t=5 min. UAP56H2-mRFP and P15H1-mRFP showed homogeneous localization in the single expression at both t=0 and t=5 min (compare with **Supplemental Figure S4, C and D**), while PININ-mRFP localized mainly in one large and several small NBs upon single expression at t=0 and t=5 min (compare with **Supplemental Figure S4E**). Hence, these three markers adopted the localization of FIT-GFP upon co-expression and suggest that FIT NBs have a speckle function.

Scale bar: 2 μm. Arrowheads indicate colocalization within NBs. G = GFP; R = mRFP. Fluorescence protein analysis was conducted in transiently transformed *N. benthamiana* leaf epidermis cells, following the standardized FIT NB analysis procedure. Representative images from four to seven independent experiments are shown. For data with type I markers (no colocalization) and type II markers (partial colocalization) see **Supplemental Figure S** and **Figure 5**.

Figure 7

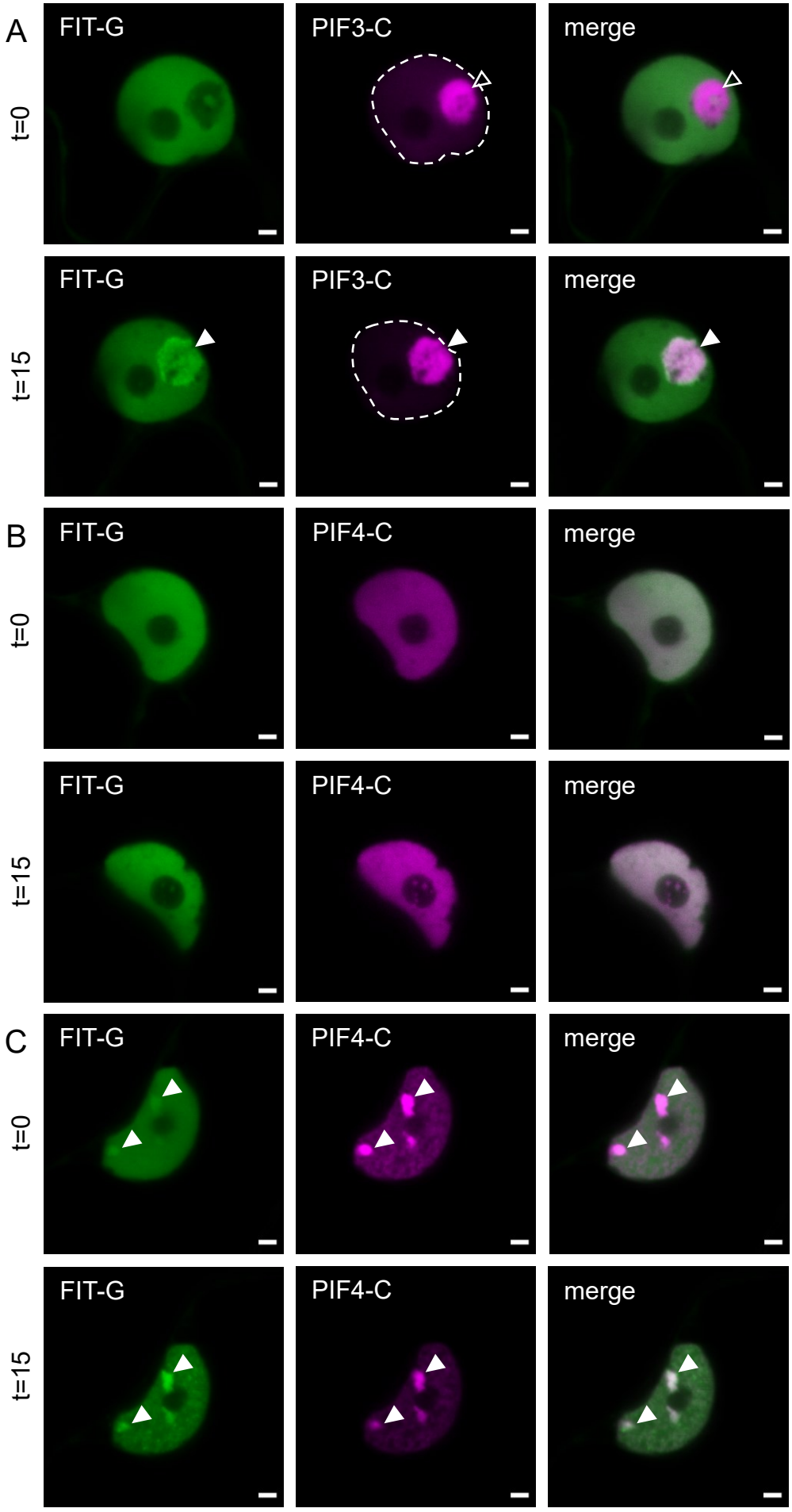
A
t=0
FIT-G
PIF3-C
merge
t=15
FIT-G
PIF3-C
merge
B
t=0
FIT-G
PIF4-C
merge
t=15
FIT-G
PIF4-C
merge
C
t=0
FIT-G
PIF4-C
merge
t=15
FIT-G
PIF4-C
merge

Figure 7: FIT colocalized with photobody (PB) markers in distinct PBs.

Confocal images showing localization of FIT-GFP and PB markers upon co-expression in the nucleus at t=0 and t=15 min. Co-expression of FIT-GFP with A, PIF3-mCherry, and B and C, PIF4-mCherry, in B, showing a typical pattern with absence of NBs (ca. 50% of nuclei), in C, showing a typical pattern with presence of NBs (ca. 50% of cells). When FIT-GFP was co-expressed with PB markers, FIT NBs did not appear at t=5 min, but instead, FIT-GFP colocalized with PB markers in PBs at t=15 min. A, PIF3-mCherry localized predominantly to a single large PB at t=0 and t=15 min. FIT-GFP colocalized with PIF3-mCherry in this single large PB at t=15 min. B, PIF4-mCherry and FIT-GFP were both homogeneously distributed in the nucleoplasm at t=0 and t=15 min. In C, FIT-GFP colocalized with PIF4-mCherry in PBs at t=0 and t=15 min. The same localization patterns were found for PIF3-mCherry and PIF4-mCherry upon single expression (compare with **Supplemental Figure S5**). Hence, FIT-GFP was recruited to the two distinct types of PIF3 and PIF4 PBs, whereas PIF3 and PIF4 were not recruited to FIT NBs. This suggests that FIT NBs are affected by the presence of PIF3- and PIF4-containing PBs and a connection to light signaling exists.

Scale bar: 2 µm. Arrowheads indicate colocalization in PBs. G = GFP; C = mCherry. Fluorescence protein analysis was conducted in transiently transformed *N. benthamiana* leaf epidermis cells, following the standardized FIT NB analysis procedure. Representative images from four to six independent experiments are shown.

Figure 8

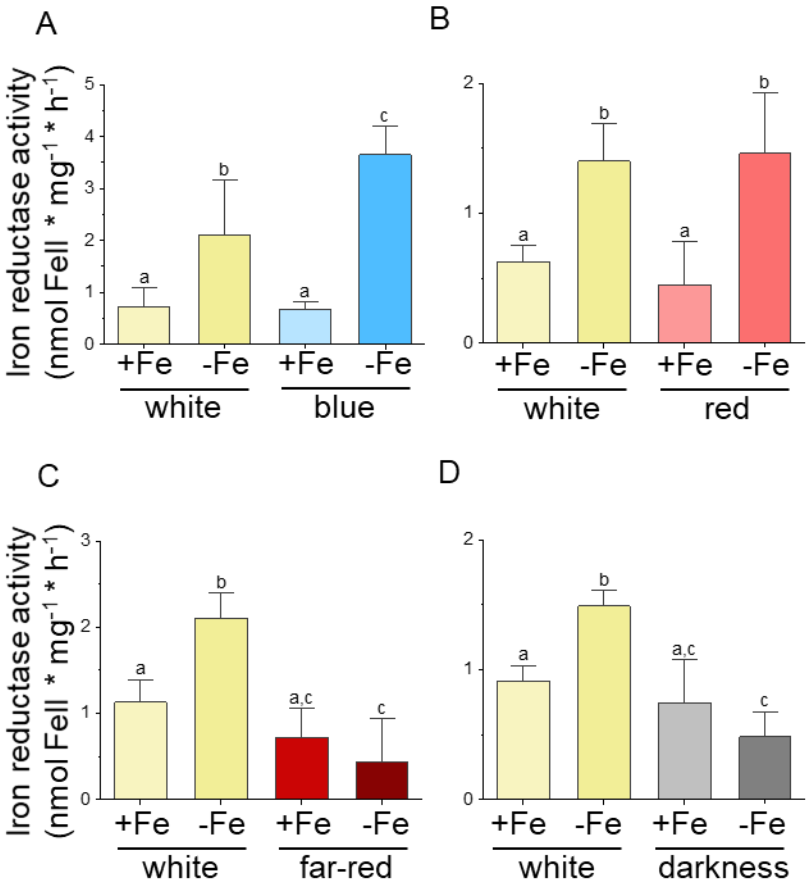
A
B
C
D
Iron reductase activity
(nmol FeII * mg-1 * h-1)
+Fe
-Fe
white
blue
red
far-red
darkness
a
b
c
a,c

Figure 8. Root iron reductase activity is promoted under blue light.

Root iron reductase activity assay on 6-d-old Arabidopsis seedlings grown under white light for 5 d under iron deficient and iron sufficient conditions and then exposed for 1 d to blue, red, far-red light or darkness, or in parallel as control to white light. A, Induction of iron reductase activity upon iron deficiency versus sufficiency was higher under blue light than compared to the white light control. B, Exposure to red light did not change the iron reductase activity compared to the white light control. C-D, Plants exposed to far-red light and darkness did not show induction of iron reductase activity under iron deficient conditions compared to the iron deficient conditions.

Two experiments were conducted, one representative result is shown. Bar diagrams represent the mean and standard deviation of four replicates with four seedlings each (n=4). Statistical analysis was performed with one-way ANOVA and Tukey post-hoc test. Different letters indicate statistically significant differences ($P < 0.05$).

Figure 9

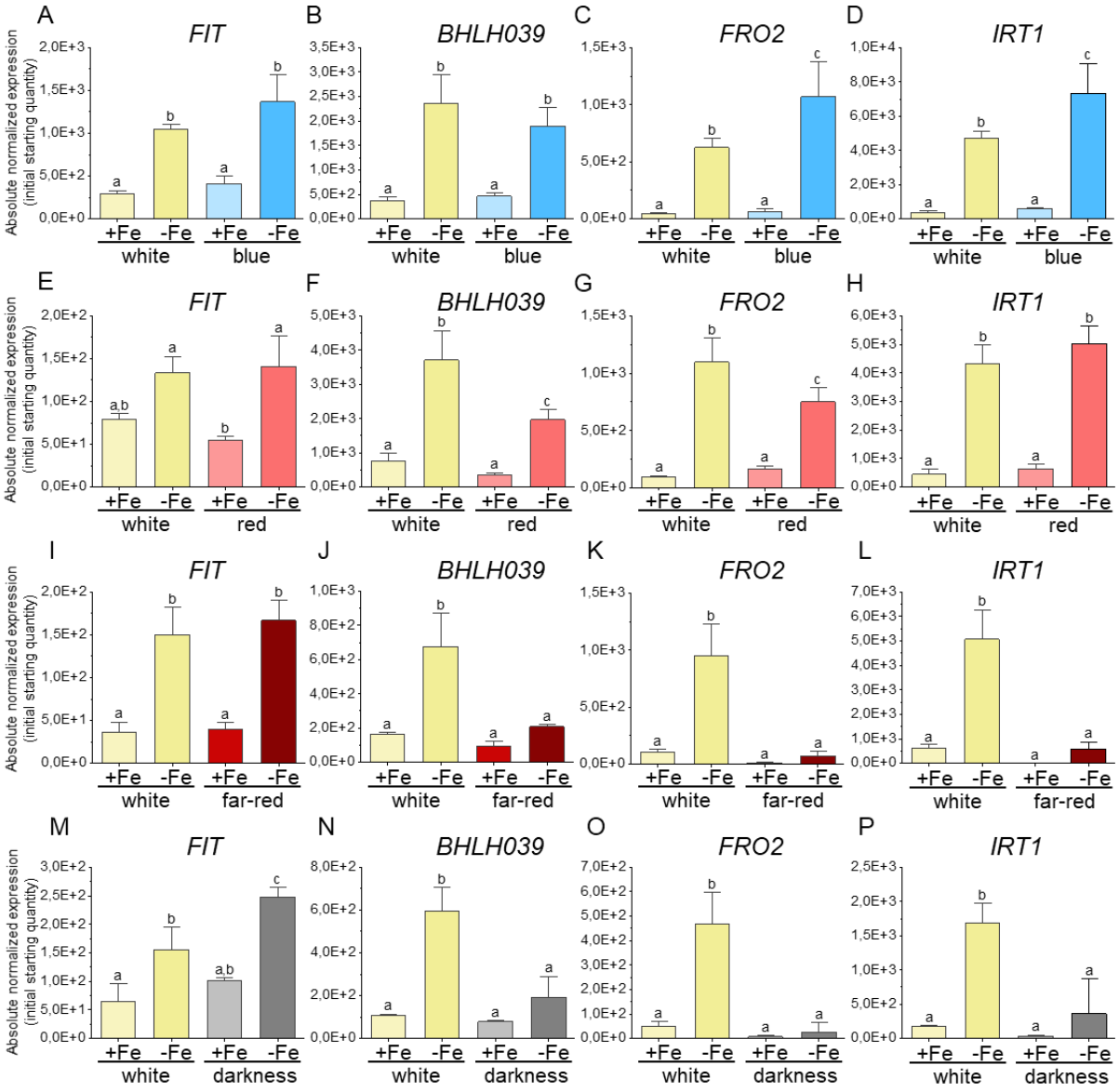
A
FIT
B
BHLH039
C
FRO2
D
IRT1
E
FIT
F
BHLH039
G
FRO2
H
IRT1
I
FIT
J
BHLH039
K
FRO2
L
IRT1
M
FIT
N
BHLH039
O
FRO2
P
IRT1
Absolute normalized expression
(initial starting quantity)
+Fe
-Fe
white
blue
red
far-red
darkness

Figure 9. Induction of FIT target gene expression is enhanced under blue light.

Gene expression analysis of iron deficiency genes *FIT*, *BHLH039*, *FRO2*, and *IRT1* on 6-d-old Arabidopsis seedlings grown under white light for 5 d under iron deficient and iron sufficient conditions and then exposed for 1 d to blue, red, far-red light or darkness, or in parallel as control to white light. A-B, *FIT* and *bHLH039* gene induction in response to low iron supply did not change after blue light exposure compared to the white light control. C-D, *FRO2* and *IRT1* gene expression increased after blue light exposure in iron deficient conditions compared to respective iron sufficient condition and white light control. E, *FIT* gene expression did not change after red light exposure compared to the white light control. F-G, *BHLH039* and *FRO2* gene expression decreased after red light exposure in iron deficient conditions compared to respective iron sufficient condition and white light control. H, *IRT1* gene expression did not change after red light exposure compared to the white light control. I, *FIT* gene expression did not change after far-red light exposure compared to the white light control. J-L, *BHLH039*, *FRO2*, and *IRT1* gene expression decreased after far-red light exposure in iron deficient conditions compared to white light deficient condition, comparable to the respective iron sufficient condition and iron sufficient white light control. M, *FIT* gene expression was higher in darkness under iron deficient conditions compared to respective iron sufficient condition and white light control. N-P, *BHLH039*, *FRO2*, and *IRT1* gene expression decreased after being exposed to darkness in iron deficient conditions compared to white light deficient condition, comparable to the respective iron sufficient condition and iron sufficient white light control.

Two experiments were conducted, one representative result is shown. Bar diagrams represent the mean and standard deviation of three replicates with twelve seedlings and two technical replicates each (n=4). Statistical analysis was performed with one-way ANOVA and Tukey post-hoc test. Different letters indicate statistically significant differences ($P < 0.05$).

Figure 10

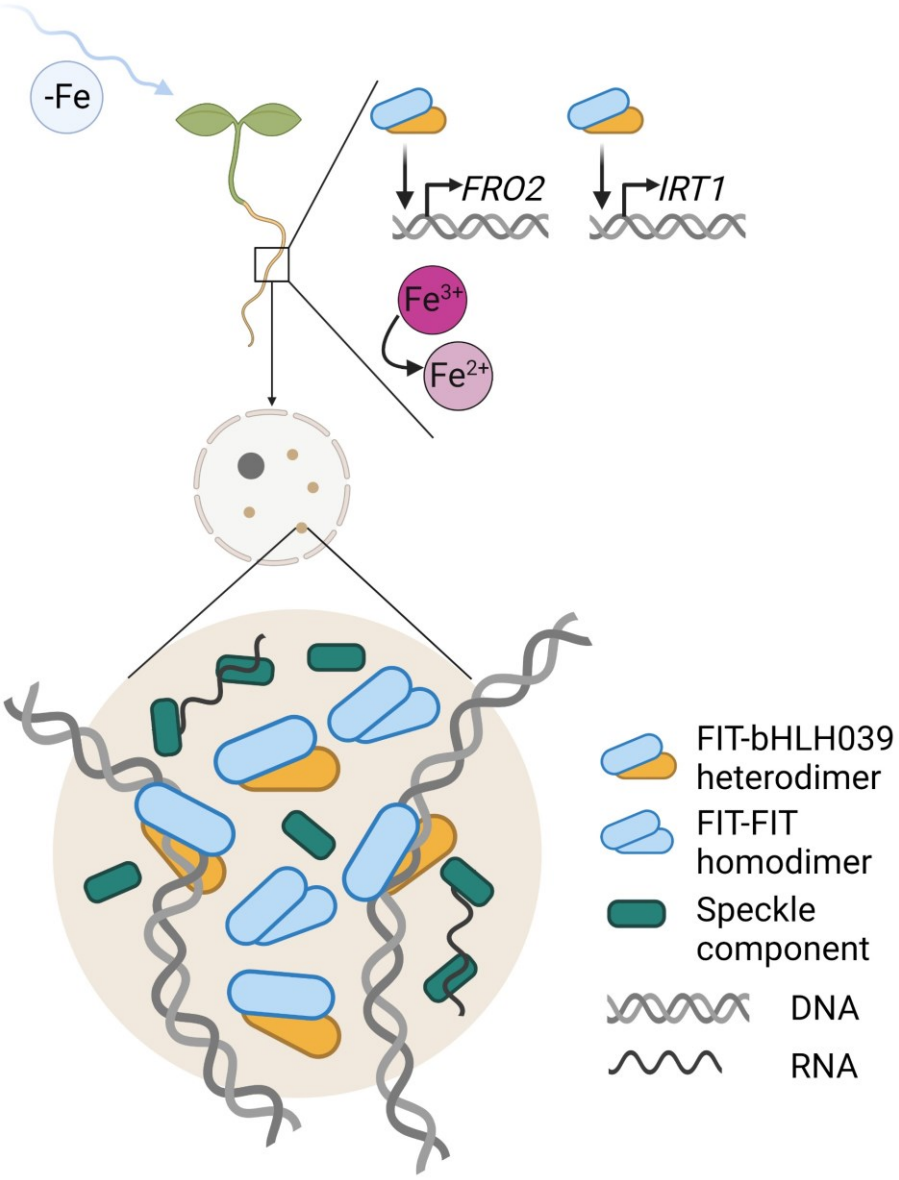
-Fe
FRO2
IRT1
Fe3+
Fe2+
FIT-bHLH039 heterodimer
FIT-FIT homodimer
Speckle component
DNA
RNA

Figure 10: Summary model illustrating the effect of blue light on FIT NB formation and iron uptake, suggesting that FIT NBs are related to transcriptional and posttranscriptional regulation in speckles and that blue light has a promoting effect on iron uptake.

FIT accumulates in FIT NBs upon induction with blue light. FIT NBs are reversible, dynamic and of circular shape and may undergo LLPS. FIT homodimers and FIT-bHLH039 heterodimers are present in FIT NBs. FIT-bHLH039 is an active TF complex for upregulating the expression of iron acquisition genes in roots (Gratz et al., 2019). Hence, FIT NBs are subnuclear sites related to transcriptional regulation and because of their colocalization with speckle components, also to speckles. Blue light enhances root iron reductase activity and gene expression of *FRO2* and *IRT1*, all of which are downstream of FIT-bHLH039. In summary, FIT NBs are blue light-inducible subnuclear sites where active TF complexes of FIT and bHLH039 accumulate, linking transcriptional and posttranscriptional regulation in speckles with a promoting blue light effect on iron uptake.

Figure 1

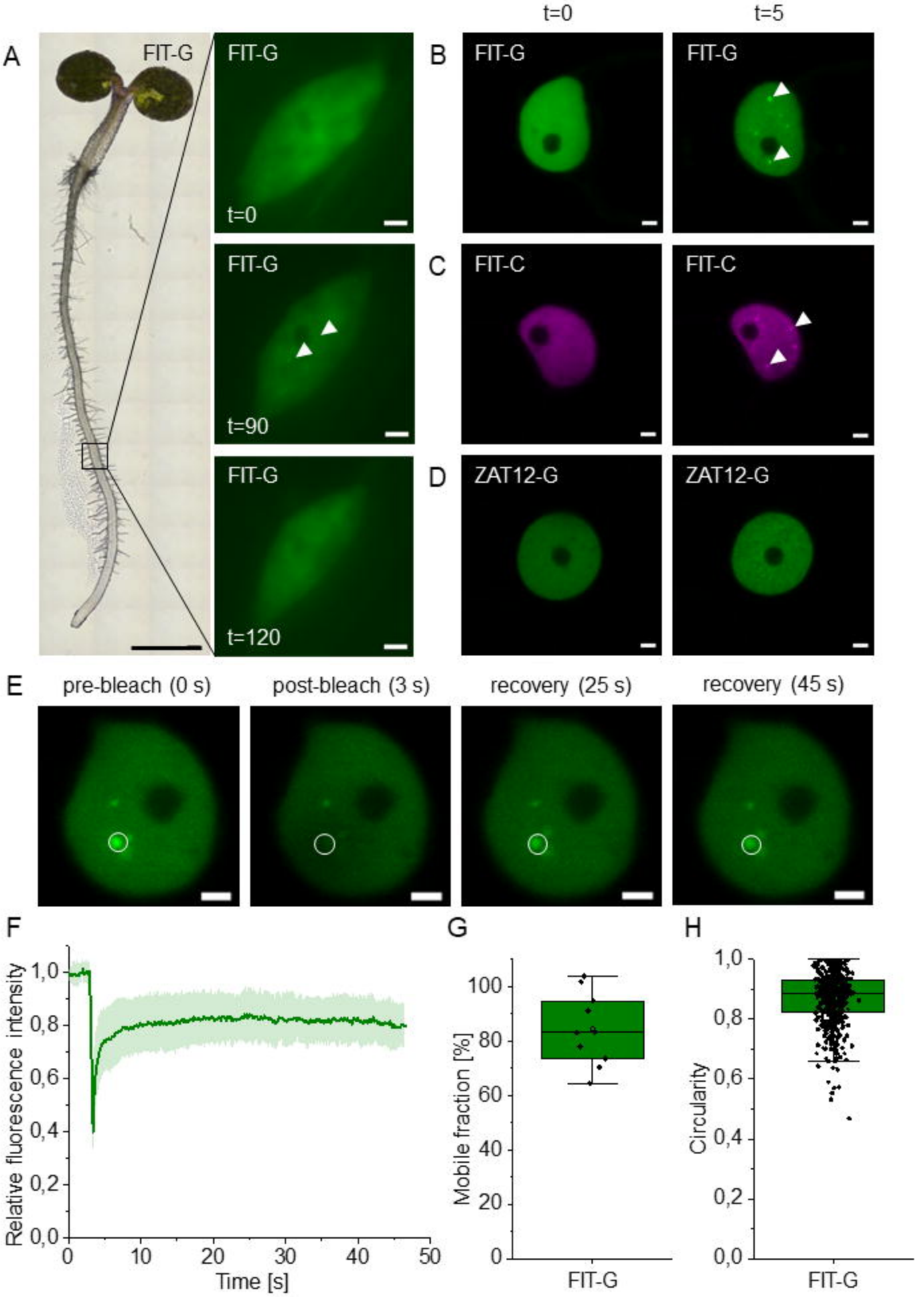
A
FIT-G
FIT-G
t=0
FIT-G
t=90
FIT-G
t=120
B
t=0
t=5
FIT-G
FIT-G
C
FIT-C
FIT-C
D
ZAT12-G
ZAT12-G
E
pre-bleach (0 s)
post-bleach (3 s)
recovery (25 s)
recovery (45 s)
F
Relative fluorescence intensity
Time [s]
G
Mobile fraction [%]
FIT-G
H
Circularity
FIT-G

Figure 2

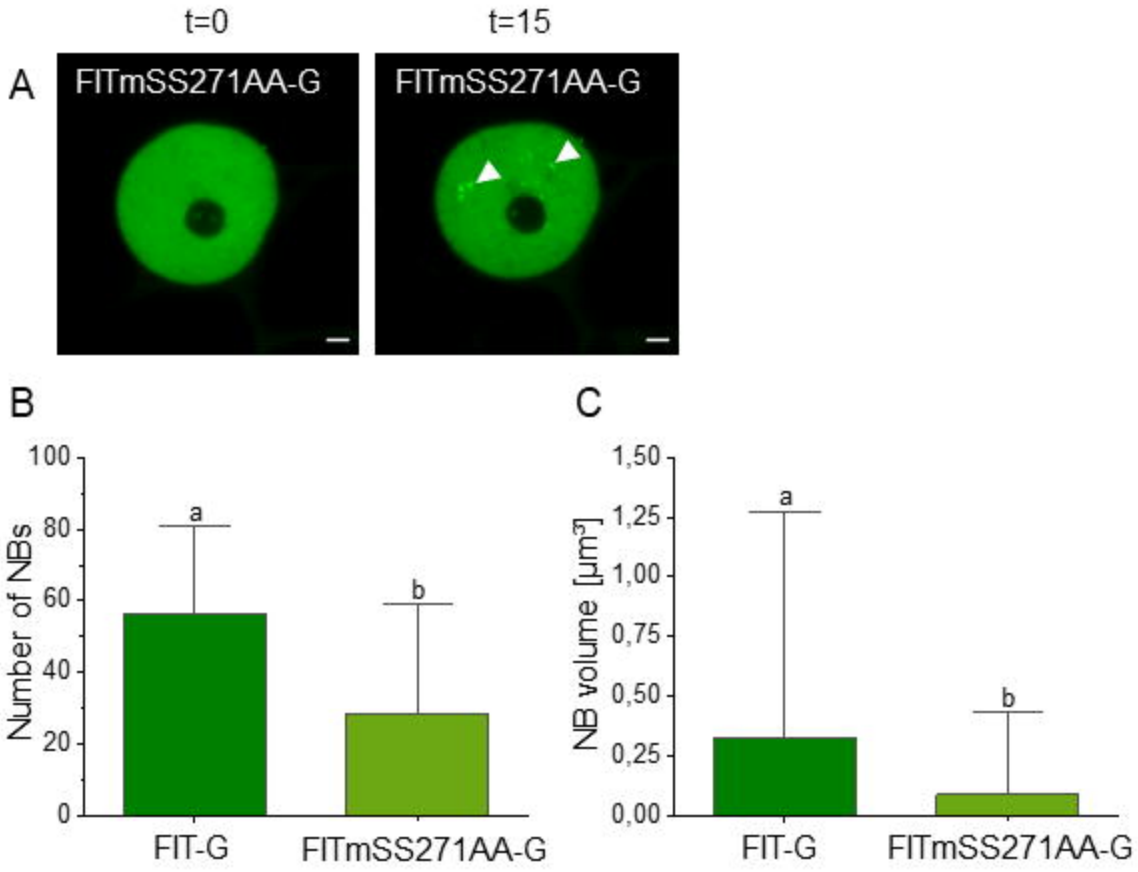
t=0
t=15
A
FITmSS271AA-G
FITmSS271AA-G
B
Number of NBs
100
80
60
40
20
0
a
b
FIT-G
FITmSS271AA-G
C
NB volume [µm³]
1,50
1,25
1,00
0,75
0,50
0,25
0,00
a
b
FIT-G
FITmSS271AA-G

Figure 3

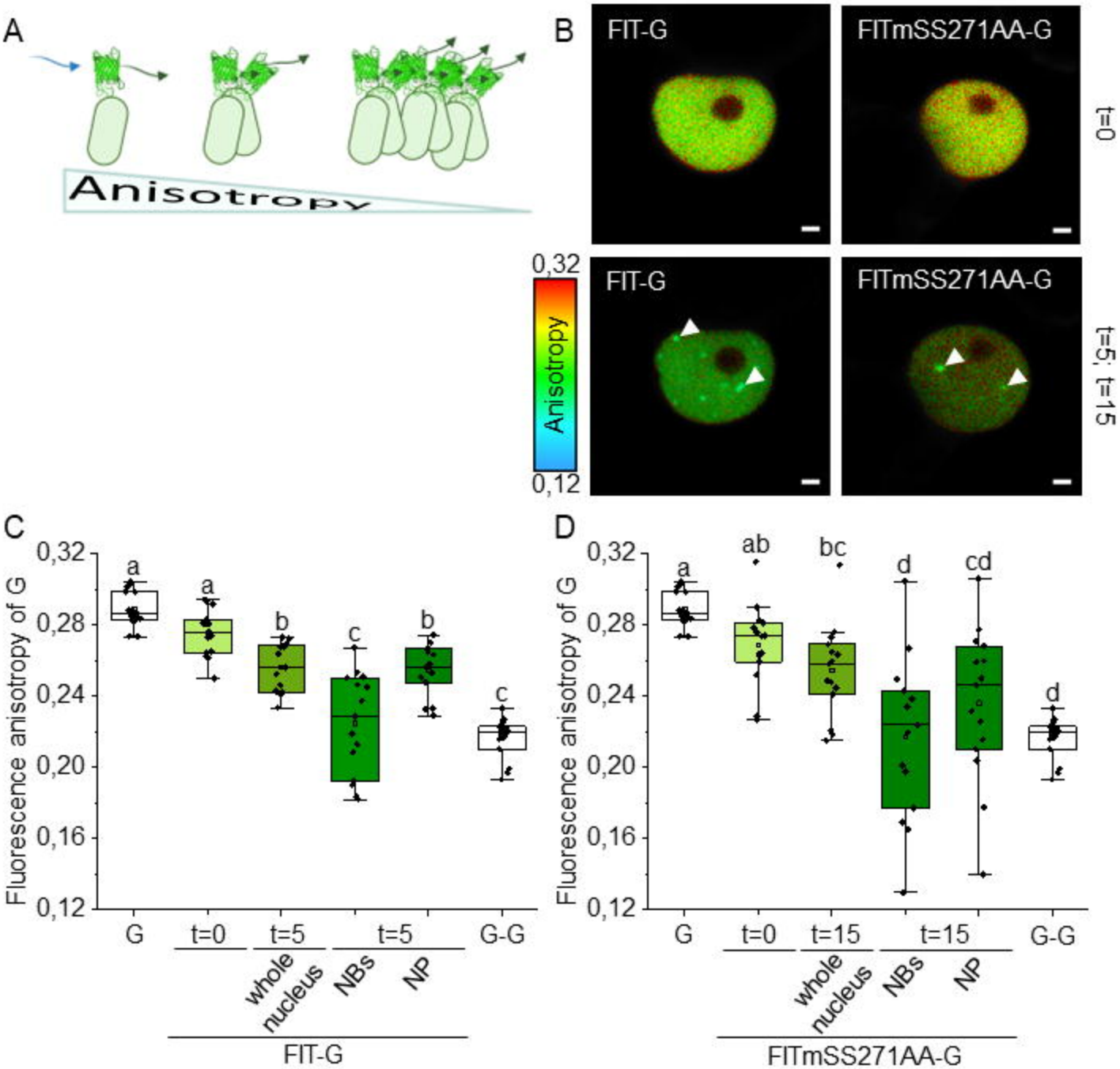
A
Anisotropy
B
FIT-G
FITmSS271AA-G
t=0
t=5; t=15
0,32
Anisotropy
0,12
C
Fluorescence anisotropy of G
0,32
0,28
0,24
0,20
0,16
0,12
a
a
b
c
b
c
G
t=0
t=5
t=5
G-G
whole nucleus
NBs
NP
FIT-G
D
Fluorescence anisotropy of G
a
ab
bc
d
cd
d
G
t=0
t=15
t=15
G-G
whole nucleus
NBs
NP
FITmSS271AA-G

Figure 4

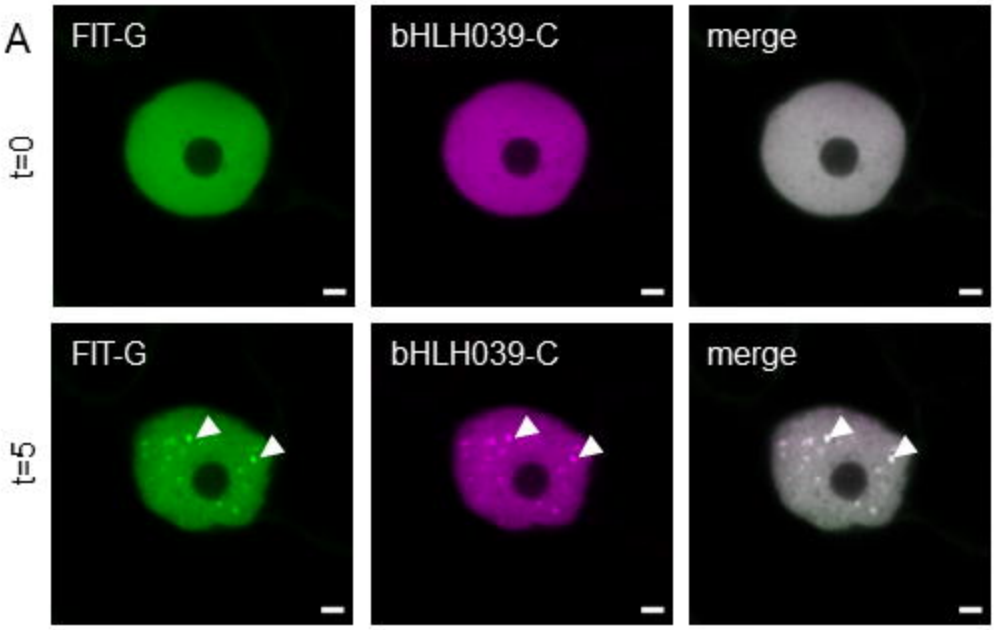
A
FIT-G
bHLH039-C
merge
t=0
t=5

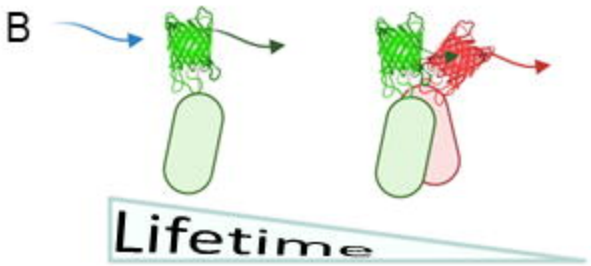
B
Lifetime

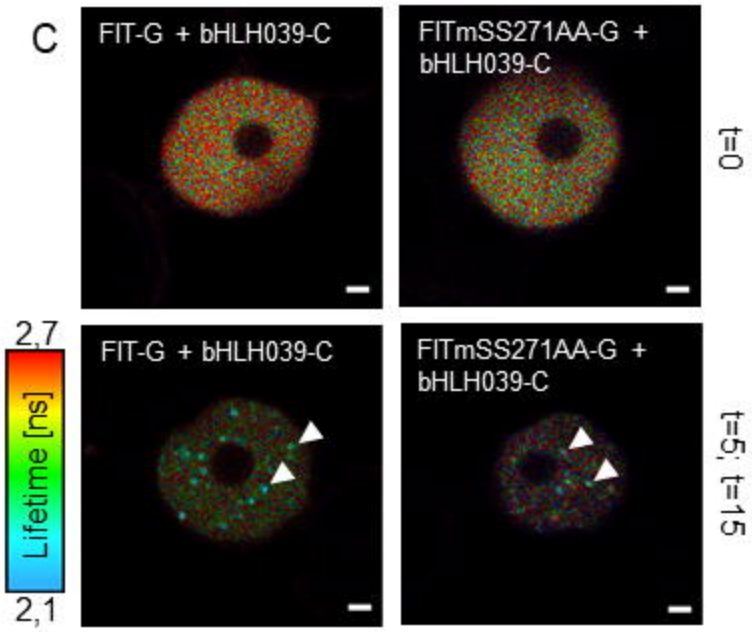
C
FIT-G + bHLH039-C
FITmSS271AA-G + bHLH039-C
t=0
t=5, t=15
2,7
Lifetime [ns]
2,1

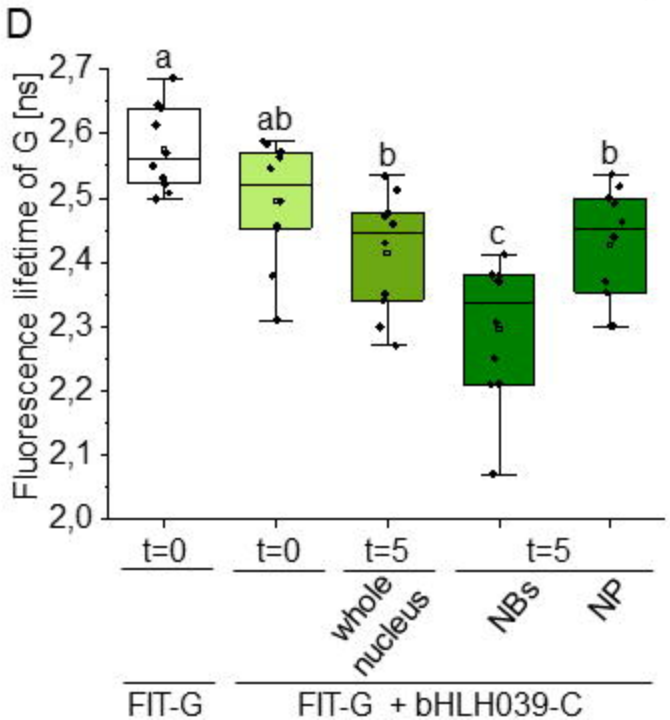
D
Fluorescence lifetime of G [ns]
2,7
2,6
2,5
2,4
2,3
2,2
2,1
2,0
a
ab
b
c
b
t=0
t=0
t=5
t=5
whole nucleus
NBs
NP
FIT-G
FIT-G + bHLH039-C

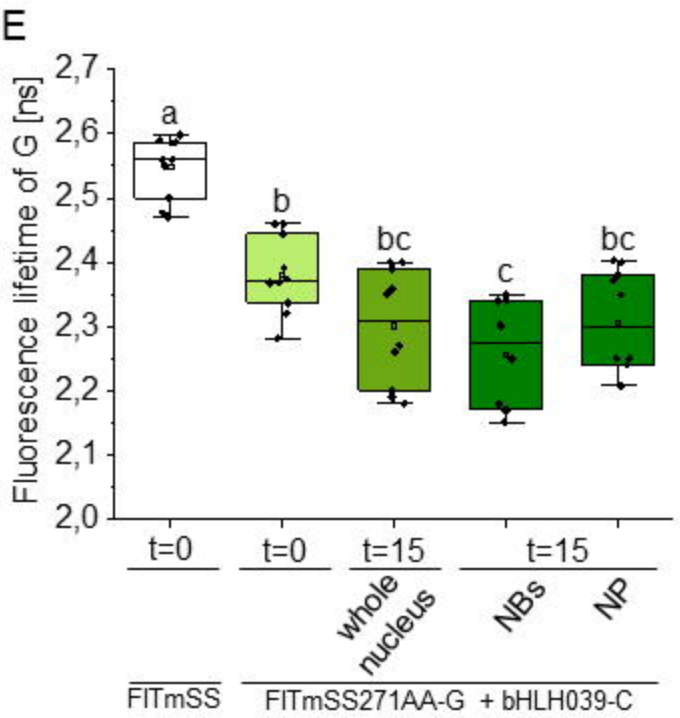
E
Fluorescence lifetime of G [ns]
2,7
2,6
2,5
2,4
2,3
2,2
2,1
2,0
a
b
bc
c
bc
t=0
t=0
t=15
t=15
whole nucleus
NBs
NP
FITmSS
FITmSS271AA-G + bHLH039-C

Figure 5

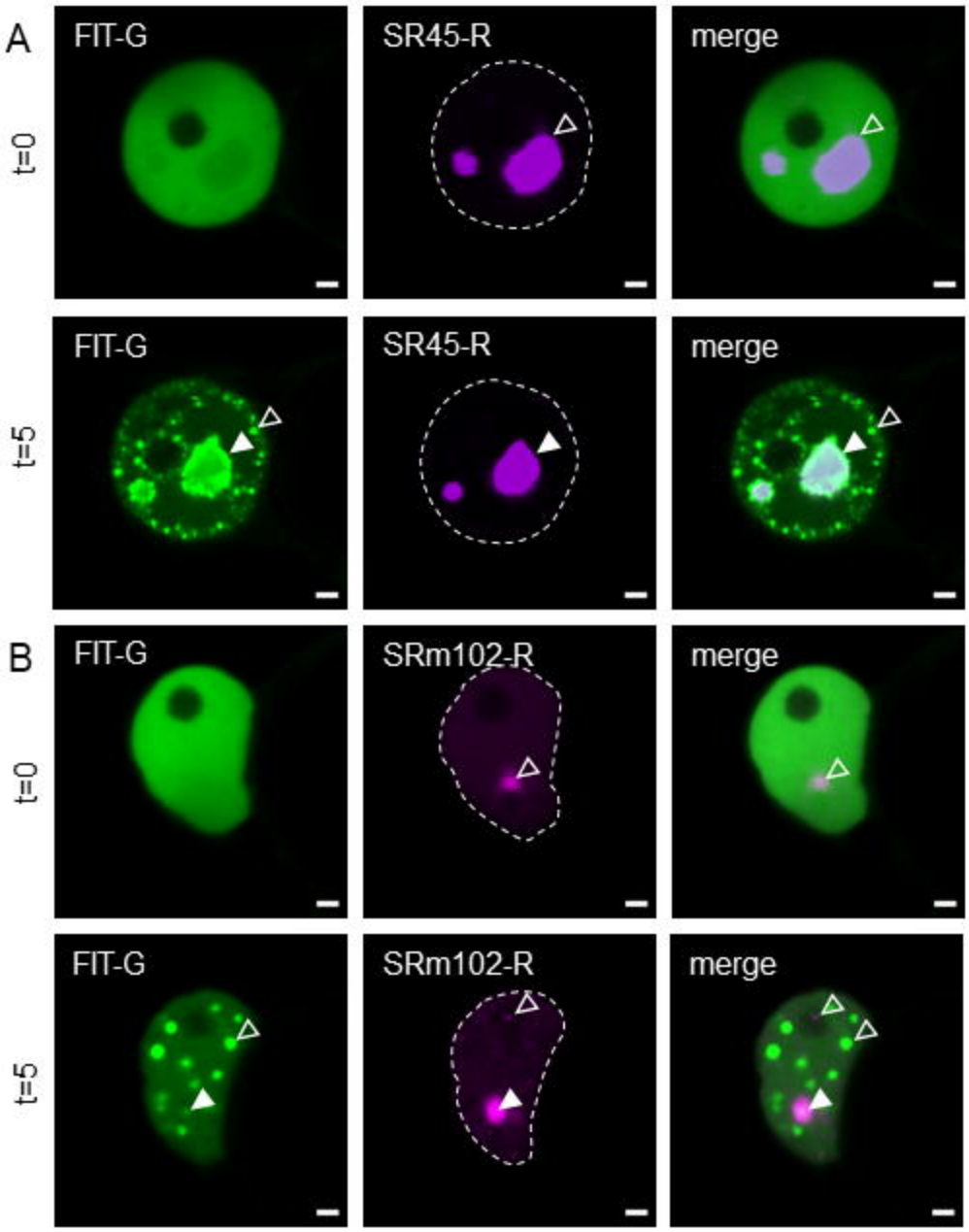
A
FIT-G
SR45-R
merge
t=0
FIT-G
SR45-R
merge
t=5
B
FIT-G
SRm102-R
merge
t=0
FIT-G
SRm102-R
merge
t=5

Figure 6

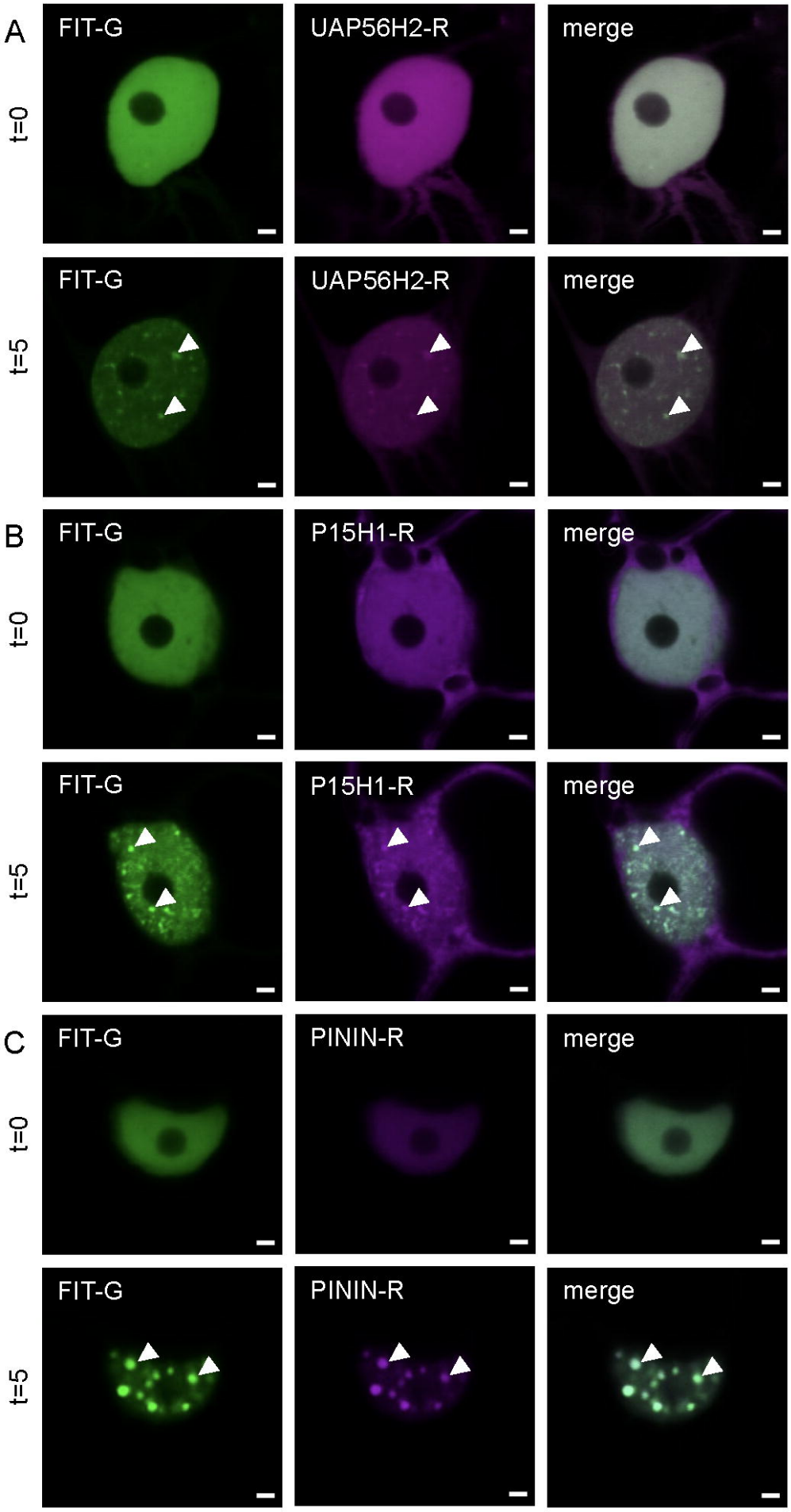
A
t=0
FIT-G
UAP56H2-R
merge
t=5
FIT-G
UAP56H2-R
merge
B
t=0
FIT-G
P15H1-R
merge
t=5
FIT-G
P15H1-R
merge
C
t=0
FIT-G
PININ-R
merge
t=5
FIT-G
PININ-R
merge

Figure 7

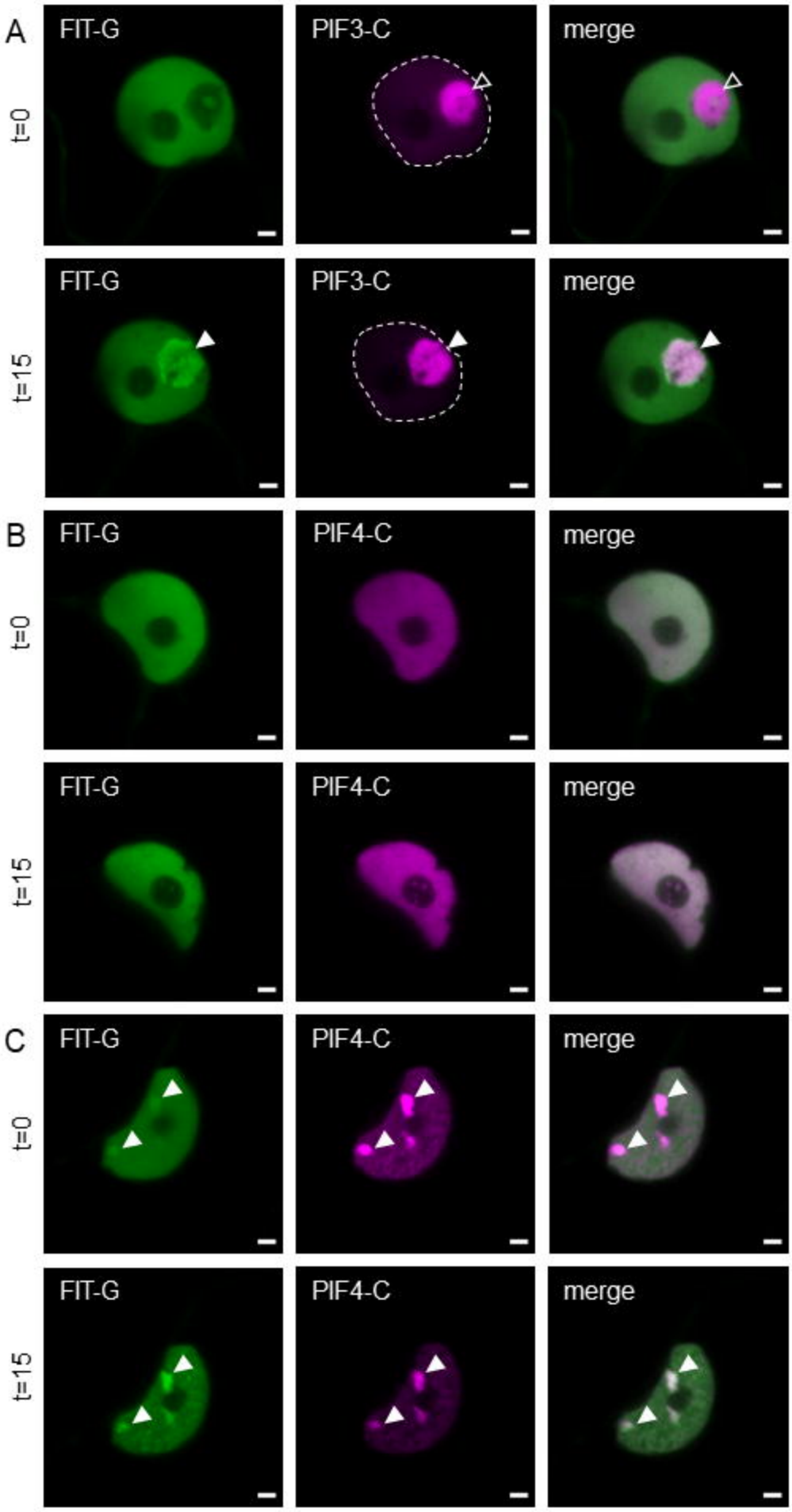
A
t=0
FIT-G
PIF3-C
merge
t=15
FIT-G
PIF3-C
merge
B
t=0
FIT-G
PIF4-C
merge
t=15
FIT-G
PIF4-C
merge
C
t=0
FIT-G
PIF4-C
merge
t=15
FIT-G
PIF4-C
merge

Figure 8

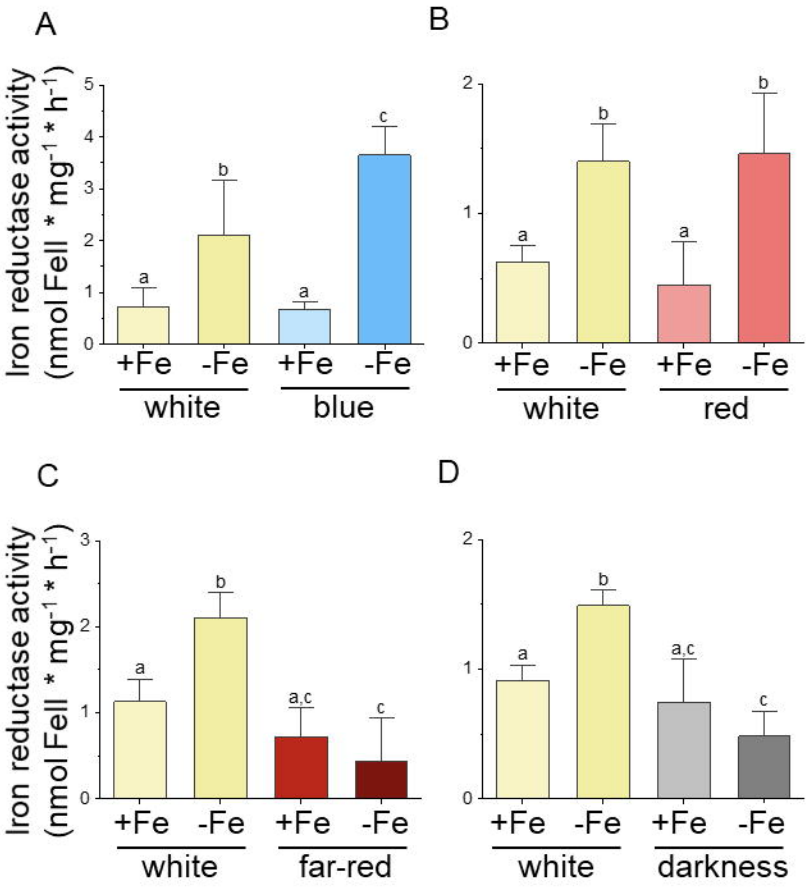
A
B
C
D
Iron reductase activity
(nmol FeII * mg-1 * h-1)
+Fe
-Fe
white
blue
red
far-red
darkness
a
b
c
a,c

Figure 9

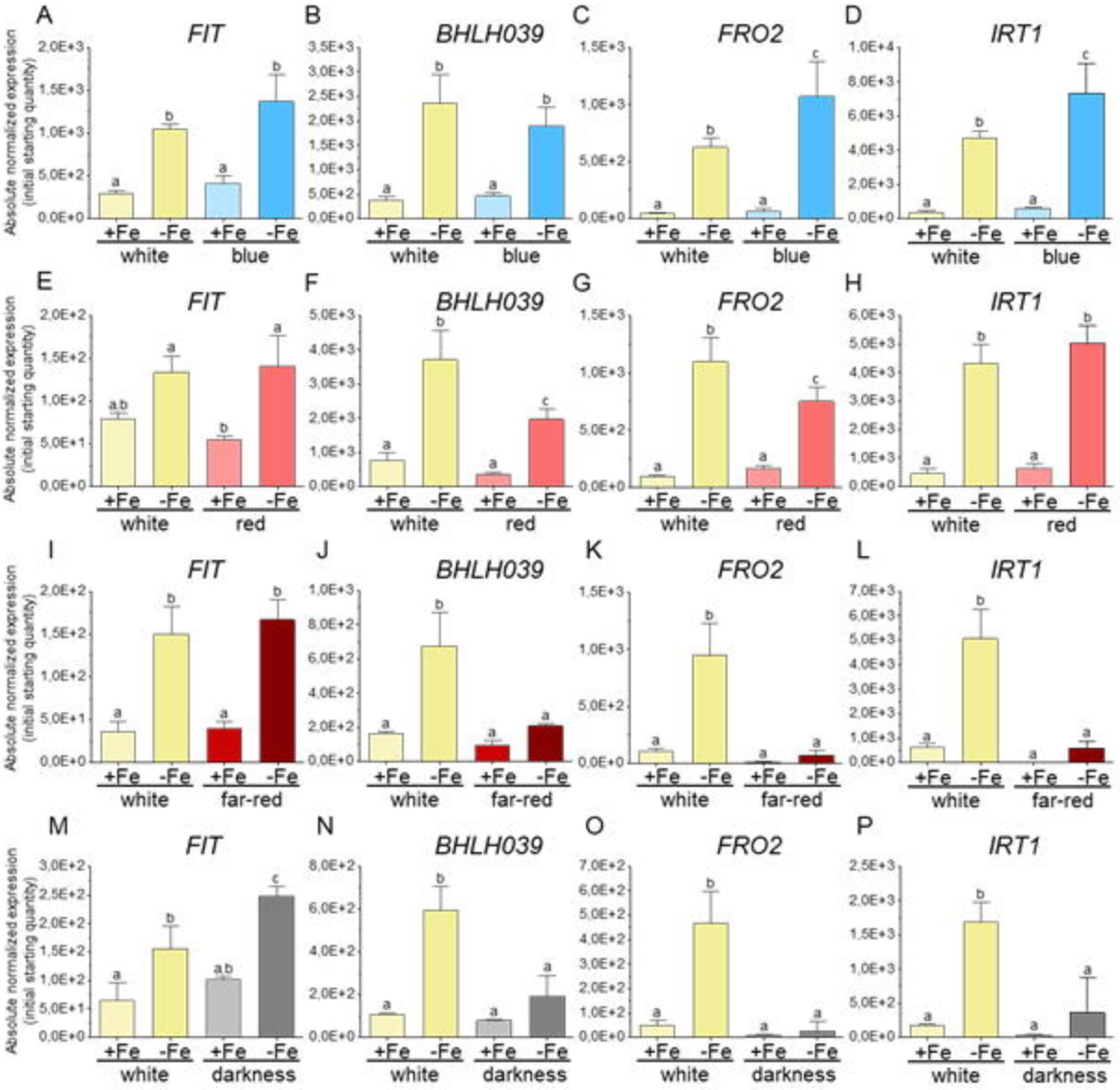
A
FIT
B
BHLH039
C
FRO2
D
IRT1
E
F
G
H
I
J
K
L
M
N
O
P
Absolute normalized expression
(initial starting quantity)
+Fe
-Fe
white
blue
red
far-red
darkness

Figure 10

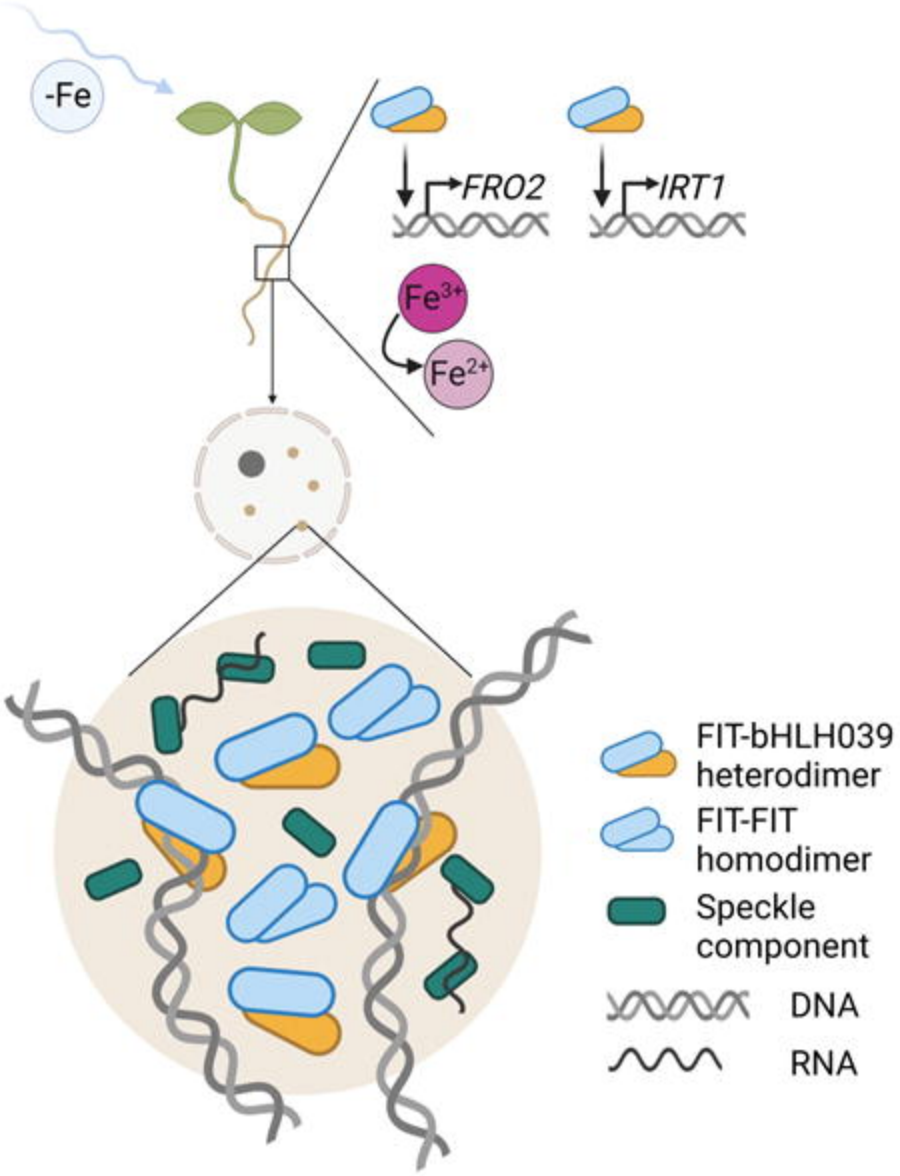
-Fe
FRO2
IRT1
Fe3+
Fe2+
FIT-bHLH039 heterodimer
FIT-FIT homodimer
Speckle component
DNA
RNA